INSTITUTO TECNOLÓGICO Y DE ESTUDIOS SUPERIORES DE MONTERREY

CAMPUS MONTERREY

DIVISIÓN DE INGENIERÍA Y ARQUITECTURA

TECNOLÓGICO DE MONTERREY®

PROGRAMA DE GRADUADOS EN INGENIERÍA

SURFACE ROUGHNESS MONITORING AND PREDICTION IN A HIGH SPEED END MILLING PROCESS IN ALUMINUM AND STEEL ALLOYS

TESIS

PRESENTADA COMO REQUISITO PARCIAL PARA OBTENER EL GRADO ACADÉMICO DE
MAESTRO EN CIENCIAS
CON ESPECIALIDAD EN SISTEMAS DE MANUFACTURA

POR:
DAVID FERNANDO VILLASEÑOR GONZÁLEZ

MONTERREY N.L. DICIEMBRE DE 2005

INSTITUTO TECNOLÓGICO Y DE ESTUDIOS SUPERIORES DE MONTERREY

DIVISIÓN DE INGENIERÍA Y ARQUITECTURA
PROGRAMA DE GRADUADOS EN INGENIERÍA

Los miembros del Comité de Tesis recomendamos que la presente Tesis del Ing. David Fernando Villaseñor González sea aceptada como requisito parcial para obtener el grado académico de Maestro en Ciencias con especialidad en:

SISTEMAS DE MANUFACTURA

COMITÉ DE TESIS

Dr. Ciro A. Rodríguez González
ASESOR

Dr. José Ramón Alique López
CO-ASESOR
Instituto de Automática Industrial
Madrid, ESPAÑA

Dr. Horacio Ahuett Garza
SINODAL

Dr. Rubén Morales Menéndez
SINODAL

APROBADO

Dr. Federico Viramontes Brown
Director del Programa de Graduados en Ingeniería

Diciembre de 2005

DEDICATORY

To my parents Juan David and María del Carmen

To my sister Carolina

To Ana María Ferran

To all my friends

ACKNOWLEDGEMENTS

To my adviser, Dr. Ciro Rodríguez González for sharing its knowledge and the time dedicated to my work. For the opportunity given for my research stance at the Instituto de Automática Industrial in Madrid, Spain.

To Dr. Horacio Ahuett and Ruben Morales for their support as advisors in my thesis work. To Dr. Arturo Molina for the opportunity given to belong to the Mechatronics Research Center and supporting my master studies at the ITESM.

Special thanks to Dr. José Ramón Alique for the opportunity given to belong to his research team at the IAI in Madrid and guiding my research work.

To my partners at the IAI, Fernando and Adriana for their support throughout the testing phase and the rights given to modify their software.

To the Centro de Sistemas Integrados de Manufactura for supporting me in my master studies.

To M.C. Miguel de Jesús Ramírez Cadena, for his advices, confidence friendship and constant support throughout my studies.

To my family for the opportunity given to study at the ITESM and their support in every decision taken.

To Nico, Laura, Ricky, Saulo, María Augusta, Joaquín, Luis Canché, Juan Camilo, Nathalie, Andrés, Victor and Jasso for their friendship, their support and all the great moments we shared.

To my friends from Colombia, Costa Rica, España and Brasil, master partners and teachers of the Manufacture department.

SUMMARY

The present study seeks to monitor and predict surface roughness in a high speed end milling process. Five specific objectives are sought in this study:

1. Establish a technological platform in which process monitoring is possible at high frequency sampling.
2. Analyze and predict the forced vibrations (Acc[x]) produced by the spindle speed and cutting conditions.
3. Determine the effect that the controllable parameters (spindle speed, depth of cut, feed per tooth and feed rate) together with forced vibrations have on the final Surface roughness (Ra).
4. Analyze and predict the machine vibrations (Acc[x]) produced by the spindle speed and its proper feed rate (V_f).
5. Create efficient surface roughness predictors for (7075-T6, 6061-T6 Aluminum and 1045 Steel) different materials in high speed end milling operations, using statistical analysis tools.
6. Compare theorical and estimated surface roughness models.

Accelerometers and CNC variables are tested to experimentally acquire data of the machining process in order to develop a model in which the surface roughness of parts is predicted. Process parameters and dynamic vibrations are used to develop the model using regression statistical tools. While experimenting, tool diameter, parts material, and depth of cut are remained constant. Once the model is obtained, final experimentation is made to corroborate its reliability. Finally, a concluding study is made to determine the individual effect of each parameter with the surface roughness.

TABLE OF CONTENTS

LIST OF FIGURES

LIST OF TABLES

LIST OF SYMBOLS

AccRes	Resultant acceleration
a_p	Axial Depth of Cut (mm)
a_x	Vibration in the x axis (mm/s^2)
a_y	Vibration in the y axis (mm/s^2)
a_z	Vibration in the z axis
B	Coefficients for multiple regression analysis
D	Tool diameter (mm)
fn	Feed per revolution
fz	Feed per tooth (mm/tooth)
g	Acceleration basic unit
r	Toroidal end mill radius/turning insert radius
R_a	Average surface roughness (μm)
R_{max}	Maximum surface roughness (μm)
R_{th}	Theorical surface roughness (μm)
S	Spindle Speed (rpm)
V_c	Cutting Speed (m/min)
V_f	Feed Rate (mm/min)
z	Number of cutting edges

Chapter 1: Introduction

The present study is made with the objective of continuing with an extended research in the topic of surface quality and the machining parameters involved in it. In order to narrow the topic of the present these, it will be focused in the surface quality of parts machined in a High Speed end-Milling (HSM) process. To achieve such objectives, a software based data acquisition platform is developed to measure variables through different sensing methods, allowing future research. A methodology, next explained, is followed to end with a resulting model which will help to predict a value for surface roughness in an end milling process. Similarly it will be understand the impact of each parameter analyzed in the final output quality characteristics.

1.1 Antecedents

Several attempts have been made to model the surface roughness of parts in machining processes. Dislike a turning process, an end-milling process has greater complexity. Models obtained by researchers have included a great number of parameters concluding that all of them have an effect on the final surface texture of the part. It is important to mention that almost none of these research works include vibrations as an independent factor related with the quality of parts and most of them have worked with low spindle speeds which are not a characteristic of an HSM process. Even though vibrations has an specific influence depending on several factors such as machine rigidity, tool wear, setup parameters, etc. a first attempt to include vibrations into an equation to predict surface roughness will be made.

1.2 Objectives

The present study has the objective to determine a relationship between machining parameters and vibrations, jointly with their corresponding effect on the

surface quality of the parts machined, in a high speed end milling process. Four main objectives are sought in this study:

1. Establish a technological platform capable of monitoring a high speed machining at high frequency sampling.
2. Determine the effect that the controllable parameters, spindle speed, depth of cut, feed per tooth and feed rate, have on the final Surface roughness (Ra) in aluminum and steel alloys machining.
3. Analyze and predict the machine vibrations (Acc[x]) based in machining parameters.
4. Create efficient surface roughness predictors for 3 different materials using statistical analysis tools.
5. Compare theorical versus measured Ra.

1.3 Methodology

Obtaining the objectives proposed involves numerous steps and tools of several fields of study: electronics, computer systems, statistics and mechanics. Software such as LabView from National Instruments, is essential for the acquisition and visualization of the data obtained and the interaction with its sensors. The next methodology, in Figure 1, is simple which requires no more explanation, each step is accompanied with the tools used and in the gray column the results obtained from the completion of each step is displayed.

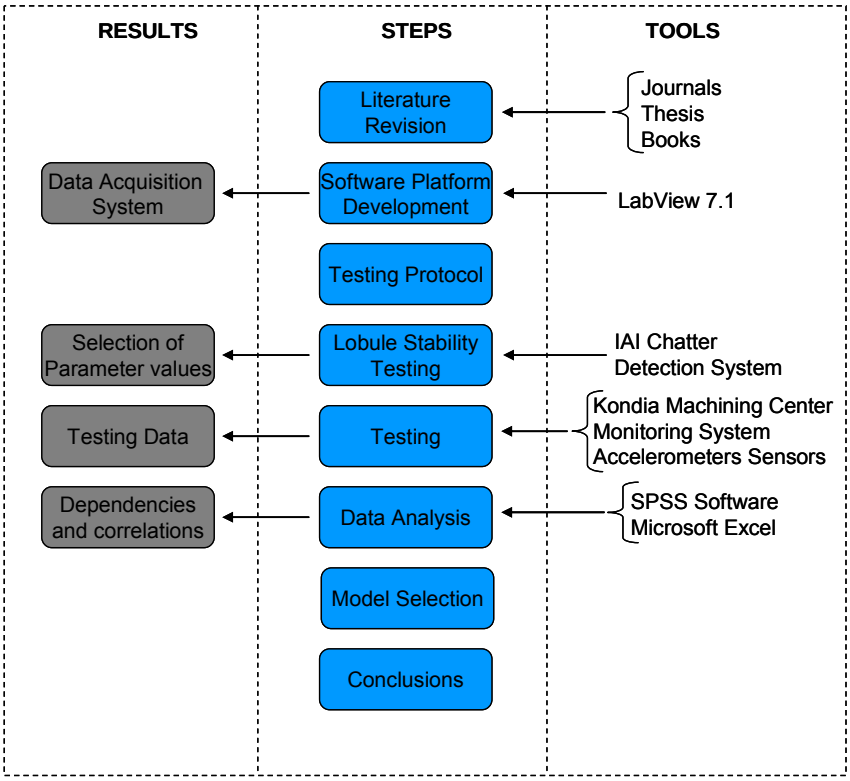

Figure 1. Methodology followed during the development of the present study. Blue boxes shows the steps made, gray boxes the result of each step and at the right the tools employed in each step.

Chapter 2: High Speed Machining

2.1 Introduction to High Speed Machining

The High Speed Machining (HSM) technology was born in the last decades focused on increasing productivity in manufacturing industries. Due to the high spindle and feed rate velocities, less time is required to manufacture parts, and so, less production costs. Because it's a relatively new technology, lots of studies have been and are being made around the topic, most of them centralized in the surface quality of parts. Drivers and motor technological advances have made possible to achieve speeds up to 30000 rpms and high feed rates, mostly in the aeronautic and aerospace industries. But the increment of such parameters has highlighted a tremendous problem in machining centers: their capability to control and monitor the process.

Compared to conventional milling process, where relatively low velocities are used, controls and sensors of HSM machines have not been enough to support high velocity sensing and control. Thus, researchers' efforts to develop successful monitoring systems for further control have been made. Even though these objectives are reached, one more step must be accomplished: to ensure that a high surface quality of parts can be obtained. With low surface quality, the time saved in a HSM process will be consumed in further processes to give parts the surface quality needed. According to the bibliography which can be found at the end of this these, Table 1 was constructed to show all variables that have been found to affect surface quality of parts. In further chapters, the development of a fast and accurate multisensor platform will be explained. This platform was developed in order to analyze some of these variables that influence the surface quality of parts in these HSM processes.

Tool Variables	Setup Variables	Workpiece Variables
Tool Geometry	Spindle Speed	Workpiece Material
Tool Nose Radius	Feed Rate	Workpiece Hardness
Tool Diameter	Depth of Cut	Workpiece Geometry
Number of teeth	Approach Angle	
Tool Wear	Stepover	
Tool Vibration		
Tool Material		
Machine-Tool Rigidity		

Table 1. Parameters and variables that influence the surface quality of machined parts in an end milling process.

2.2 Why High Speed Milling?

It is very important for the metalworking industry to reduce costs in manufacturing, for such reason the development of high speed machines has been inspired. It is important also to recognize that high speed machining technology is relatively new, thus there is not enough knowledge on the most suitable shop procedures for these processes. These and other reasons are found to justify the research on such topic.

HSM implies high spindle speed, feed rates, or both. It could not be standardized a certain speed to be consider a high speed milling process, due to the condition and complexity of the process and the materials used, but it is known that HSM helps to improve productivity compared to a conventional milling method. The problem surges in which parameter settings to choose to achieve great quality parts if such process nature is not well know.

The development of material technology is driving the research on faster machining methods. New harder and resistant materials, mostly from automotive and aeronautic industries, cannot be machined with conventional processes.

The objective of this study is to get knowledge of few aspects of the nature of high speed milling focused on parts quality. Some more years must pass in order to get full knowledge and be capable of controlling a huge amount of parameters involved in a process to achieve specific purposes. Actually, without a complete knowledge in the topic, it can be ensure that high speed milling processes have the following advantages over conventional milling:

- With the ability of increasing speed over six times, HSM will reduce production times and consequently production costs.
- Generating low cutting forces with HSM than with conventional milling, it is now possible to produce thinner-walled parts than normal.
- A single HSM has the potential to replace 2 or 3 conventional mills.

The development of such machinery is driving other areas involved in this industry to develop new technologies to satisfy the users of HSM. These evolutions involve:

- Complex and more resistant tools.
- Higher speed spindles.
- More complex control systems.
- Development on sensorial systems.
- Development on safety systems.
- New and more precise CNC systems.
- More rigid and resistant machine structures.
- Complex clamping methods.
- Research and development of new coolant methods.

For all these reasons and the need of knowledge in this area, this these focus its research in High Speed Milling.

2.3 Literature Review

One of the greatest challenges in machining is to achieve the maximum rate of cutting material, minimizing at the same time the tool wear, maintaining the surface and dimensional quality in all parts [Correa, 2004]. Nowadays, researchers have focused their work in determining which parameters affect these machining aspects. In this study we will center our attention in surface quality. Surface roughness is the most representative parameter to represent the part surface texture. Currently the most common term to define surface roughness is Ra, Figure 2, other terms such as Rmax, Ry, Rq, etc. are less used. Ra is defined as the average value or surface roughness through a distance [Amaral and Chong, 2002].

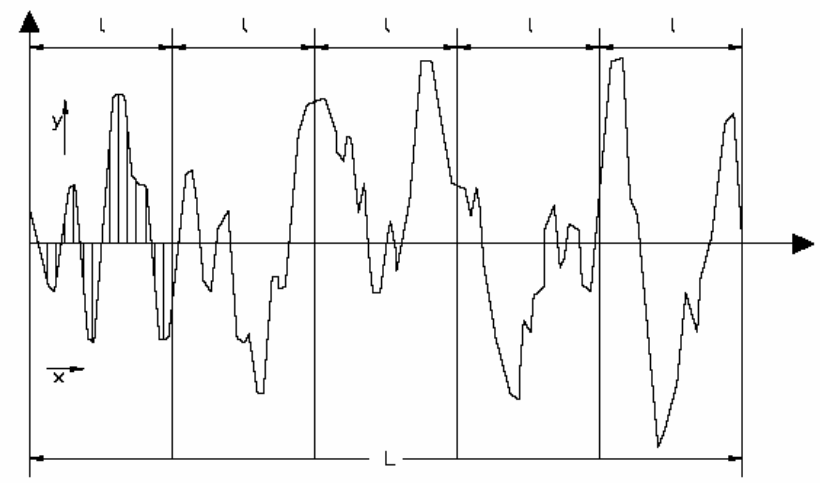

Figure 2. Surface Roughness parameter Ra representation over a specific length [Lou, Mike. et al, 1998].

Researchers have modeled the machining process in order to obtain an equation which help to predict the superficial roughness in parts [Boothroyd and Knight, 1989].

$$Ra = \frac{f_n^{\,2}}{32r} \qquad \text{(Equation 1)}$$

Equation 1 shows the ideal surface roughness in turning, where Ra is the average value of surface roughness through a distance, f_n is the feed per revolution and r the tool radius. In addition to the geometric parameters in equation 1, researches have found that the surface roughness is affected by a great number of parameters and aspects in more or less magnitude. Models, such as the one of Lou, had include parameters like spindle speed, feed rate and depth of cut to determine Ra [Lou et al, 1999]. In other investigation Mandara left the depth of cut constant and varied the tool size getting the same results as Lou, which are, all parameter evaluated have an effect on surface roughness [Mandara et al, 1999].

Table 2 shows some relevant studies made by researchers related to the prediction of surface roughness.

Article name	Authors	Article Objective	Observations	Conclusions
Optimization of feedrate in a face milling operation using a surface roughness model (October 1999)	Dae Kyun Baek Tae Jo Ko Hee Sool Kim (South Korea)	Create a surface roughness prediction based on geometric calculus of the axial and radial insert runouts. Process: face milling	Velocities used: Feed Rate 127 mm/min Spindle Speed 370 rpm Maximum Velocities: Vc = 116 m/min	A surface roughness predictor was created with prediction errors of 3 µm average. Measured surface roughness are about 13 and 20 µm.
Simulation of surface roughness and profile in high-speed end milling (2001)	Ki Yong Lee Myeong Chang Kang Yung Ho Jeong Deuk Woo Lee Jeong Suk Kim (South Korea)	Present a method for simulating the machined surface using the acceleration signal instead of using cutting forces. A geometric end milling model was used for modeling the end milling offset and tilt angle. Process: Profiling	Velocities used: Feed per tooth: 0.05 mm/t Spindle Speed 10000-15000 Max Velocities: Vc = 471 m/min	The frequency analysis is used to obtain the dominant frequencies which are included in the model to obtain the surface roughness predictions. Errors vary in maximum 0.50 µm.
Surface roughness model for en milling: a semi-free cutting carbon casehardening steel (EN32) in dry condition (October 2000)	A. Mansour H. Abdalla F. Meche (Egypt, UK)	Develop a mathematical model that utilizing the response surface roughness methodology and method of experiments to predict the surface roughness. Process: face milling	The milling process was in dry conditions. Models and design of experiments too complex. Max Velocities: Vc = 38 m/min	Confidence intervals for Ra prediction were created.
Experimental study of surface roughness in slot end milling AL2014-T6 (May 2003)	Ming-Yung Wang Hung-Yen Chang (Taiwan)	Analyze the influence of cutting condition and tool geometry on surface roughness when slot end milling AL2014-T6. Process: slot end milling	Parameters considered were cutting speed, feed, depth of cut, concavity and axial relief angles of the end cutting edge of the end mill. Max Velocities: Vc = 80 m/min	Using response surface models two theoretical models were created for dry machining and with coolant.
An adaptive-network based fuzzy inference system for prediction of workpiece surface roughness in end milling (October 2001)	Ship-Peng Lo	Predict the workpiece surface roughness after the end milling process with an adaptive network based fuzzy inference system. Process: N/A	Three milling parameters were analyzed, spindle speed, feed rate and depth of cut. Max Velocities: Vc = 89 m/min	The predicted surface roughness values derived from ANFIS achieved very satisfactory accuracy.
This these		Process: Grooving	Vc = 830 m/min maximum.	For steel and aluminum alloys

Table 2. Relevant articles reviewed in the literature research phase.

2.4 Proposed Modeling Approach

Several techniques can be used to obtain a final model for surface roughness. In this study regression methods will be used because of their simplicity, effectiveness and the allowance of using high exponential orders. As explained in the introduction of this work vibration and surface roughness will be our final predicted dependant values. Our dependant variables will be feed rate, spindle speed and depth of cut. Further study could be considered using different techniques to obtain the model in order to compare efficiency and processing time. Average surface roughness (Ra) will be kept as the unique term analyzed to get uniformity in the results of the experimentation phase. Next figure shows the proposed modeling approach for this study.

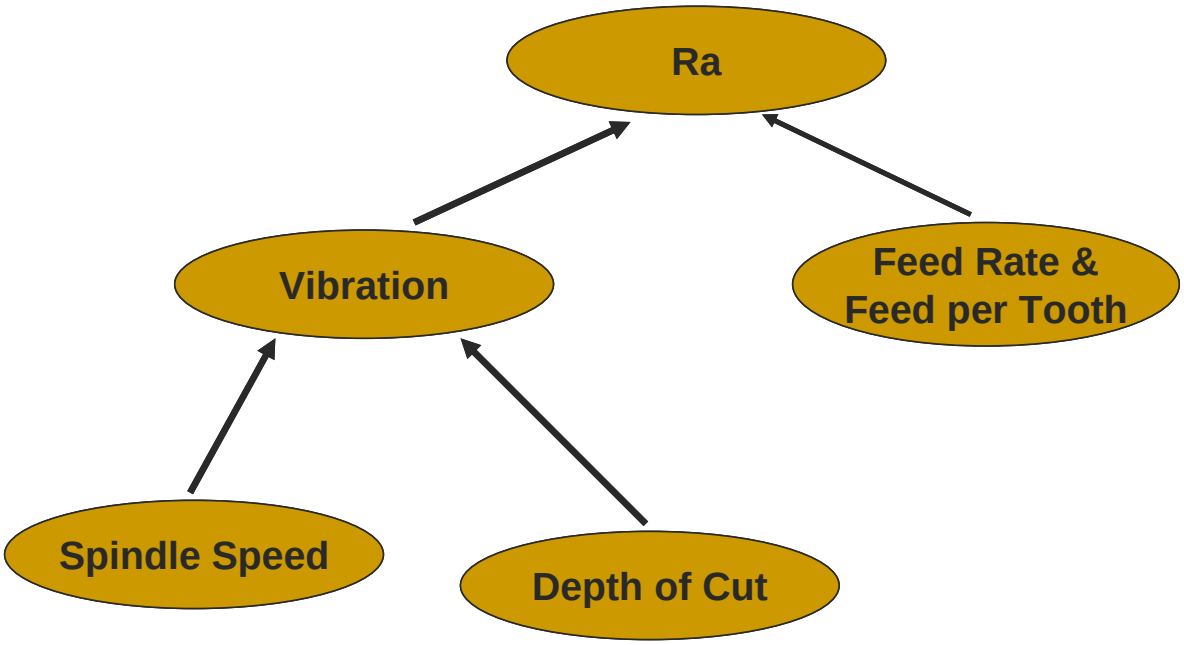

Figure 3. Proposed modeling approach scheme.

In this modeling approach two equation are obtained: one to predict vibrations and a second to predict surface roughness. Figure 3 shows the variables that help predict each parameter.

Chapter 3: Machining Monitoring System

3.1 Introduction

The present chapter is intended to give an overview of how a machine monitoring system (MMS) is composed. For better understanding, the whole MMS is divided into instrumentation levels. These levels can be seen in Table 3, where it is shown which type of instrumentation belongs to each level. Starting from the end milling machine, up to the computer, where the results are displayed and analyze, every possible instrument that was intended to use in the system is briefly explained. It is not the purpose of this these to deeply explained their operating mechanism but at least to know which function they have in the whole system. In order to acquire deeper information on the instrumentation, the bibliography shown at the end of this study should be consulted.

Level	Instrumentation
Level 1	All type of sensors: accelerometers, acoustic emission, proximity, proper machine system, etc.
Level 2	Signal conditioners: amplifiers, filters, etc.
Level 3	Signal digitalizing/acquisition: Data Acquisition Cards, specific data acquisition devices, etc.
Level 4	Computer and software for signal displaying and processing.

Table 3. Instrumentation levels classification.

3.2 Instrumentation

According to the levels of instrumentation showed, Figure 4 explains the instrumentation setup that will be used for variable information acquisition of the end milling process. It is important to mention that the instrumentation showed was selected due to their properties related to the variables of interest. It is open to the researcher the instrumentation they want to used, but normally it is limited by the cost of the system. At the end of this chapter, a brief resume of several

instrumentation systems used by researchers will be shown. Next, each integrant of the system will briefly be explained. Technical information, data sheets and manufacturers can be found on appendix A.

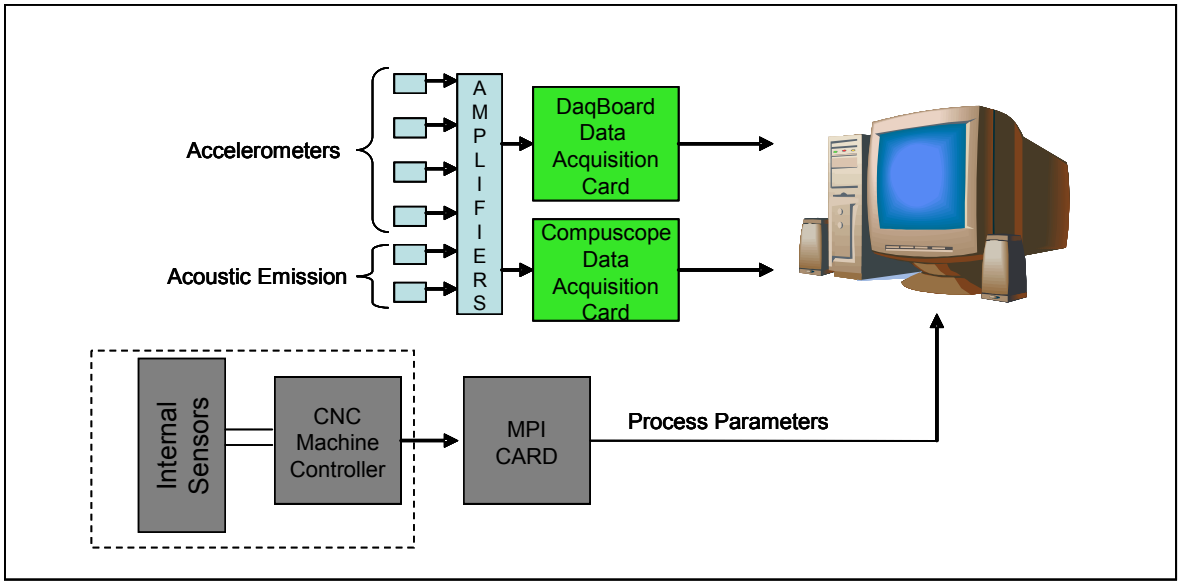

Figure 4. Instrumentation setup for data acquisition.

3.3 Sensors

Sensors constitute the first level of a monitoring system. Simply, they function as human senses in order to produce electrical signals depending on what is happening in the environment. They can greatly improve the functionality of a system, but in the same way it increases its complexity. In-Process Sensors (IPS) are able to obtain signals under the harsh environment of a milling process, for example. IP sensors are used to generate control signals to improve both the control and productivity of manufacturing systems [Dornfeld, 2003]. Numerous type of IPS have been developed to make monitoring systems more reliable. Accelerometers, acoustic emission sensors, microphones and dynamometric bases are some IPS used to measure parameters affecting the surface finishing of parts.

3.3.1 Accelerometers

Accelerometers are piezoelectric sensors which are commonly used to measure vibrations and accelerations in most monitoring systems with industrial applications such as predictive maintenance, aerospace, automotive, medical, process control, etc. These sensors come in many types depending on the operation principle. Generally most accelerometers have a crystal which generates a signal when it is compressed by a force or 'g' force. The signal delivered by these sensors is commonly treated as m/s^2. Further integration of data could give us measures as velocities or distances [Transductores y medidores electrónicos, 1977]. Data could be worked either in time or frequency domain. This signal could then be amplified and measure by an acquisition system which will then process it to convert it to the units of interest. Most accelerometers are housed in order to be used under harsh environment circumstances.

Before choosing an accelerometer it is important to know in which order of frequencies we are sensing. The signal emitted by these sensors is very accurate up to the resonance frequency, where the error increases dramatically [Brüel & Kjaer, 1998]. For our experimentation phase, six accelerometers are used to measure vibrations in the machining process. Three are located in the upper part of the machine closed to the spindle, other three are placed in the working table. Only the three located in the spindle will be used to build the model. In further chapters, the signal generated by each sensors is analyze in order to determine what influence does the location of the sensor had in the measured signal. Figure 6 shows the location in the spindle of the three accelerometers.

Figure 5. Typical axial accelerometer [Endevco Homepage]

3.3.2 Acoustic Emission Sensors

Acoustic emission sensors have the same principle as the accelerometers; the only difference is that they do not use a seismic mass. Instead they use a ceramic disk or cylinder with a thickness of a few mm. Acoustic emission sensors are not widely known in engineering. They can be used as vibration sensors with very low amplitude and of very high frequency (in orders of 10 KHz to over 1 MHz). Depending on the type of sensor and its application, the sensitivity of an AE sensor can be given in V/um when the sensor is used to measure surface displacement motion, or in V/(mm/s) when the sensor is intended to measure surface velocity.

AE sensors are now starting to be used in numerous processes with monitoring purposes such as:

- Metal cutting
- Metal forming such as stamping and deep drawing
- Extruding plastic melts, specially filled melts
- Indicating the stress level in bolts
- Monitoring of welding processes
- Machinery condition monitoring and incipient failure detection
- Monitoring of aircraft structures.

Actually AE sensors are being used in research for tool break detection and wear in metal cutting processes. Researchers have tended to frequently use

accelerometers instead AE sensors due to their frequency range development, their simplicity to reduce noise, calibration methods and available bibliographic information.

AE sensors have the greatest sensitivity to the critical process conditions in precision machining, with the lowest noise level. Other sensors such as force and vibration sensors suffer from inaccuracies due to their low sensitivity in the extremely high frequency range, where most of the micro cutting activities are sensed [Dornfeld, 2003]. If the signal of interest is vibrations purely related to the cutting process, not to mechanical effects, AE sensors must be a good option.

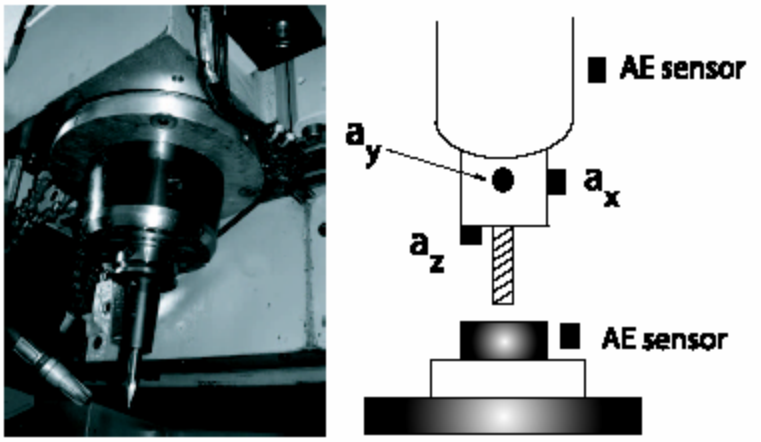

Figure 6. Sensor types and location in the machining center.

Two acoustic emission sensors are used to sense vibrations in the high speed milling process for this study. Further analysis is made in order to determine the differences found on the experiment results, due to the used of different type of sensors (AE and Accelerometers).

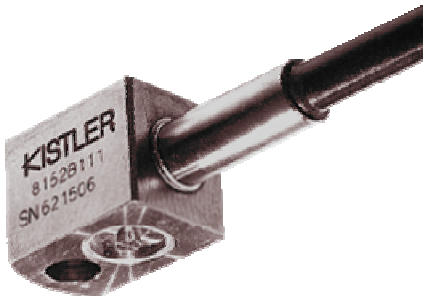

Figure 7. A Kistler 8152B Acoustic Emission Sensor [Kistler Homepage]

3.3.3 Microphones

In the effort of searching different ways of measuring vibration on machining process, microphones were tested. As conventional microphones, industrial microphones emit signals due to vibrations caused by sound waves. These sound waves are emitted directly from the machining process. Their sensibility is directly related with the area of the sensor diaphragm. This factor is very important at the time of selecting the correct microphone [Transductores y medidores electrónicos, 1977]. Normally, the signal emitted by these sensors is measured in dB. The principal disadvantages detected on microphones are their low sensitivity and their reaction to environmental noise. It resulted very difficult to suppress noise signal caused by environmental noises of machining floors. Because their closed placement to the tool and workpiece, and their difficulty in the signal processing, these sensors were excluded from the machine instrumentation for the experimentation of the present study.

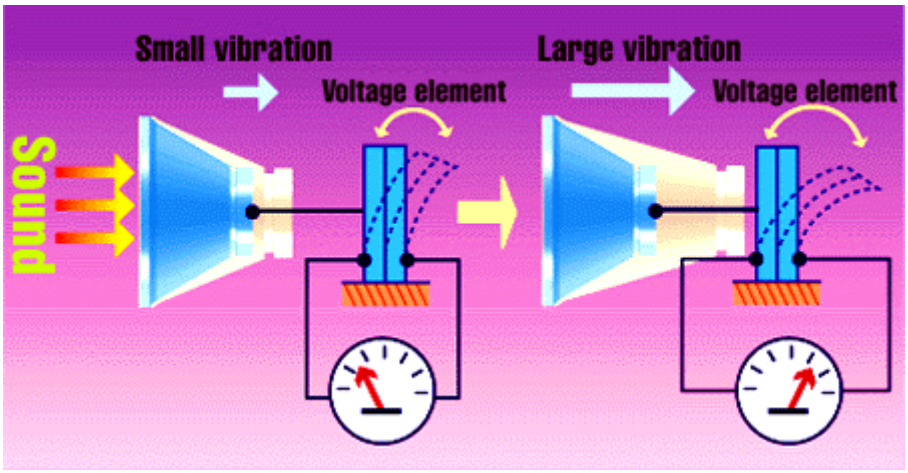

Figure 8. Microphone function principle [How stuff works homepage].

3.3.4 Multicomponent Force Sensors

Force sensors are also widely used in manufacturing process monitoring. A common force sensor has the same anatomy as a piezoelectric sensor. It has a piezoelectric material which reacts emitting an electrical signal due to a compression or expansion force. In most sensors the signal emitted in a

compression force is positive. Multicomponent force sensors are devices with several built in common force sensors or dynamometers. These sensors are placed in order to detect two, three or more axes of measurement. These are mainly built with quartz and for high temperature or high sensitive applications. 3-component force sensors have a pair of quartz elements cut for longitudinal piezoelectric effect for measuring the compression force (the z component Fz) and a pair of quartz elements cut for the shear effect each for measuring the shear components (the x component Fx and the y component Fy) of the acting force [Gautschi, G, 2003]. The output of these devices is normally connected to a charge amplifier. The sensors could be connected in parallel so the output of the multicomponent sensor would be the sum of forces, or they could be measured separately.

Due to the need of a high number of amplifiers and the cost of the equipment, forces will not be measured in this work. The possibility of measuring forces in a high speed milling process will lead to interesting findings and should be included later in a machining model. Actually these sensors are being used to develop control systems, controlling parameters such as spindle speed and feed rate for specific purposes, like tool wear and surface roughness.

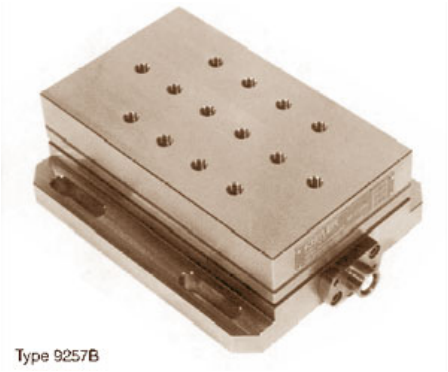

Figure 9. Kistler multicomponent force sensor, includes dynamometers in three axis [Kistler Homepage].

3.4 Data Acquisition Cards

After signal amplifiers, Data Acquisition Cards (DACs) constitute the third level of instrumentation. DACs are electronics cards dedicated to signal acquiring and processing. Equally as sensors, several characteristics must be taken into account in order to select and appropriate DAC for a monitoring system. These characteristics include:

- Sampling Rate
- Input Tension
- Number of Analog Channels
- Number of Digital Channels
- Internal RAM Memory

Sampling rate prevails as the most important factor involved in selecting a DAC. This parameter is defined as the velocity at which the acquisition card will obtain data, this is, the maximum number of samples per second that will be obtained from the system. It is important to know that the number of data per sampling can also be configured. As computers with RAM Memory, this important factor heavily influences the cost of the DAC. A good sampling rate is considered to be around 100 kHz, depending on the measuring needs.

Input tension is the maximum voltage the DAC will deliver or admit from external components. Expressed in volts, normally DACs input voltage can be, +/-5V, +/-10V or +/-12V. The input tension is directly related with the sensor for signal acquisition and with the type of channel, digital or analog, which are explained later.

The number of analog and digital channels depends on the number of sensors and their output voltage. For example, accelerometers and acoustic emission sensors deliver a continuous voltage between 4 and -4 V. Due to the fact that digital channels function with TTLs, they can either emit or accept 5V or 0V signals. Then accelerometers and AE sensors must be used with an input analog channel. Sensors such as proximity, where 5 or 0V are produced with or without detection respectively, use digital channels.

Some advanced DACs are available with internal memory. The advantage of these cards is that they acquire and can process part of the signal obtained. This will avoid the computer processor to become slower during the signal acquisition. Their main disadvantage is the high cost.

For data obtaining and processing, three DACs are used in the experimentation related to this study. Daq2000 and Daq2005 from Iotech are responsible of the accelerometers signal and a CompuScope 1602 from Gage Applied will acquire the signal from the AE sensors.

Figure 10. Gage CompuScope 1602 acquisition card. Their analog inputs were used to acquire information from AE sensors at 2.4 Mhz maximum [Gage-applied Homepage].

3.5 Amplifiers

Amplifiers are used in electronic systems to increment devices output signals making possible for computers to be detected and analyzed. Most of sensorial instrumentation detects and emits signals in order of millivolts. These signals must be amplified so variations in detection can be clearly identified. Amplifiers can be divided into two categories: operational amplifiers and charge amplifiers.

Operational amplifiers principle consists mainly in amplifying directly the voltage received by the sensor [Chicala, 2004]. These amplifiers are mainly use in applications were signals will be treated in millivolts. Requiring signals in other

units, such as velocity or acceleration units requires further software conversion, incrementing processing time. Depending on the amplifying factor its how sensitive the detection to sensor variations will be. Amplification factor must be adjusted taking into consideration the voltage ranges of the acquisition cards. Using amplifications which outputs voltages higher that DACs capacities may result into hardware damage.

Charge amplifiers have the same purpose than operational amplifiers, but their output its proportional to the charge received by the sensor [Chicala, 2004]. The voltage delivered by these type of amplifiers is proportional, in a scale, to the signal detected by the sensors. For such reason sensitivity and scale information must be configured to the amplifier. This information must be obtained from the sensor properties.

The accelerometers used for our study use a charge amplifier for each sensor. The amplifier used is a Kistler 5011 as shown in Figure 11. The configuration and connection scheme can be consulted in Appendix B.

Figure 11. 5011 Kistler Charge Amplifier use with each accelerometer. [Kistler Homepage]

3.6 Data Acquisition Software

Most of sensorial systems used for data acquisition in machining does not provide a display unit itself, for such reason it is needed to develop a PC Multisensorial platform which make possible the analyzing and saving of the acquired data. There is many software specialized in manipulating and controlling information acquired from sensorial units, some of these software are Mathlab,

DaqView, LabView, etc. All of them have weak and strong points which are described next.

- Mathlab.- Excellent software for control of processes and communication with acquisition cards. Easy programming makes this software an excellent choice. One of its weak points is that is not suitable for displaying information graphically.

- DaqView.- Software provided with acquisition cards. It is used mostly as a test software due to its simplicity and cost. It does not provide great programming capabilities, for such reason its application is limited.

- LabView.- For much the best visualization and easy programming software. It provides a complete library of preprogrammed functions which can be easily used. Its programming is completely graphical, but it can be programmed by some languages such as C, C++, etc. Its step by step function is a powerful tool which helps correcting and understanding complex programs.

LabView version 7.1 is the tool used to create the software which helped to obtain data and save it into disk so it can be analyzed. It also shows real time information graphically. This software, produced by National Instruments, counts with pre-realized VIs (named given to the graphical blocks) which makes the communication simple with the Daqs (2000 and 2005) and the Compuscope 1602. This is a very important aspect to consider before choosing the right software, and even more important, the acquisitions cards that are going to be used. Appendix C shows both VIs mentioned and their input and output signals.

Figure 12 shows a snapshot of the software developed, which has the next capabilities:

- Simultaneous and coordinated acquisition of data from three different acquisition cards, the Daqboard 2000, the Daqboard 2005 and the Compuscope 1602.
- The software was named Multiple Sensor Acquisition Platform due to the ability of getting numerous signals from different sources and sensors, such as accelerometers, acoustic emission sensors and CNC variables.

- An HMI which shows, in real time, the acquisition of different data.
- Ability to change acquisition configurations in its HMI.
- Simultaneous to data from acquisition cards, it acquires and shows information from the process. This is done through the MPI installed in the milling machine. For more information on the MPI consult appendix D.
- Finally it has the capability of saving all information showed in a .txt file in order to be analyzed after the process is finished.

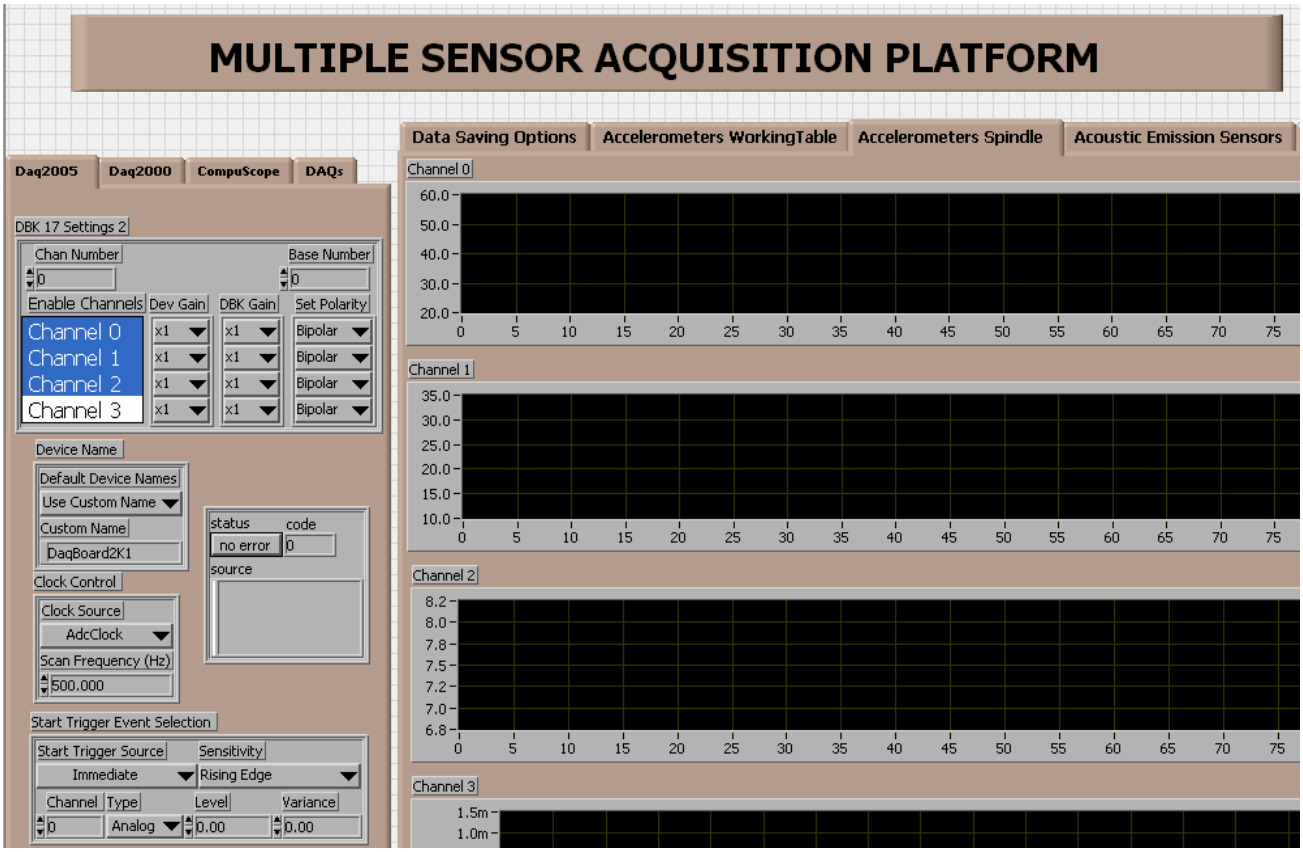

Figure 12. MAP, acquisition platform developed to gather sensorial information of the machining process and vibrations.

3.7 State of the Art

Insufficient documentation about developed monitoring systems exist. In the information that could be gathered a trend is followed by researchers. Similar sensors and developing platforms are used. Labview and Mathlab predominate as

the programming languages mostly used. Accelerometer and acoustic emission sensors are also widely used.

While more sensors are used in the monitoring system more difficult becomes the process and its location. Some researchers such as Lou and Chen uses proximity sensors to capture process parameter information like spindle speed. Using open architecture controls such as the 840D of Siemens provides the possibility of avoiding this kind of sensors that sometimes obstruct machine movements.

Compared to this monitoring system there are some differences in the way of acquiring information. Most researchers found in literature use a system as the one showed in Figure 13.

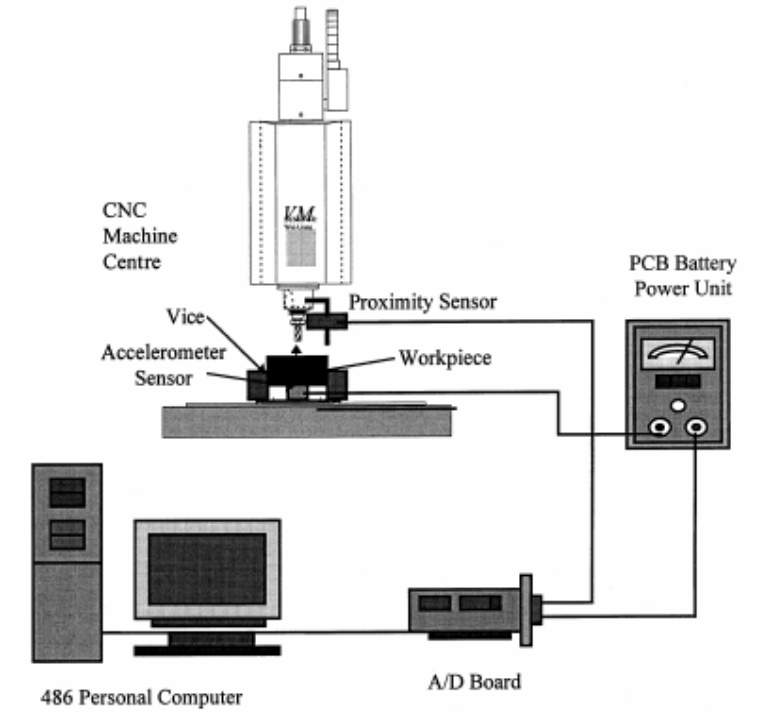

Figure 13. Lou and Chen experimental setup [Lou and Chen, 1999].

This system uses a proximity sensor in order to measure with an accelerometer the vibrations during one tool revolution. This way, they measured Vpr Vibration per revolution. In our case, the vibrations are measured all the way through the groove.

3.8 Conclusions

The monitoring system developed has several advantages over typical systems used by researchers. Some of these advantages are:

- Avoids using sensors to gather machining parameter information, such as spindle speed, depth of cut and feed rate.
- Capture simultaneously information from several acquisition cards.
- All information is gathered once, this means data obtained at a certain time corresponds to the instant of acquisition of all other cards.
- Cards and channel can be shut down if they are not going to be used. This reduces processing time.
- Information is saved in a txt file which helps in further data analysis.

Chapter 4: Design of Experiments

4.1 Introduction

A phase of high importance in the present work is the design of experiments and testing. In this chapter all conditions selected for experimentation will be supported. In the next section, the methodology followed during the whole research will be graphically shown.

4.2 Methodology

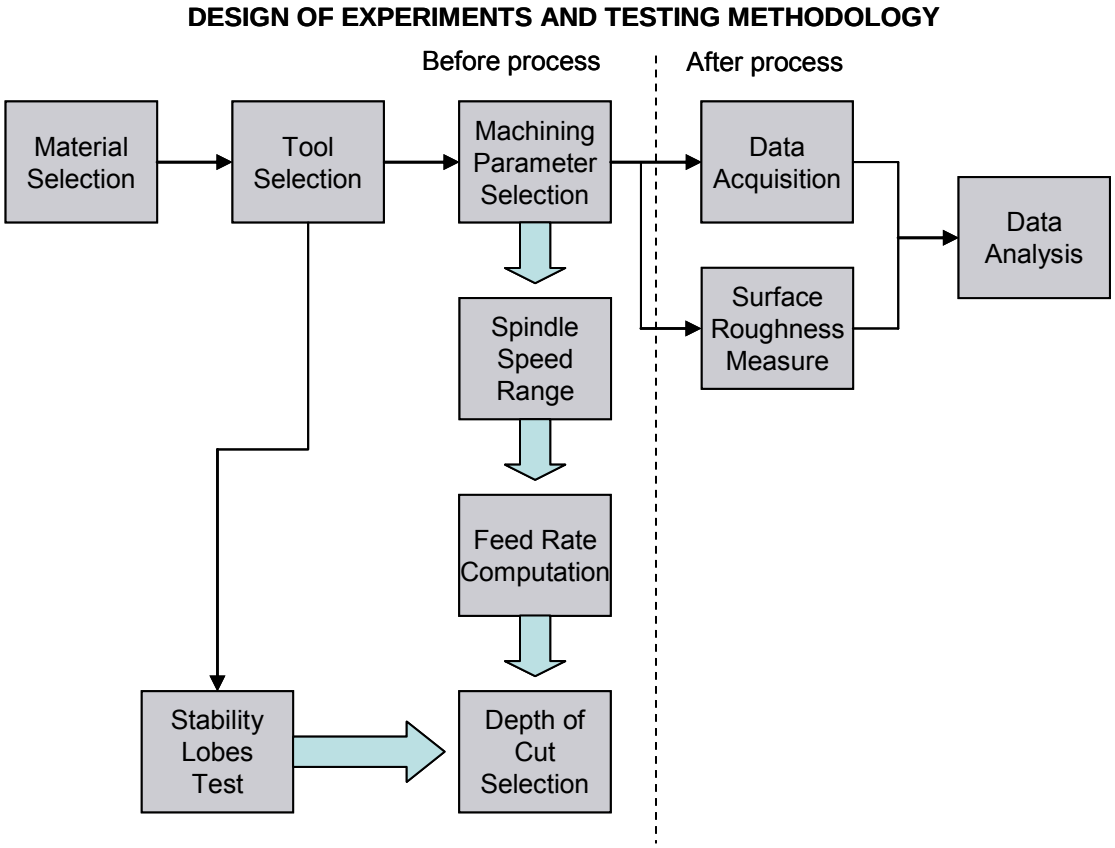

Figure 14. Design of experiments and testing methodology. Divided in two phases, the before process and the after process.

4.3 Material Selection

In the beginning of this these was commented that the present work is focused on High Speed Machining Processes. Some of the industries in which high speed processes are applied are aeronautics and automotive. For such reason the selection of materials was based on this assumption.

All the materials used are actually employed in parts produced by these industries. They were carefully selected in order to permit a comparison and a representative conclusion of the present work. Three materials were used in the experimentation phase, 7075-T6 Aluminum, 6061-T6 Aluminum and 1045 Steel. The following table shows some important characteristics of these materials that lead to its selection.

	7075-T6 Aluminum	6061-T6 Aluminum	1045 Steel
Composition	Si: 0.40	Si: 0.721	C: 0.43-0.50
	Fe: 0.50	Fe Cu: 0.408	Mn: 0.60-0.90
	Cu: 1.2-2.0	Mn: 0.109	P max: 0.040
	Mn: 0.30	Mg: 0.937	S max: 0.050
	Mg: 2.1-2.9	Zn: 0.176	Si max: 0.20-0.35
	Zn: 5.1-6.1	Ti: 0.051	
	Ti: Zr0.20	Pb: 0.002	
	Cr: 0.18-0.28	Cr: 0.072	
Brinell Hardness	145	88	220

Table 4. Composition of the materials used in the experimentation.

It was intended to use different materials which covered a wide range of hardness, in this case, Brinell Hardness from 88 to 220 will show its effect in surface quality and sensorial acquisition. Appendix E shows details of the material properties.

4.4 Tool Selection

Basing the experimentation phase on variations on material and as consequence on its hardness, made difficult to remain constant the rest of

machining parameters such as machining tool, range of spindle velocities, depth of cut, feed rates, etc. Even though it looked impossible, most of these parameters depended directly from the tool selected for each material, then, careful tool selection helped to remain in equal condition as possible all the experiments. A unique tool manufacturer was selected for all materials to avoid differences in the results due to the final tool treating.

The relation of the material with its tool is as follow:

- 7075-T6 Aluminum Tool Model: 30.6215
- 6061-T6 Aluminum Tool Model: 30.6215
- 1045 Steel Tool Model: 30.6472

Table 5 shows the model of each Karnasch tool used for the three materials tested, as its characteristics according to the manufacturer catalog.

Tool Model	Tool Specifications	Recommended Process Parameters
30.6215	Diameter = 12 mm	Cutting Velocities m/min = 300-1000
	Radius = 1.5 mm	Feed per tooth mm = 0.08 – 0.18
	Tooth number = 2	RPM Range = 8000 - 26000
30.6472	Diameter = 10 mm	Cutting Velocities m/min = 300 – 400
	Radius = 1.5 mm	Feed per tooth mm = 0.065
	Tooth number = 2	RPM Range = 12000 - 16000

Table 5. Tool characteristics and recommended process parameters.

Note: The RPM range was obtained according to equation 2.

$$S = \frac{Vcx1000}{dx\pi} \qquad \text{(Equation 2)}$$

where:

S = Spindle Velocity

Vc = Cutting Velocity

d = Tool Diameter

As the table shows, the diameter of the tool had to be changed for its use in steel, in order to maintain the radius of the tool constant. The radius of the tool is known to have a greater effect in the surface roughness than the diameter, this way the changes on surface quality from one material to another will not be greatly affected by the tool characteristics. More information from the tools used may be found in appendix F.

4.5 Machining Parameter Selection

A key issue to ensure representative results in the experimentation phase is machining parameter selection. Ranges from every parameter must be selected to avoid getting out of the limits permitted by the tool, the machine and the material. The stability lobes were an important tool that helped to choose the correct machining parameters, avoiding the influence of the machine static vibrations in the result. The stability lobes are explained in the next section.

Three machining parameters had to be defined for the experimentation phase: spindle speed (*S*), feed rate (*Vf*) and depth of cut (*ap*). Each of these parameter is greatly influenced by the tool used and the material machined. In the case of the spindle speed, it was consulted the tool catalog in order to cover all the range of possible velocities. As expected, the tool used for aluminum (30.6215) covers a wider range of speeds, than the one used in steel (30.6472). Table 6 and Table 7 show the ranges used for each parameter mentioned, in both materials.

Material:7075-T6 and 6061-T6 Aluminum	***Range***
Spindle Speed	8000 – 22000 rpm
Feed Rate	Calculated with: Vf = fz x S x Z
Depth of Cut	1.5, 2.5 and 3.5 mm

Note: fz (feed per tooth) was obtained from the catalog, using both limits of 0.08 mm/tooth and 0.18 mm/tooth. Z (number of teeth) of the tool is 2.

Table 6. Ranges in the parameters used for machining in aluminum.

Material:1045 Steel	***Range***
Spindle Speed	11000 – 16000 rpm
Feed Rate	Calculated with: Vf = fz x S x Z
Depth of Cut	0.2, 0.4, 0.6 and 0.8 mm

Note: fz (feed per tooth) was obtained from the catalog, using 0.065 mm/tooth. Z (number of teeth) of the tool is 2.

Table 7. Ranges in the parameters used for machining in 1045 Steel.

For aluminum the increments of the spindle speed in each sample is 1000 rpm, for steel each sample was machined with an increment of 500 rpm. Grooves in the material were made to get each sample of the experimentation. Parameters remained constant in each groove. Table 8 and Table 9 shows the feed rates used for all cases.

For fz = 0.08 mm/tooth (Aluminum)			For fz = 0.18 mm/tooth (Aluminum)	
RPM	Vf (mm/min)		RPM	Vf (mm/min)
8000	1280		8000	2880
9000	1440		9000	3240
10000	1600		10000	3600
11000	1760		11000	3960
12000	1920		12000	4320
13000	2080		13000	4680
14000	2240		14000	5040
15000	2400		15000	5400
16000	2560		16000	5760
17000	2720		17000	6120
18000	2880		18000	6480
19000	3040		19000	6840
20000	3200		20000	7200
21000	3360		21000	7560
22000	3520		22000	7920

Table 8. Feed Rate values used for aluminum and the 30.6215 tool

For fz = 0.065 mm/tooth (Steel)	
RPM	Vf (mm/min)
11000	1430
12000	1560

13000	1690
14000	1820
15000	1950
16000	2080

Table 9. Feed Rate values used for steel and the 30.6472 tool.

The stability lobe test was used for the depth of cut selection. Generally this method helps avoiding entering chatter zones during machining by selecting a depth of cut that produces stable machining conditions. Appendix G explains more detailed the effect of this test in the machining parameter selection.

4.6 Surface Roughness Measure

After the machining of parts follows the measuring of surface roughness. The specific machining process selected for experimentation is grooving. As Figure 15 shows, several 100 x 180 x 25 mm blocks were used for testing. In these blocks grooves were made keeping constant the machining parameters in each one. Each groove corresponds to a specific spindle speed, depth of cut and feed rate.

Figure 15. Photo of the grooving process used for experimentation.

The width of the groove depends on the diameter of the tool, 12 mm in aluminum and 8 mm in steel. A 2 mm width wall was kept between each groove, to

eliminate vibrations due to a thin wall. The numeric control program for machining was made parametric to make changes simple, it can be seen in Appendix H.

After machining a stylus profilometer was used to measure the surface roughness in the plane of the groove. Because of the anatomy of the profilometer, measurements had to be done 40 mm after the groove ends, in the sense of machining. Figure 16 shows the way the measurement was taken. A 5 mm surface was measured, obtaining the average of all data taken (Ra)

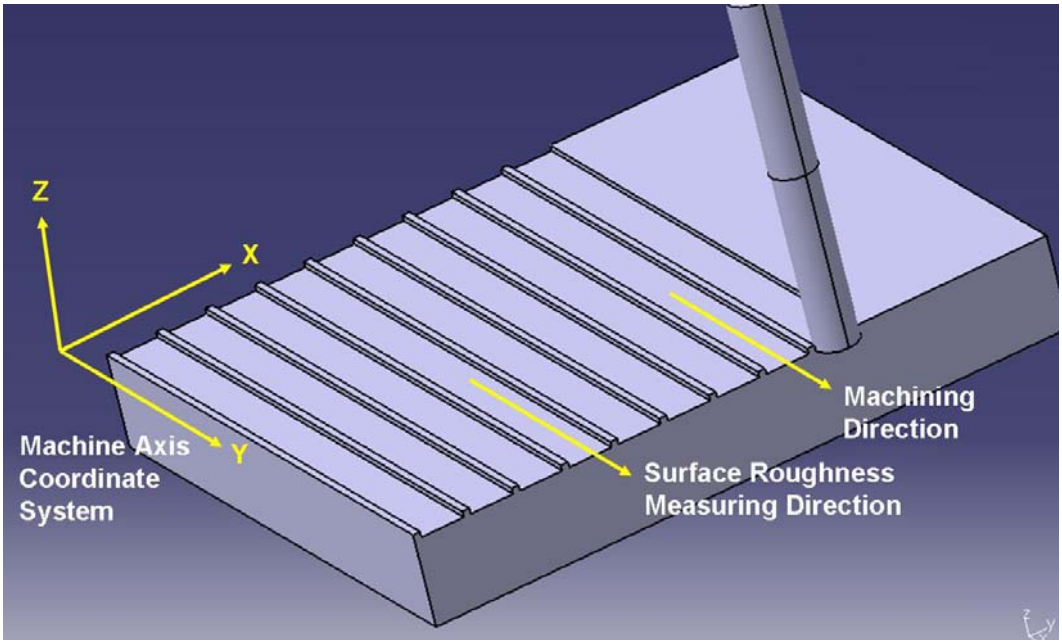

Figure 16. Measurement method description.

Chapter 5: Data Analysis

5.1 Introduction

This chapter shows the overall approach used for data analysis. Detailed tables and procedures are included in appendix I.

5.2 Experimental Results

The software application developed provided the capability of saving all data acquired for further analysis. The processing of the information was time consuming due to the size of the files. Two files are saved: a) the information of acoustic emission sensors and information from the MPI and b) the data from the accelerometers. Two files are obtained from each block machined. Then each file has information from a specific depth of cut and all the grooves made on the block. After acquiring both files they are joined in one table using a spreadsheet. The software is made considering that it has to save the same number of data in both files. Once all data joined in a table an average value of all parameters in each groove was obtained. Table 10 shows an example of a fragment of the table constructed with all data obtained.

Index	AE 1	AE 2	S	Vf	ap	a_x	a_y	a_z	…	…
22	206.04	26.55	8000	2880	1.5	214.018	194.362	26.4078	…	…
23	209.34	22.57	7999	2880	1.5	269.490	240.929	26.5423	…	…
24	205.18	23.40	7999	2880	1.5	302.068	277.816	26.6098	…	…
…	…	…	…	…	…	…	…	…	…	…

Table 10. Example of a table made from all data acquired from one block.

After getting the average of each groove made, from each sensor a table of averages was prepared. An example of such table is shown in Table 11. This table includes the surface roughness measured from the blocks. These tables were then

used to graph the results and compare vibrations with the surface roughness obtained.

S	a_x	a_y	a_z	Ra
8000	335.40	288.14	267.45	1.36
9000	430.12	330.35	262.16	1.61
10000	505.17	400.82	263.34	2.02
11000	436.41	377.22	260.00	1.90
12000	617.45	422.56	266.32	2.00
13000	568.87	405.77	256.90	2.17
14000	478.10	367.65	249.75	1.54
15000	421.96	409.78	270.28	1.80
16000	543.67	435.34	253.99	1.91
17000	458.52	362.03	253.18	1.61
18000	385.15	355.45	245.69	1.57
19000	363.78	340.83	254.69	2.32
20000	364.62	324.54	270.60	2.34
21000	444.24	379.19	277.13	2.39
22000	342.35	367.29	272.51	2.36

Table 11. Final table of averages.

As it may be seen in the previous table is obtained only one final value of vibration of each sensor and of Ra, corresponding to a spindle speed, which was maintained constant through the length of the groove.

5.3 Model Type Selection

Selecting the type of model that best fit the data is not an easy task. Several statistical analysis must be done in order to reach the best model possible. Next methodology, Figure 17 shows the suggested steps that may be followed to reach such model.

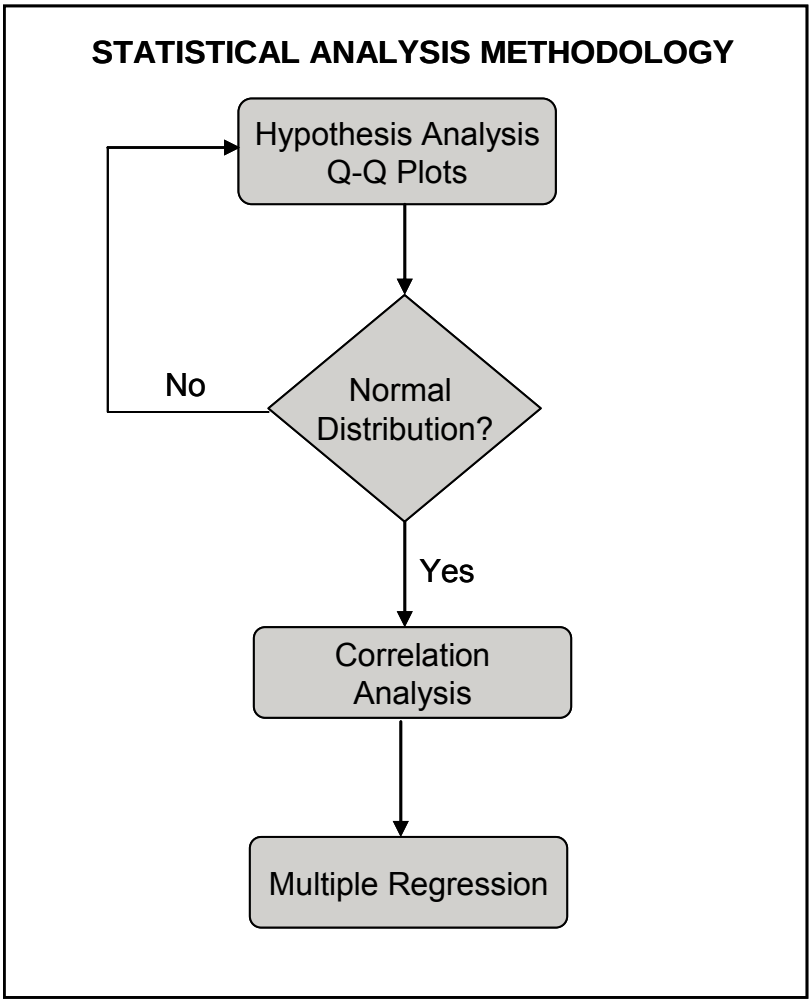

Figure 17. Statistical analysis methodology used to reach the best model to predict surface roughness.

Hypothesis analysis, Q-Q Plots refers to a hypothesis analysis to know if there is statistical evidence that the data from each population follows a certain distribution. In our case, it is important that the data follows a normal distribution because the steps that come next infer that data comes from this distribution. Next, the correlation analysis helps to determine if the factor that are intended to be part

of the model have a linear correlation with surface roughness, if not it is important to consider that the factor must be of a higher order to be influent or important in the prediction.

Finally, several multiple regression models are obtained an evaluated with its prediction capability and only the important parameters are the ones that remain in the model, making it more simple.

Chapter 6: Surface Roughness Models

6.1 Introduction

Final results are presented in this chapter. Surface roughness prediction models with their corresponding coefficients are shown. As explained in the last chapter two models are obtained for each material. The first parameters and their interactions will form a model which predicts the resultant 3 axis vibrations. Then, a second model will include the force parameters and the predicted vibration to predict the final surface roughness. For more information about the application of the regression analysis to the data, and the results of such analysis (ANOVA tables) appendix I should be consulted.

6.2 Regression Data Analysis

There are several factors resulting from the regression data analysis that are important at the time of deciding which model is more precise. The most important factor is the R Square parameter. This parameter offers a percentage of efficiency at which the model is capable of correctly predicting the surface roughness. The coefficients of the ANOVA table, which indicate the value that must be assigned to the β values of the model. It could have a negative sign, which means that has an inverse influence. In the same table there is a column assigned as P-Value, which is a statistical parameter that indicates the significance of the factors in the whole model. This parameter determines which parameter should be deleted from the model, due to its low contribution in the prediction.

An example of a regression analysis result is shown in Figure 18. The value of P-Value is given to show the correlation between all the parameters with the response. A value near cero means that the correlation is high, if it is greater than 0.05 the factor is considered with no significance. The column at the left of the table shows all the parameters being included in the model.

SUMMARY OUTPUT

Regression Statistics	
Multiple R	0.943509799
R Square	0.89021074
Adjusted R Square	0.880523453
Standard Error	0.234159999
Observations	75

ANOVA

	df	*SS*	*MS*	*F*	*Significance F*
Regression	6	30.23202941	5.038671568	91.89473623	1.20343E-30
Residual	68	3.728501552	0.054830905		
Total	74	33.96053096			

	Coefficients	*Standard Error*	*t Stat*	*P-value*	*Lower 95%*
Intercept	0.187538603	0.28136299	0.666536148	0.507323702	-0.37391217
DC	-0.156689326	0.047486059	-3.299691072	0.00154316	-0.251446226
S	-6.46305E-05	8.13461E-06	-7.945131448	2.75653E-11	-8.08629E-05
FR	0.000319417	2.6361E-05	12.11703065	1.19812E-18	0.000266815
AccX	0.000302411	0.000599014	0.504848591	0.615297416	-0.000892901
AccY	0.001331186	0.001124105	1.184218659	0.24044938	-0.000911929
AccZ	0.019964249	0.004732634	4.218421916	7.44866E-05	0.010520429

Figure 18. Example of a regression calculus results.

6.3 Model Results

As mentioned in earlier chapters, three materials were used for testing, 7075-T6, 6061-T6 Aluminum and 1045 Steel. As seen in the introduction of this chapter, models will be presented for each material. All results (tables, graphs and models) are shown in appendix I.

6.4 7075-T6 Aluminum Model

90 experiments were conducted in 7075-T6 aluminum. After several multiple regression analysis the next final model to predict the resultant acceleration was obtained. The resultant acceleration signal used in all materials is given as the square root of the sum of squares of the signals of the X, Y and Z accelerometer. Due to the nature of the process, the most relevant signals were obtained from the Y and Z axis. The X axis signal was less significant, because the grooving was made perpendicular to this axis.

$$Acc\,\mathrm{Re}\,s = -1556.44 + (0.448764 * S) + (-2.89473E-05 * S^2) + (5.86818E-10 * S^3)$$

The model is able to predict the resultant acceleration of machined parts with a 50% of effectiveness (Adjusted R-Square in the ANOVA table). It is evident that the spindle speed plays an important role in this prediction.

Figure 19, Figure 20 and Figure 21 show how the predicted resultant acceleration follows the real one at each depth of cut.

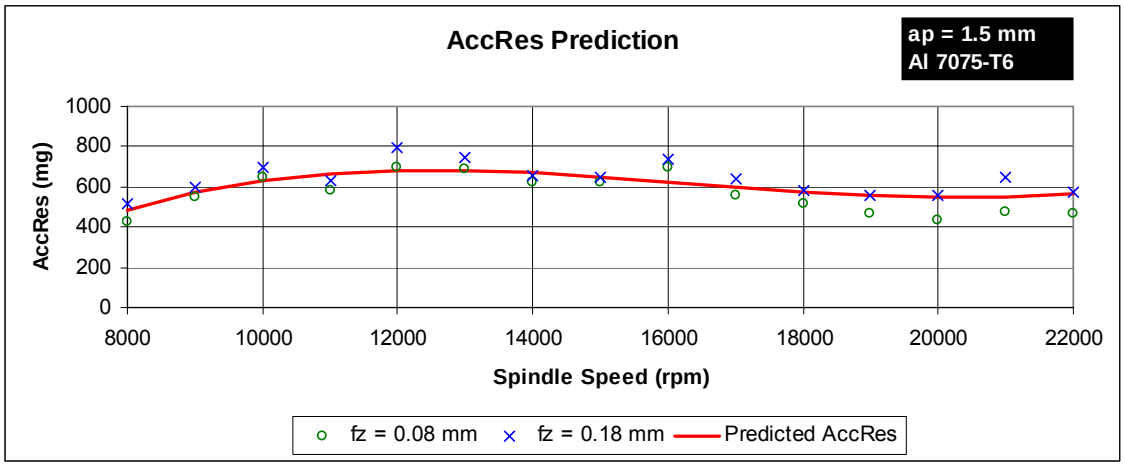

Figure 19. Resultant acceleration model response for 7075-T6 aluminum and ap = 1.5 mm.

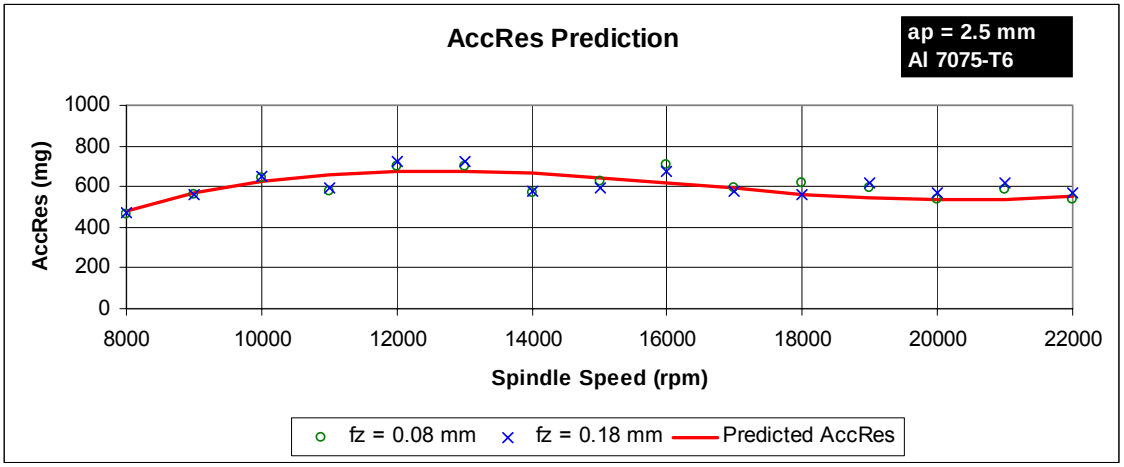

Figure 20. Resultant acceleration model response for 7075-T6 aluminum and ap = 2.5 mm.

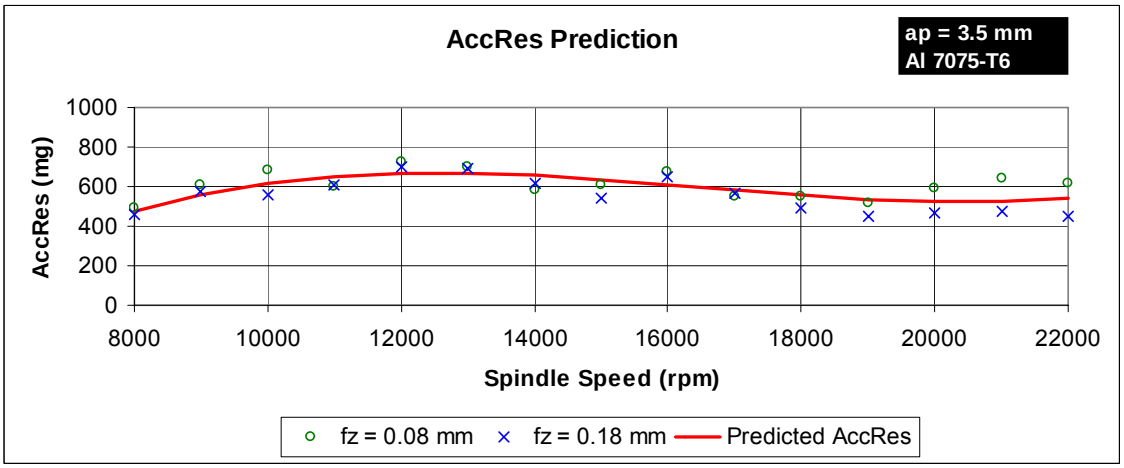

Figure 21. Resultant acceleration model response for 7075-T6 aluminum and ap = 3.5 mm.

Two other models were obtained to predict the final surface roughness of the parts machined in 7075-T6 aluminum. One corresponds to a feed per tooth of 0.08 mm/t and the other one to 0.18 mm/t. The reason to separate such models is that there is a big difference between the measured surface roughness of both values of fz. Such difference can be seen in Figure 22.

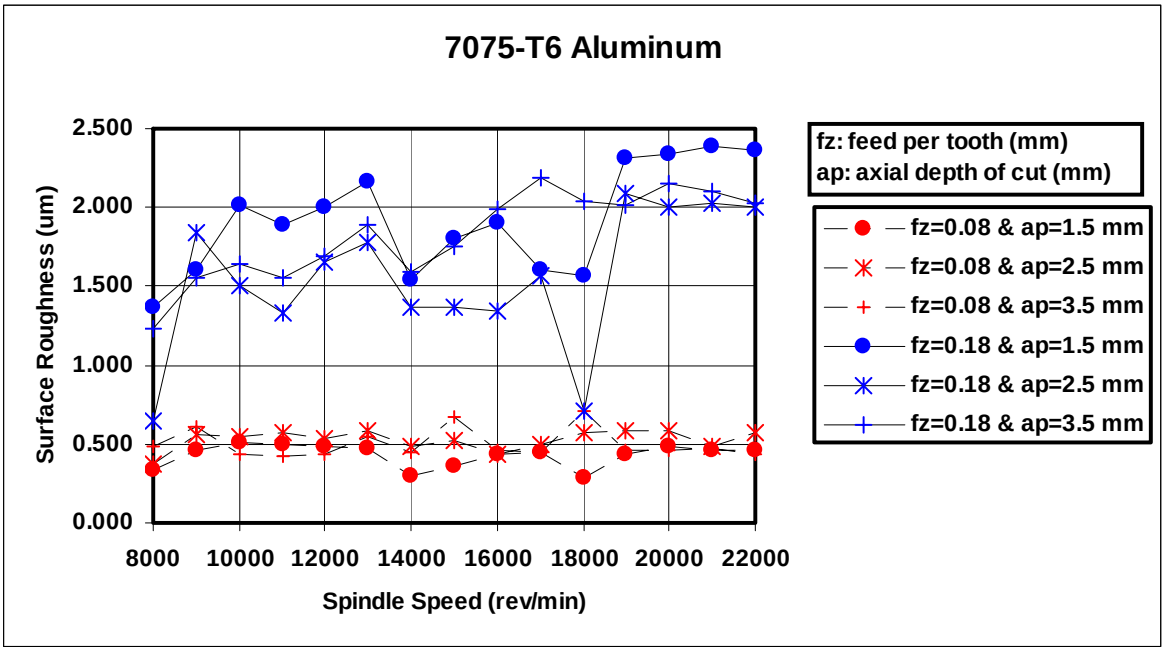

Figure 22. Feed per tooth influence on the measured surface roughness.

The model for fz = 0.08 resulted with very low precision, then it will not be shown in this chapter, and the model for fz = 0.18 mm/t has the following form.

$$Ra = -2.03638 + (0.0005969 * Vf) + (0.00525252 * Acc\,\mathrm{Re}\,s) - (8.00655E-07 * Vf * Acc\,\mathrm{Re}\,s)$$

Both summary outputs are shown in appendix I. For the first model we have an efficiency of 6%. With this data we assume that the model is not capable of making any good surface roughness prediction. In Figure 22 we can see that the values of Ra with fz of 0.08 mm/t does not change considerably with different values of spindle speed. This may be one of the reasons why the efficiency of the model resulted very low.

In the other case the model for fz = 0.18 mm/t resulted with an efficiency in prediction of 38%, much higher than the first model. Even though it is a very low value, the next figures show both models prediction capabilities comparing the measured against the predicted value.

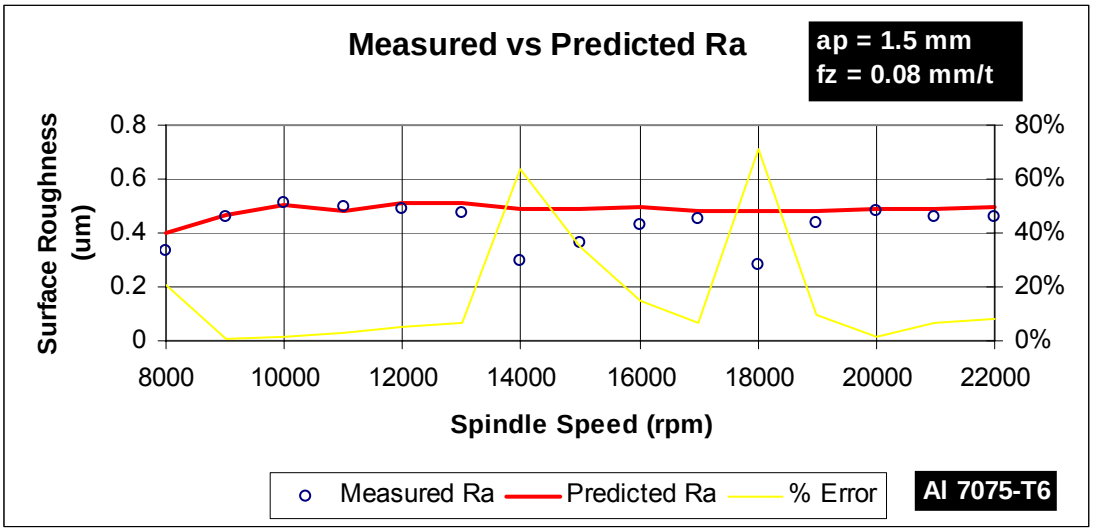

Figure 23. Measured vs Predicted Ra for 7075-T6 aluminum at an ap of 1.5 mm and 0.08 mm/t of feed per tooth.

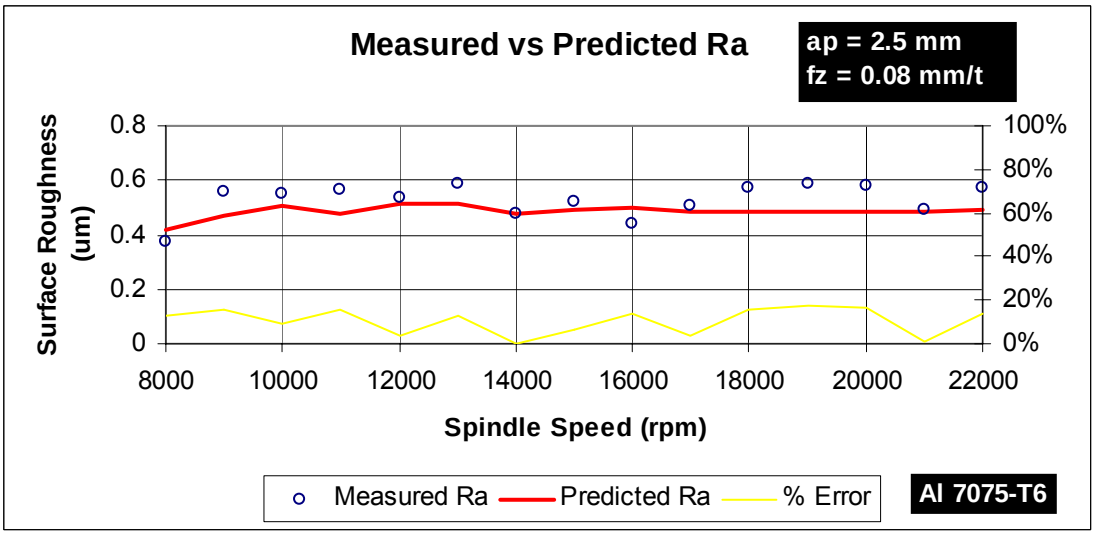

Figure 24. Measured vs Predicted Ra for 7075-T6 aluminum at an ap of 2.5 mm and 0.08 mm/t of feed per tooth.

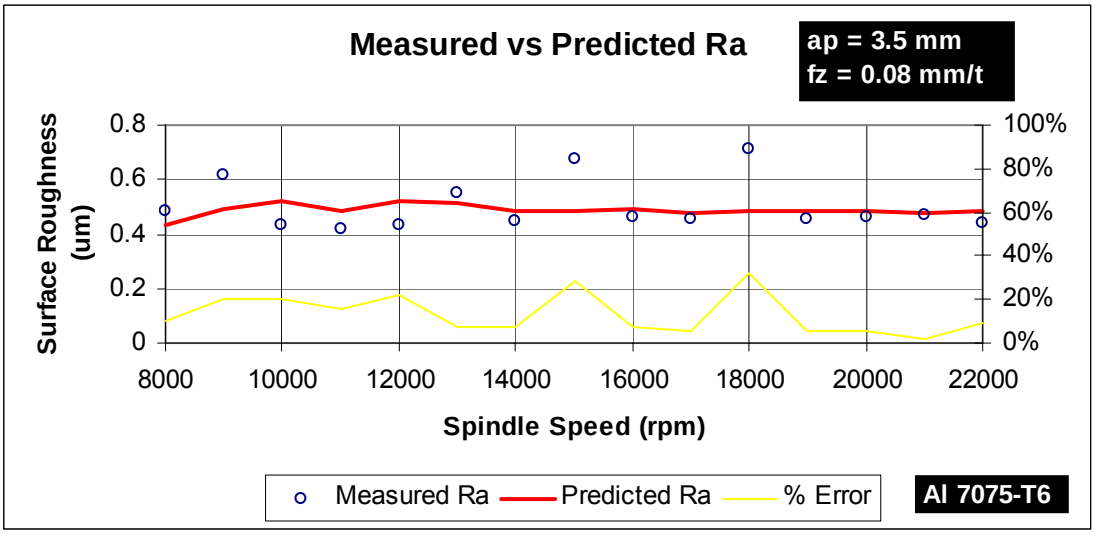

Figure 25. Measured vs Predicted Ra for 7075-T6 aluminum at an ap of 3.5 mm and 0.08 mm/t of feed per tooth.

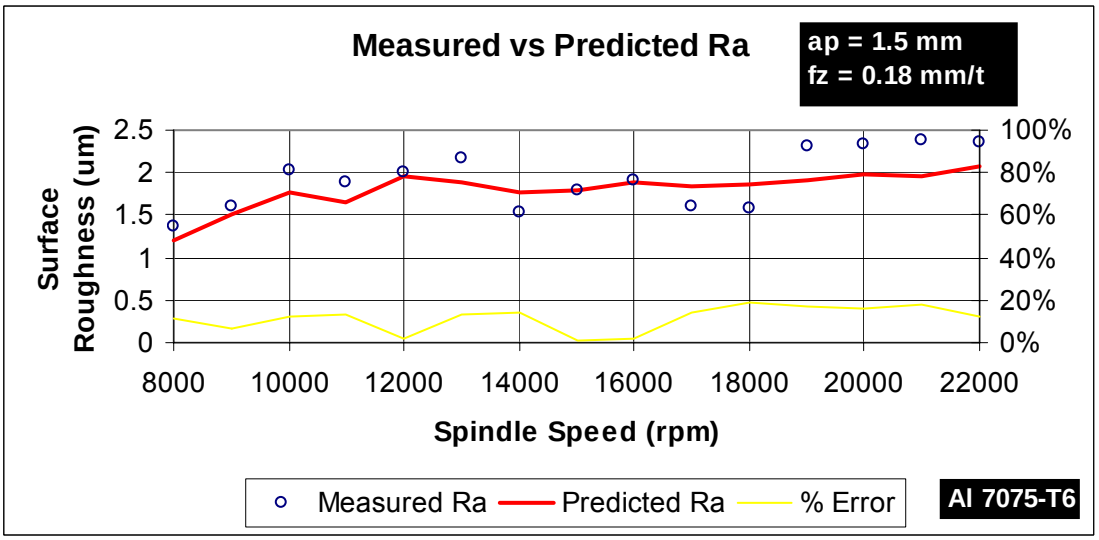

Figure 26. Measured vs Predicted Ra for 7075-T6 aluminum at an ap of 1.5 mm and 0.18 mm/t of feed per tooth.

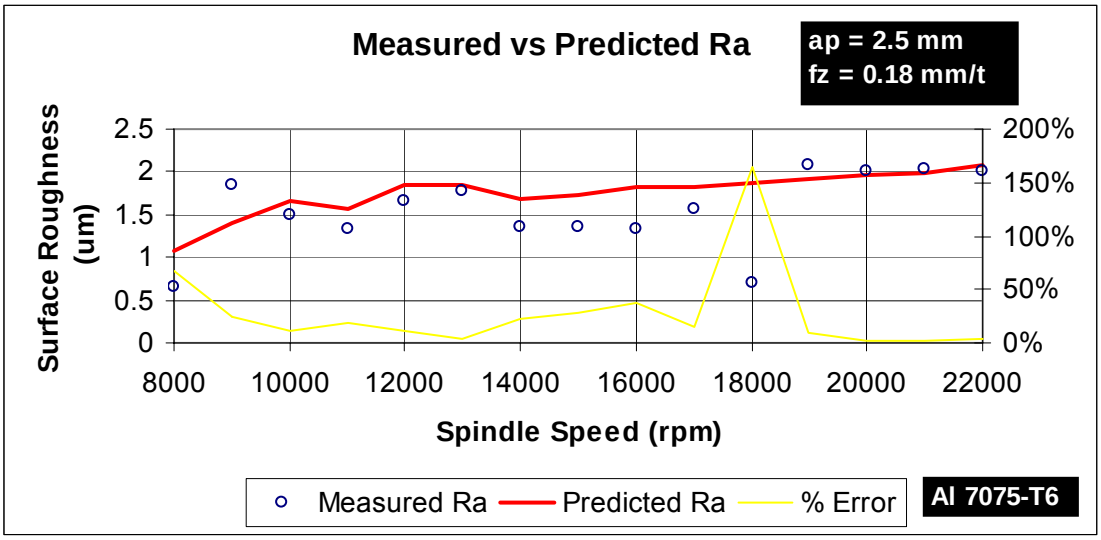

Figure 27. Measured vs Predicted Ra for 7075-T6 aluminum at an ap of 2.5 mm and 0.18 mm/t of feed per tooth.

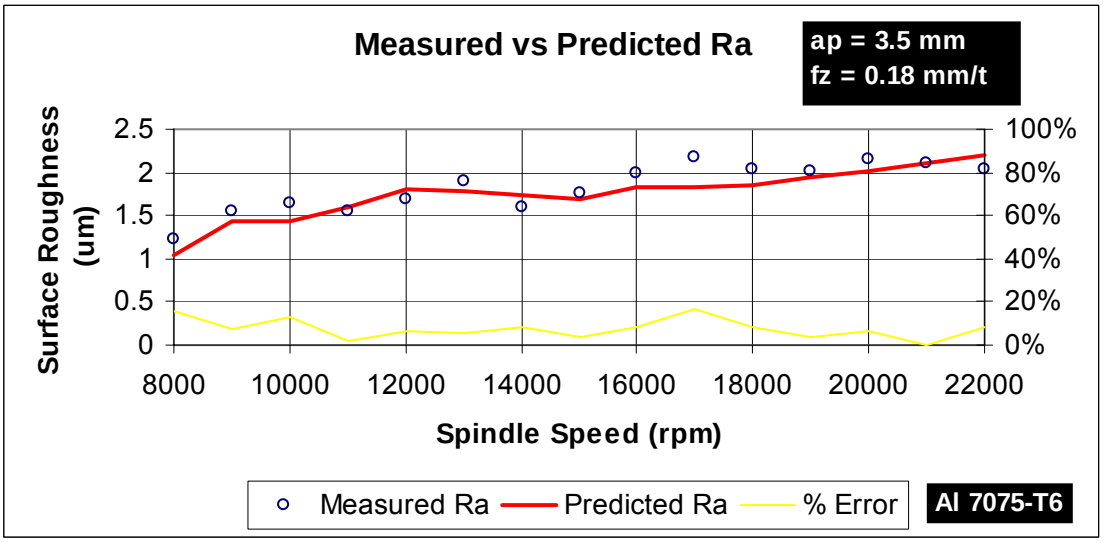

Figure 28. Measured vs Predicted Ra for 7075-T6 aluminum at an ap of 3.5 mm and 0.18 mm/t of feed per tooth.

6.5 6061-T6 Aluminum Model

A total of 90 tests were conducted in 6061-T6 aluminum (15 levels of spindle speed, 3 levels of depth of cut and 2 levels of feed per tooth). This aluminum is softer than the 7075-T6. After several multiple regression analysis the next final model was obtained to predict the resultant acceleration.

$$Acc\,\mathrm{Re}\,s = -2186.79161 - 2.1152E-13*(ap*S)^3 + (0.582462*S) - (3.7889E-05*S^2) + (7.7859E-10*S^3)$$

The model resulted able to predict 69% of the real acceleration. In this model it is more notorious the influence of the spindle speed jointly with the depth of cut. An example of how this model works is shown in Figure 30.

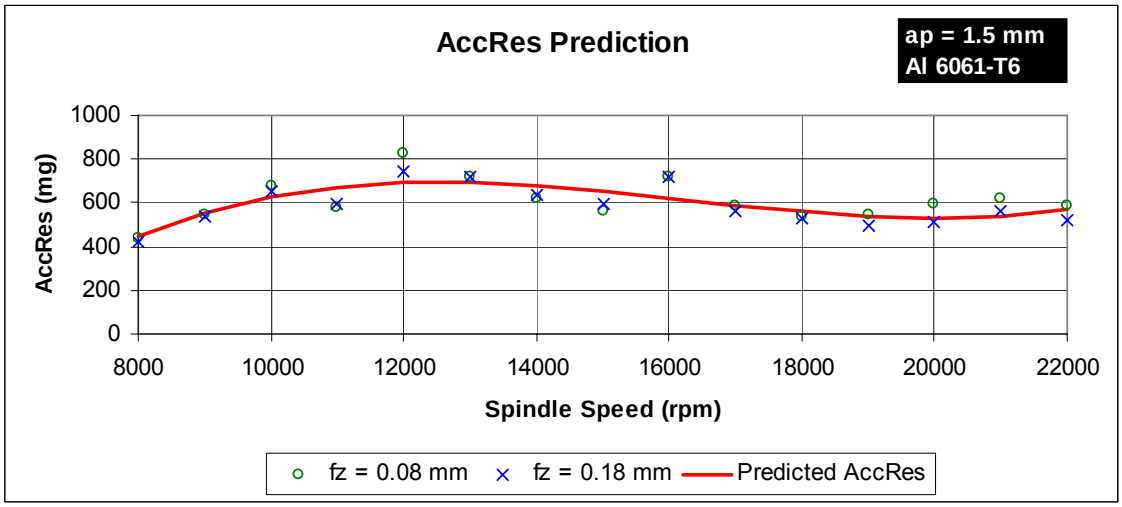

Figure 29. Resultant Acceleration prediction model response for 6061-T6 aluminum at an ap of 1.5 mm.

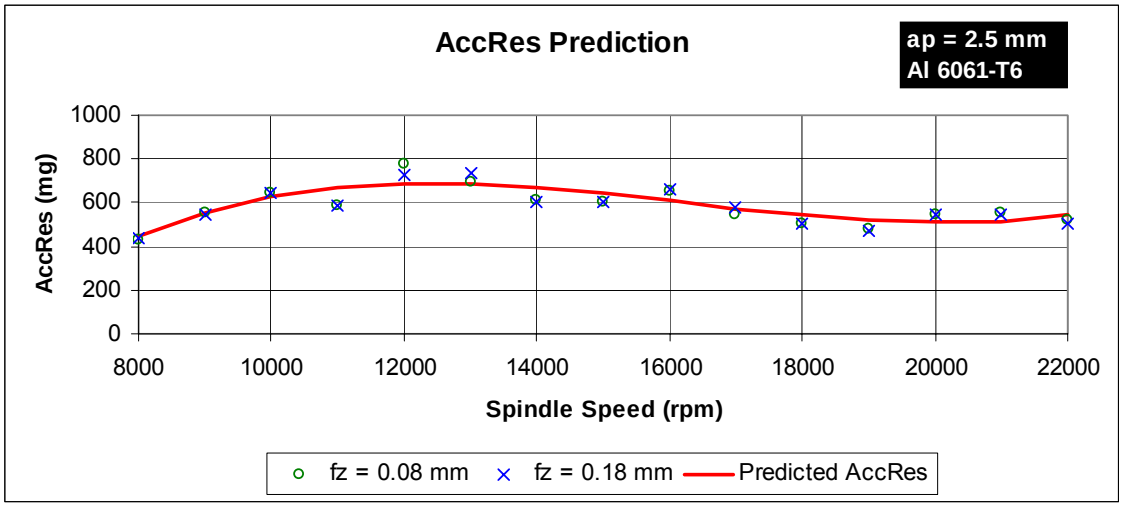

Figure 30. Resultant Acceleration prediction model response for 6061-T6 aluminum at an ap of 2.5 mm.

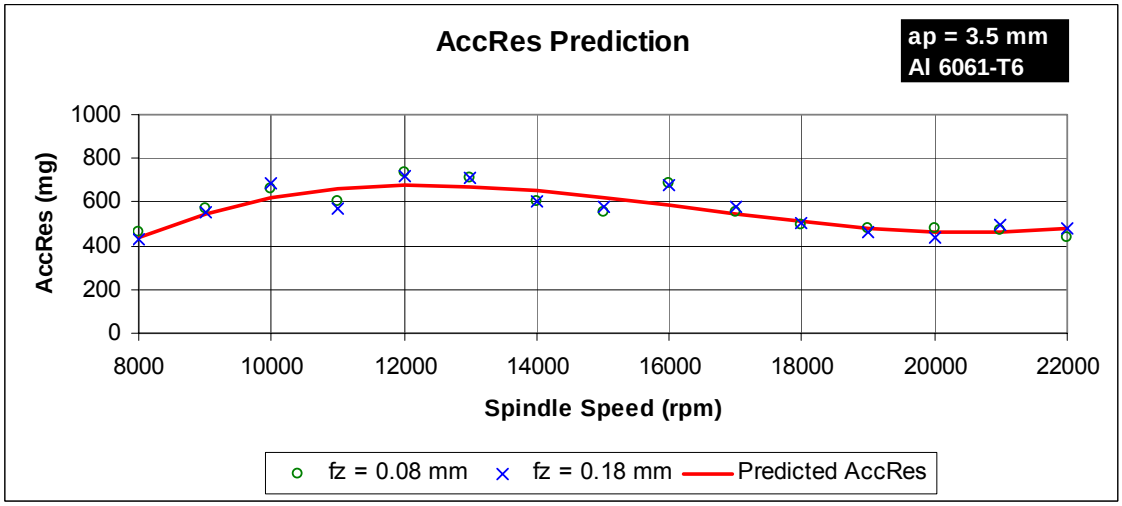

Figure 31. Resultant Acceleration prediction model response for 6061-T6 aluminum at an ap of 3.5 mm.

Two other models were obtained for this aluminum also. As in the 7075-T6 aluminum, the model for fz = 0.08 mm/t resulted very ineffective. Next equation corresponds to the model of fz = 0.18 mm/t.

$$Ra = -0.982117576 + (0.00049374 * Vf) + (0.003675913 * Acc\,\mathrm{Re}\,s) - (6.85312E-07 * Vf * Acc\,\mathrm{Re}\,s)$$

The model for fz = 0.08 mm/t works with an efficiency of 3 %, very low compared to the 46% of the higher feed per tooth model. Similar to the other

aluminum the differences between the Ra of both fz are huge. This can be seen in Figure 32.

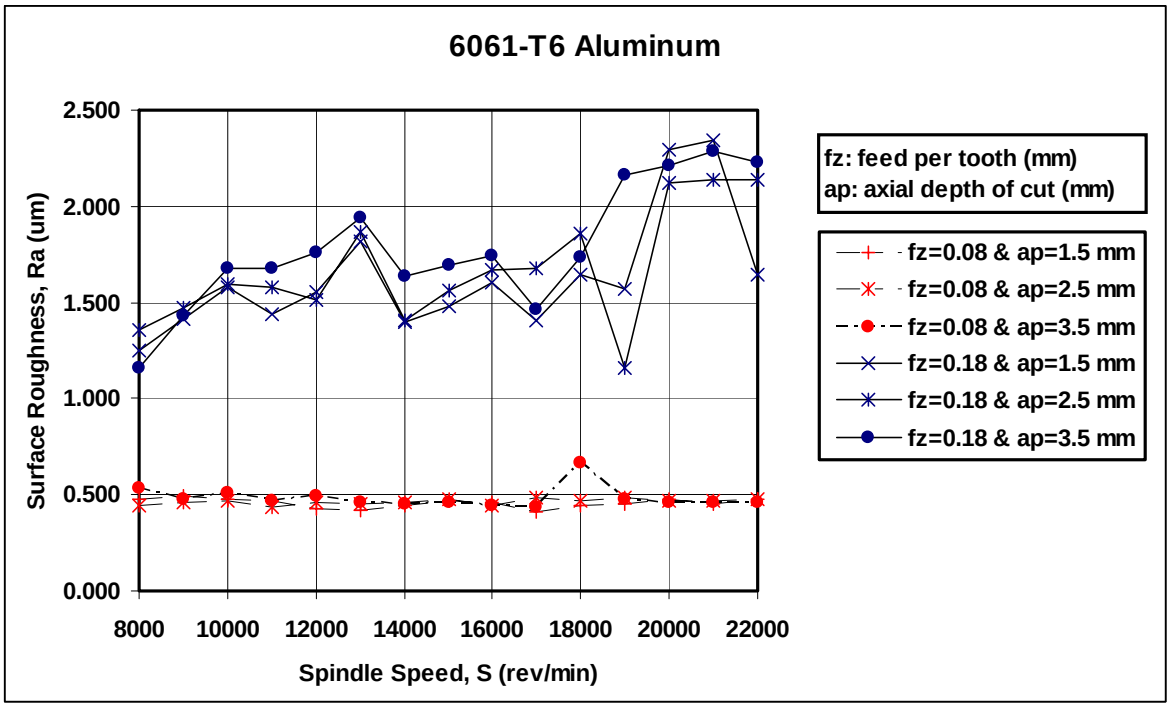

Figure 32. Feed per tooth influence on the measured surface roughness.

An example of how each model works comparing the real versus the predicted Ra is shown next.

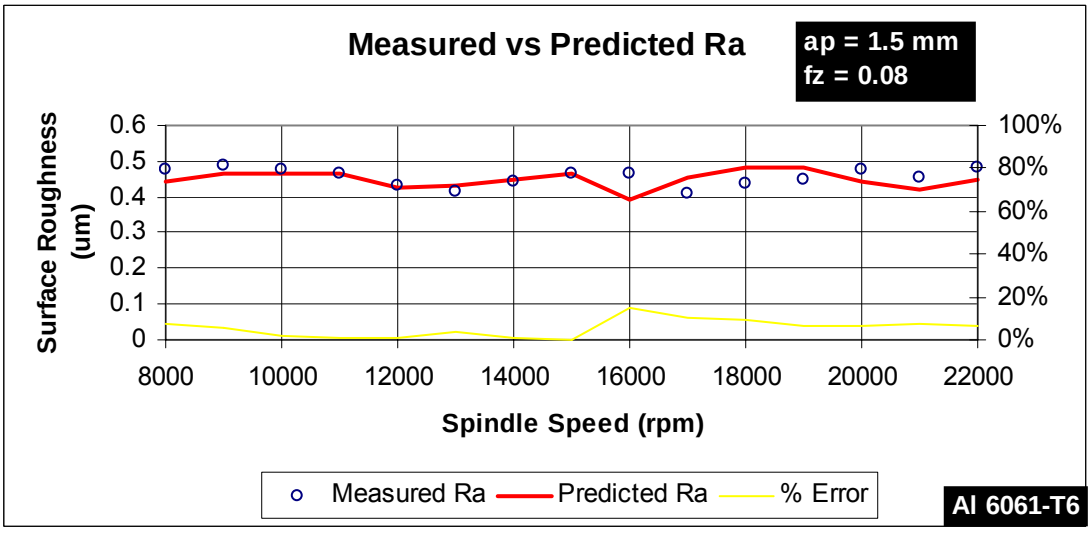

Figure 33. Measured vs Predicted Ra for 6061-T6 aluminum at an ap of 1.5 mm and 0.08 mm/t of feed per tooth.

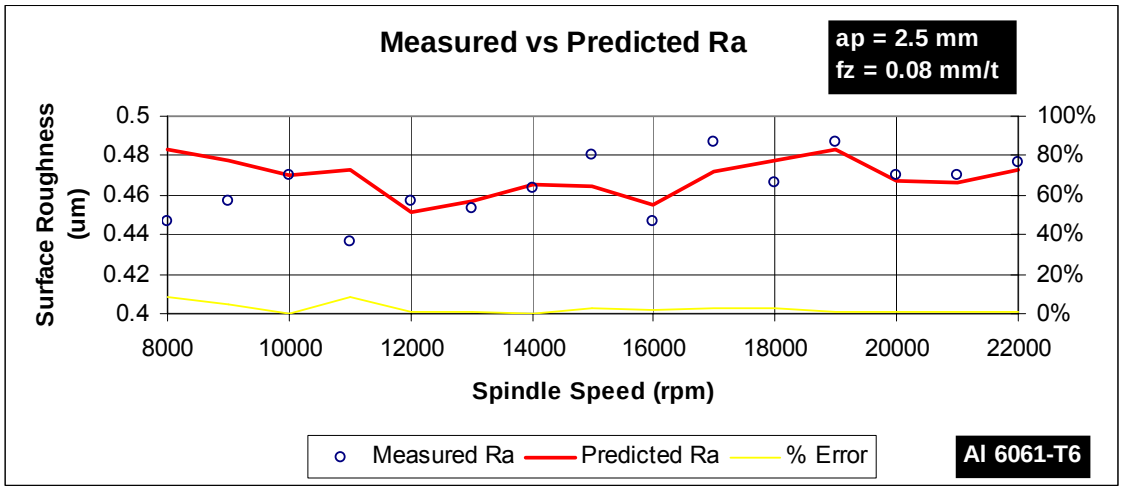

Figure 34. Measured vs Predicted Ra for 6061-T6 aluminum at an ap of 2.5 mm and 0.08 mm/t of feed per tooth.

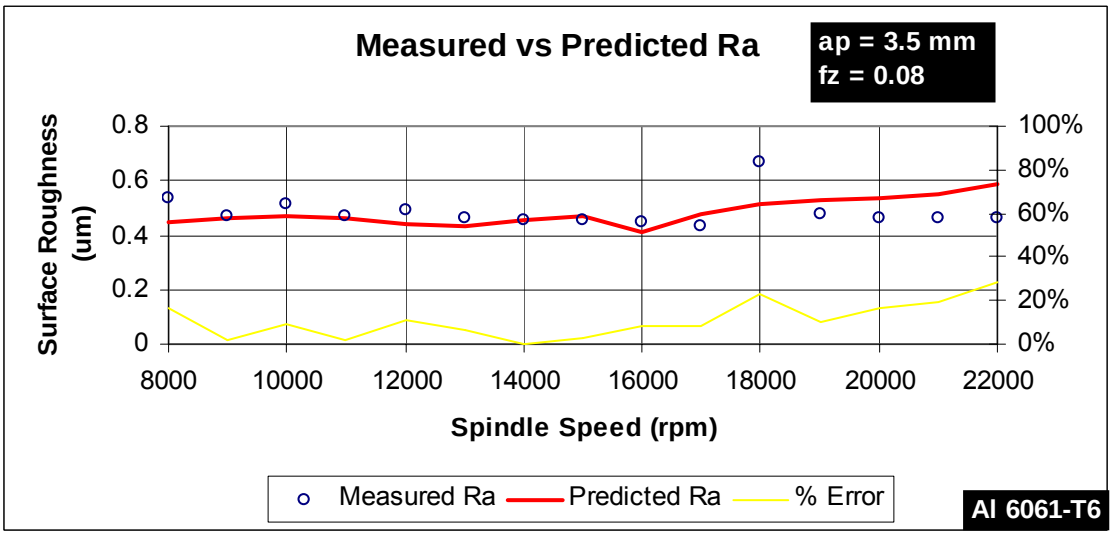

Figure 35. Measured vs Predicted Ra for 6061-T6 aluminum at an ap of 3.5 mm and 0.08 mm/t of feed per tooth.

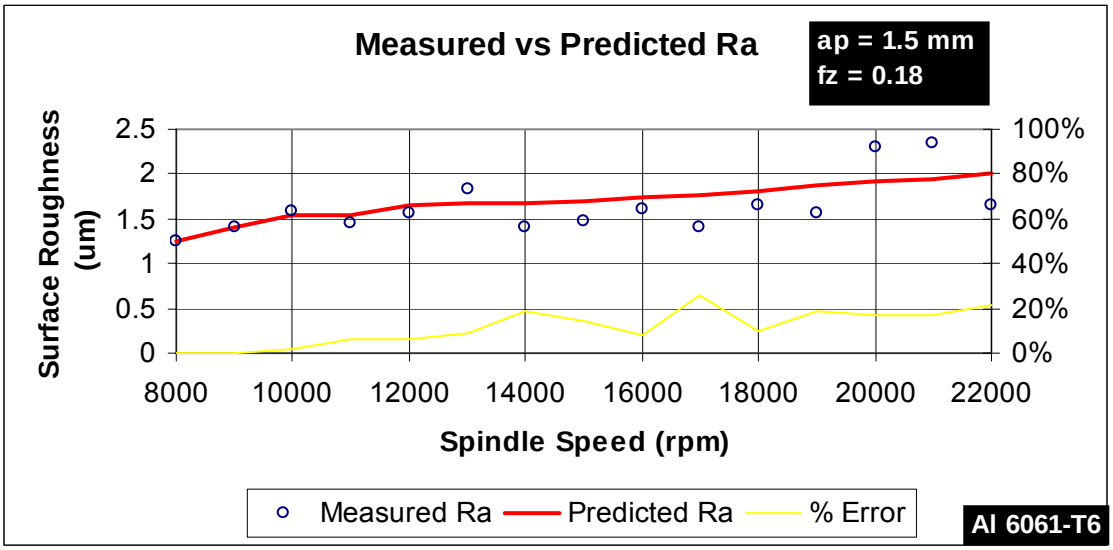

Figure 36. Measured vs Predicted Ra for 6061-T6 aluminum at an ap of 1.5 mm and 0.18 mm/t of feed per tooth.

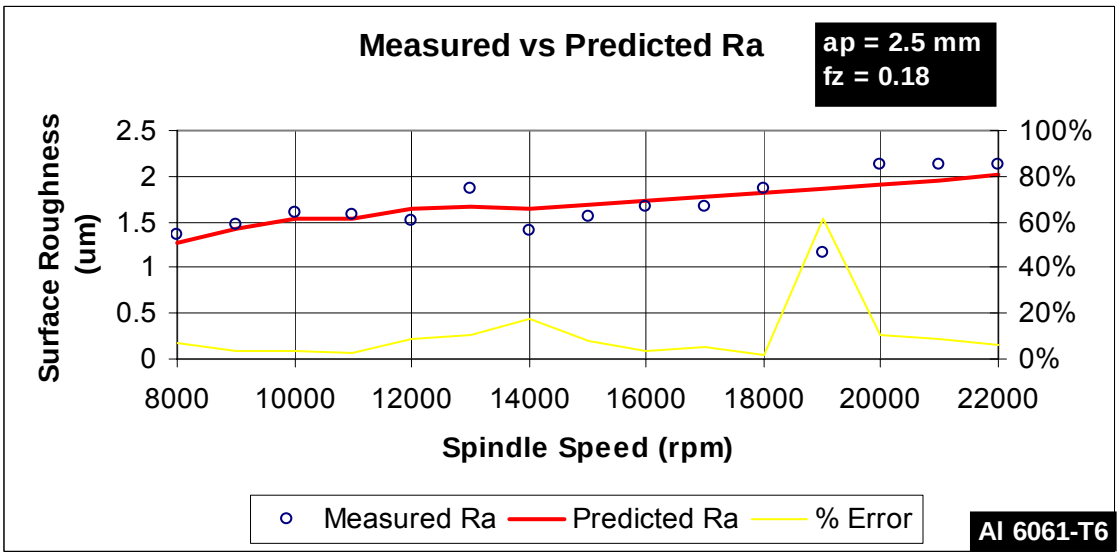

Figure 37. Measured vs Predicted Ra for 6061-T6 aluminum at an ap of 2.5 mm and 0.18 mm/t of feed per tooth.

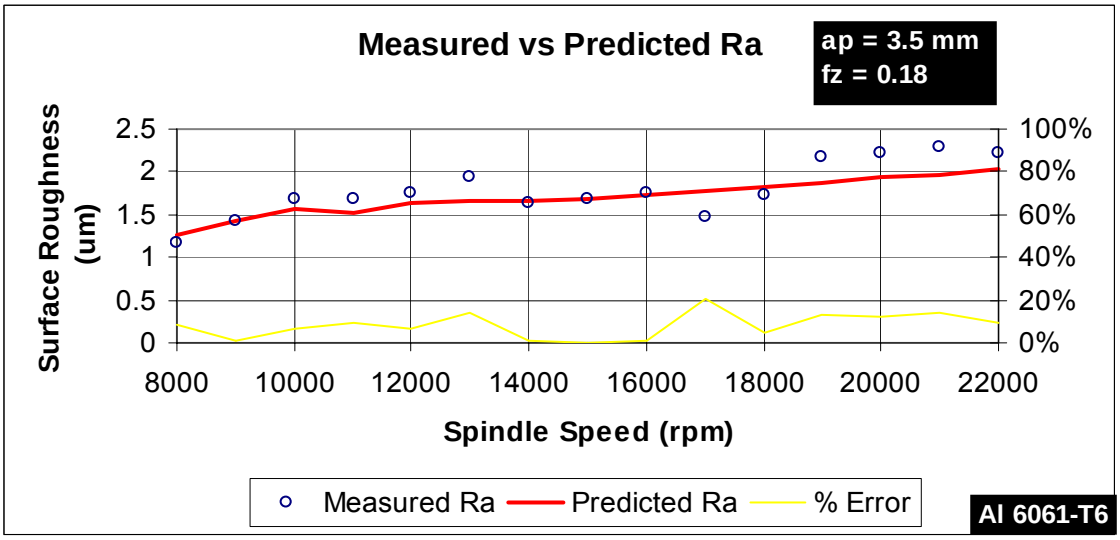

Figure 38. Measured vs Predicted Ra for 6061-T6 aluminum at an ap of 3.5 mm and 0.18 mm/t of feed per tooth.

6.6 1045 Steel Model

1045 Steel is a different case than aluminum. The tool used for this material had to be varied due to its hardness properties. It resulted impossible to continue with the same machining parameters. For this material it was used a fixed feed per tooth. This tool restriction permitted only 44 samples for testing levels and factors. The variation of spindle speed was made in increments of 500 rpm staring at 11000 up to 16000 rpm with depths pf cut of 0.2, 0.4, 0.6 and 0.8 mm. With regression analysis became difficult to get acceptable P-Values and as consequence, models with a very low effectiveness were obtained. The model to predict acceleration is shown below.

$$Acc\,\mathrm{Re}\,s = -30048.13 + (6.921679 * S) - (0.000515 * S^2) + (1.27E - 08 * S^3)$$

The model resulted with a low effectiveness of 52 %. Because only one fz was used. The behavior of this model is seen in Figure 39.

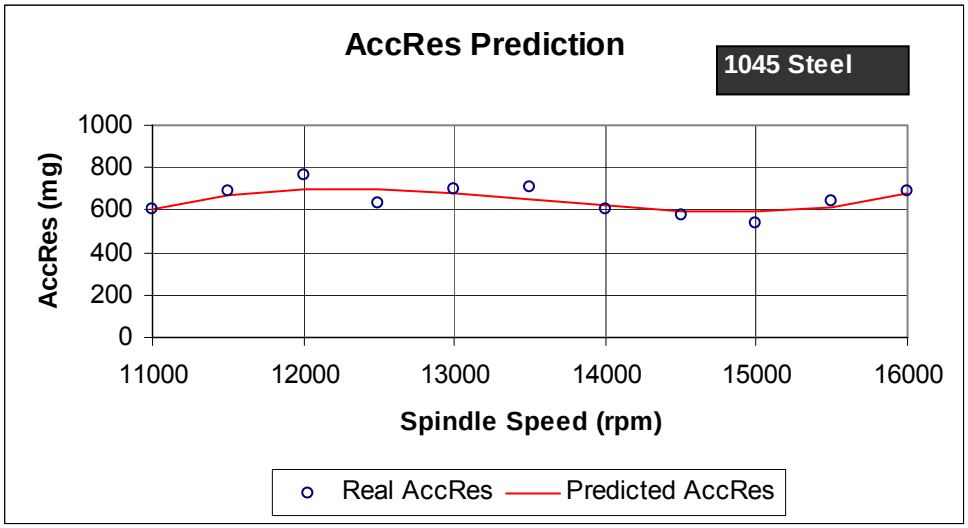

Figure 39. Resultant Acceleration prediction model response for 1045 Steel.

The influence of the spindle speed can be seen in the next graph, Figure 40, where the depth of cut does not follows any predictable behavior related to the surface roughness.

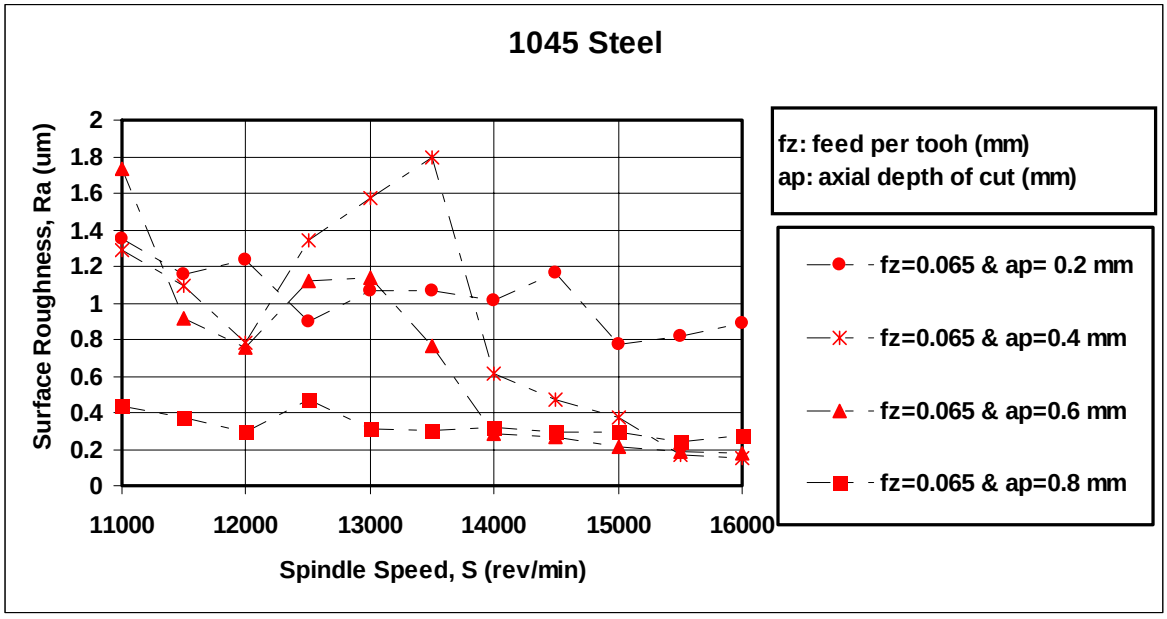

Figure 40. Axial depth influence in the measured surface roughness.

It can be seen that the effect of both axial depth of cut and spindle speed is inversely proportional to the resultant surface roughness value. This aspect influences directly in the capability of the model to predict Ra.

$$Ra = 2.847416667 - (0.001204779 * Vf)$$

This is a linear equation which may be useless to predict the surface roughness in steel. Its inaccuracy can be seen in the next figures.

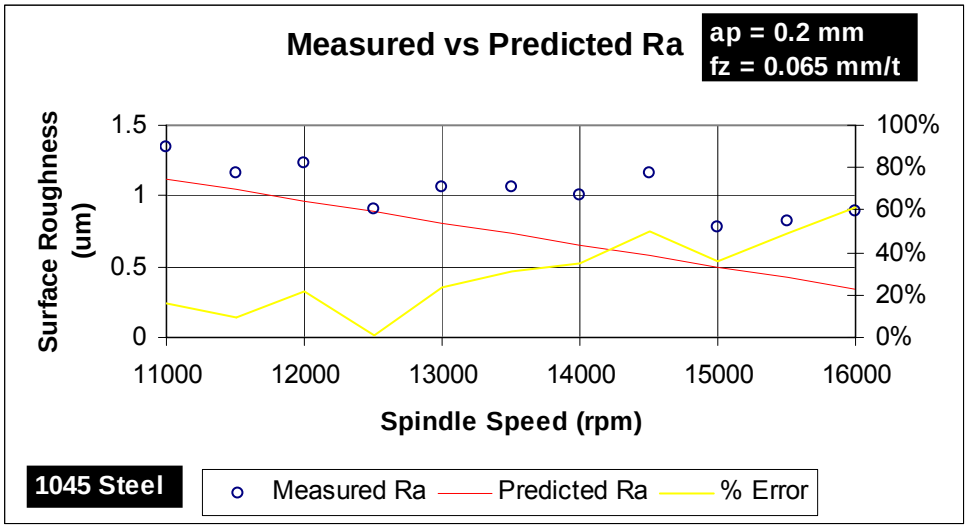

Figure 41. Measured vs Predicted Ra for 1045 Steel at an ap of 0.2 mm and 0.065 mm/t of feed per tooth.

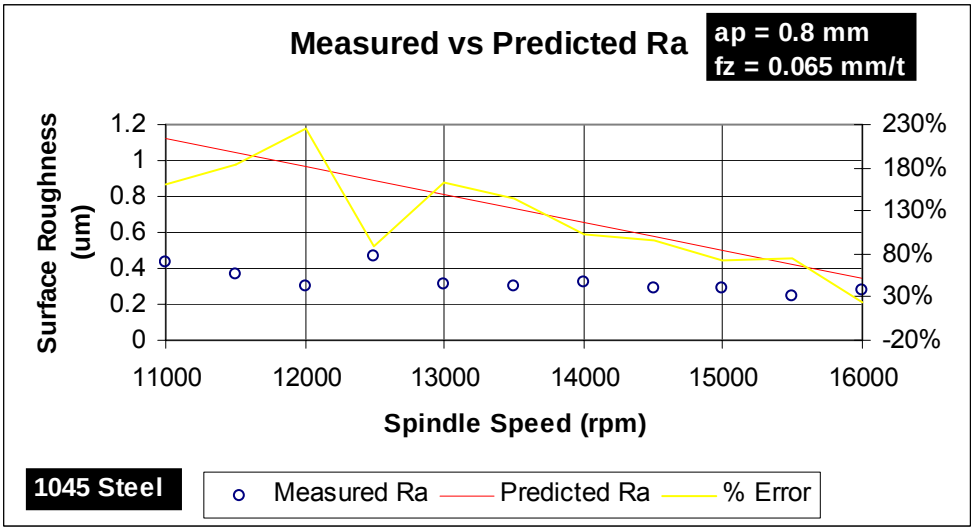

Figure 42. Measured vs Predicted Ra for 1045 steel at an ap of 0.8 mm and 0.065 mm/t of feed per tooth.

6.7 Theorical vs Real Surface Roughness

Different researchers have develop models to obtain theorical surface roughness values. Most of these models were developed through geometrical analysis and does not consider any process dynamics. In this section, two of these models will be compared with the results of surface roughness obtained in this study.

In his book, Boothroyd and Knight state that the *final surface roughness obtained during a practical machining operation may be considered as the sum of two independent effects:*

1. *The ideal surface roughness, which is a result of the geometry of the tool and the feed or feed speed.*
2. *The natural surface roughness, which is a result of the irregularities in the cutting operation.*

Taking into consideration that tools with round corner were used during experimentation, Boothroyd and Knight suggest that the following expression gives a very close value of the ideal surface roughness.

$$Ra = \frac{0.0321 f^2}{r_\varepsilon}$$

Where f is the feed and r_ε the corner radius. This expression does not consider the factors that commonly contribute to the natural surface roughness value. Some of these factors are:

1. The occurrence of chatter or vibrations of the machine tool.
2. Inaccuracies in machine tool movements such as the movement of the saddle on a lathe.
3. Irregularities in the feed mechanism.
4. Defects in the structure of the work material.
5. Discontinuous chip formation when machining brittle materials.
6. Tearing of the work material when ductile metals are cut at low cutting speeds.

7. Surface damage caused by such factors as chip flow [Boothroyd and Knight, 2006].

In the other hand there is also commonly an expression given to calculate the theorical surface roughness from the tool manufacturer. In this study, all tools used were Karnasch models. This way, we have the following expression given from the tool manufacturer.

$$R_{th} = \frac{d_1}{2} - \sqrt{\frac{d_1^{\,2} - b_r^{\,2}}{4}}$$

Where d_1 is the cutter diameter and b_r is the feed per tooth. It is important to notice that this expression gives de ideal R_{max} which is bigger than R_a.

Once both expression are shown, next graphs show the measured (natural + ideal) surface roughness compared with both ideal models just explained.

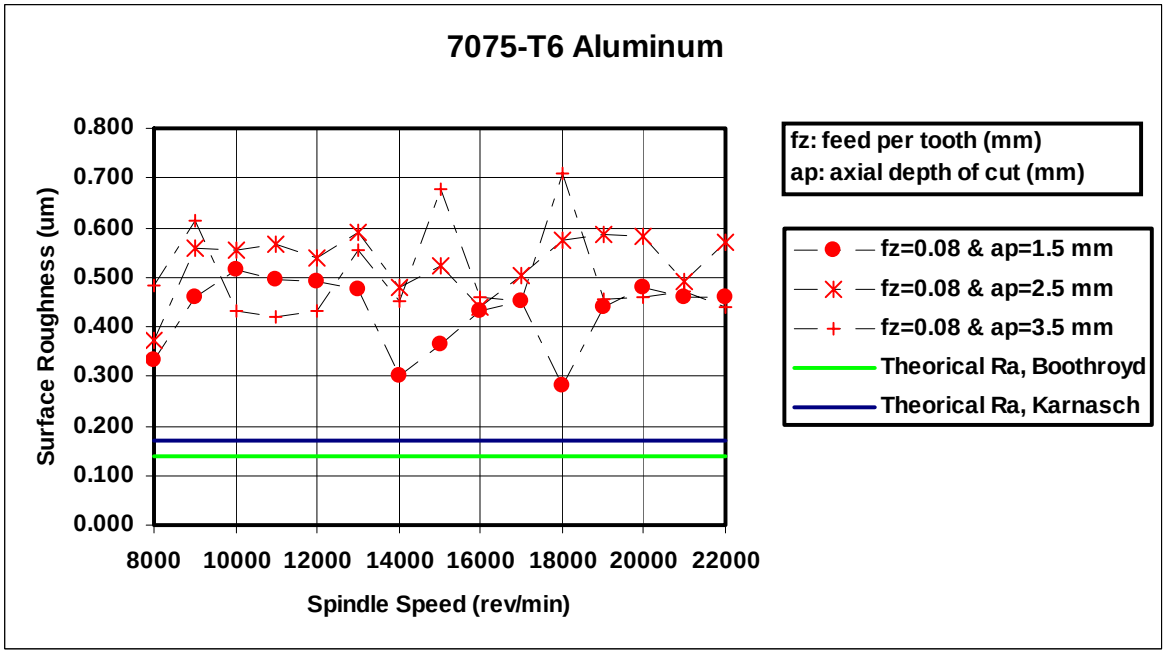

Figure 43. Measured vs ideal surface roughness comparison in 7075-T6 aluminum for fz = 0.08 mm/t.

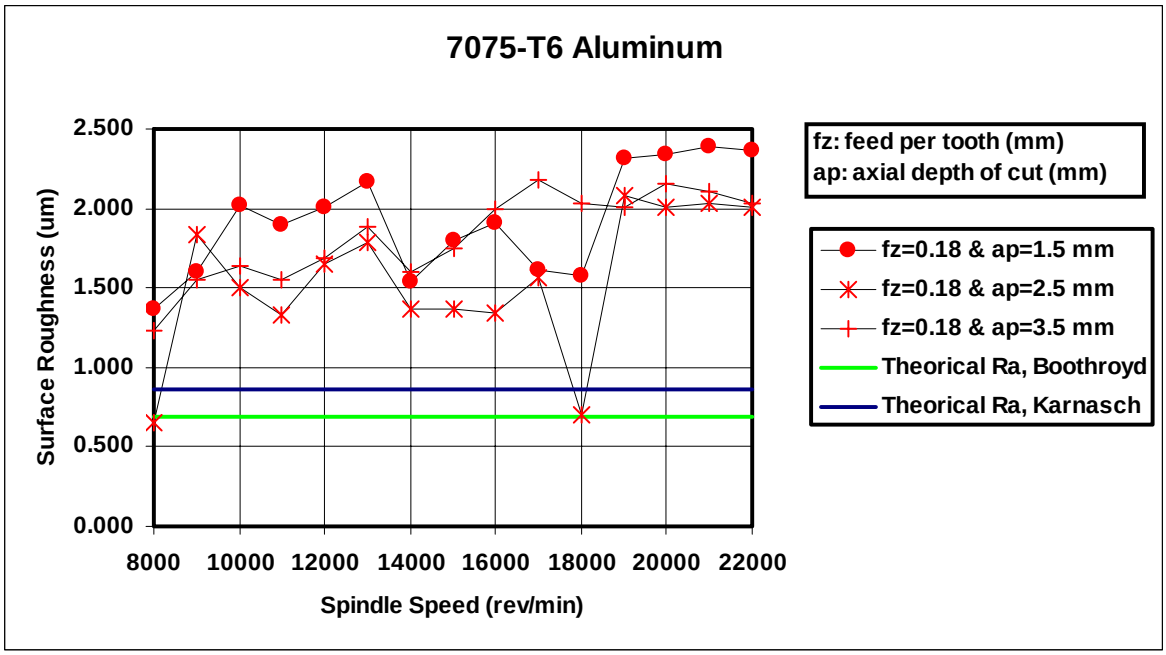

Figure 44. Measured vs ideal surface roughness comparison in 7075-T6 aluminum for fz = 0.18 mm/t.

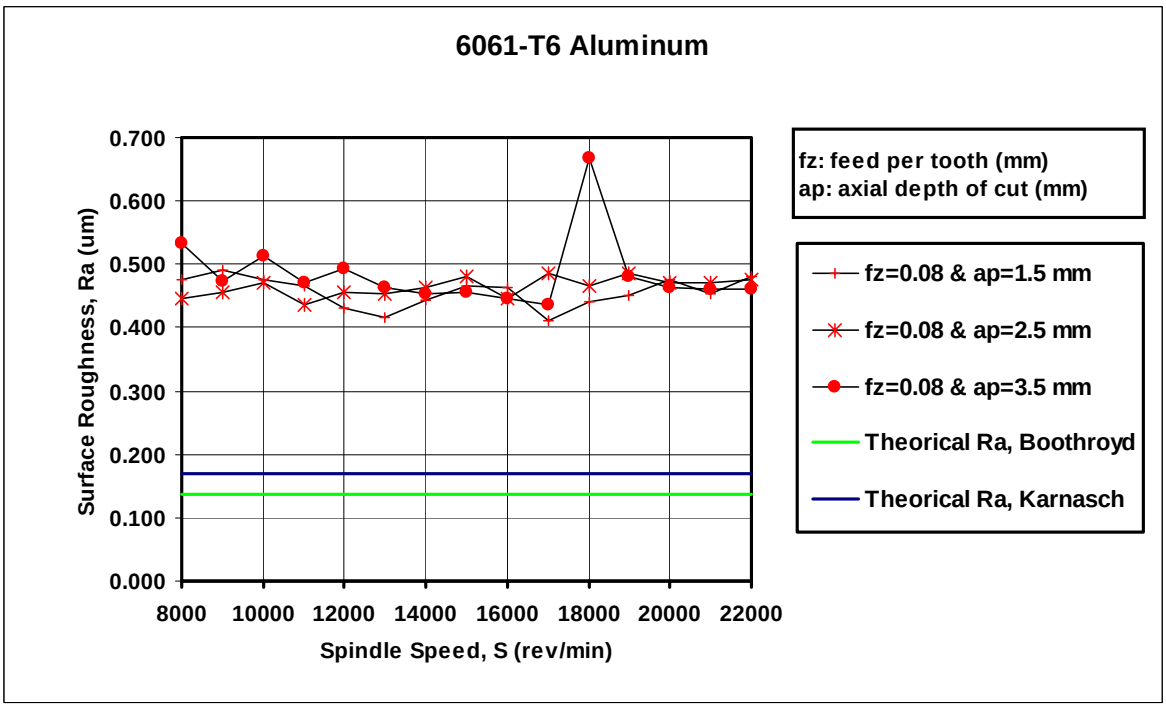

Figure 45. Measured vs ideal surface roughness comparison in 6061-T6 aluminum for fz = 0.08 mm/t.

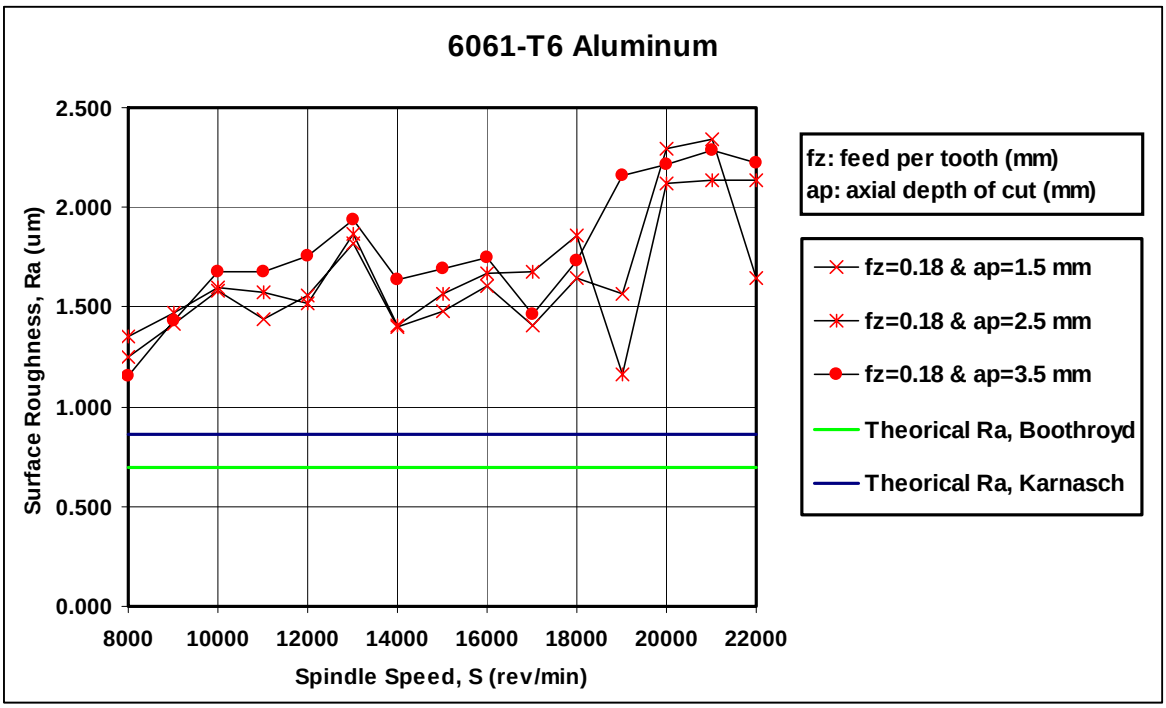

Figure 46. Measured vs ideal surface roughness comparison in 6061-T6 aluminum for fz = 0.18 mm/t.

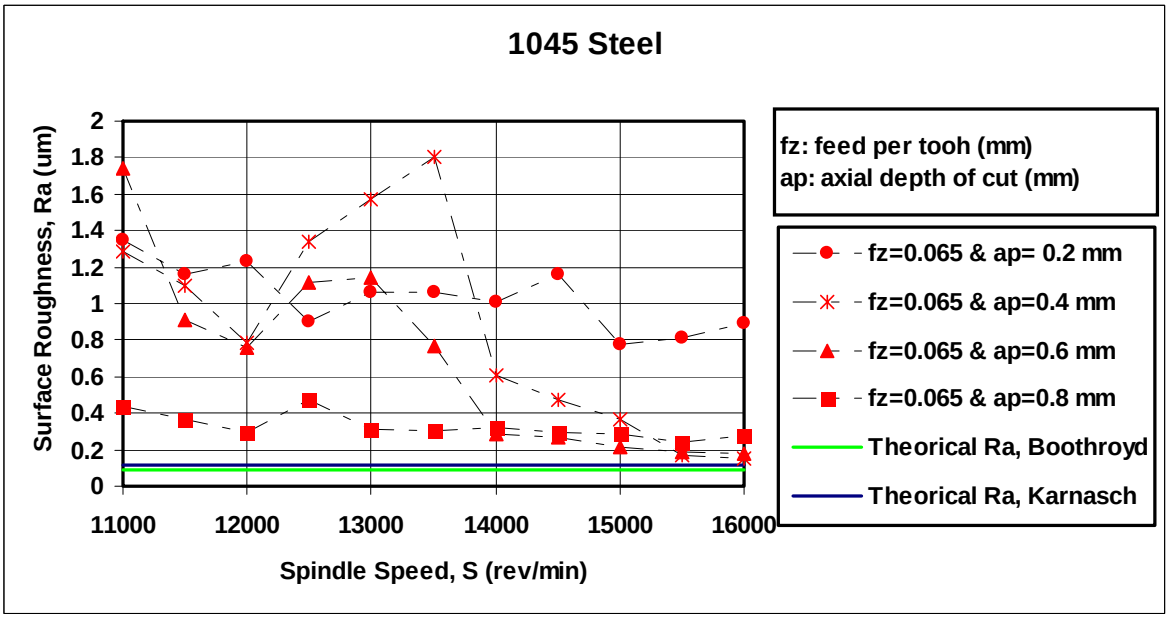

Figure 47. Measured vs ideal surface roughness comparison in 1045 steel for fz = 0.065 mm/t.

Figure 43 through Figure 47 show the theorical versus the measured surface roughness. As we can see in the graphs, the model provided by Karnasch is a little bit higher than the one from Boothroyd, but both are useful as references to know the process contribution to the surface roughness value.

This means that the difference between the measured value and the theorical value is the result of all inaccuracies that are produced during the cutting process. This conclusion can be sustained observing the next graph in which it was measured only the signal without cutting and the spindle working ate different velocities. As it was expected, the level of the signal is smaller than the ones shown before.

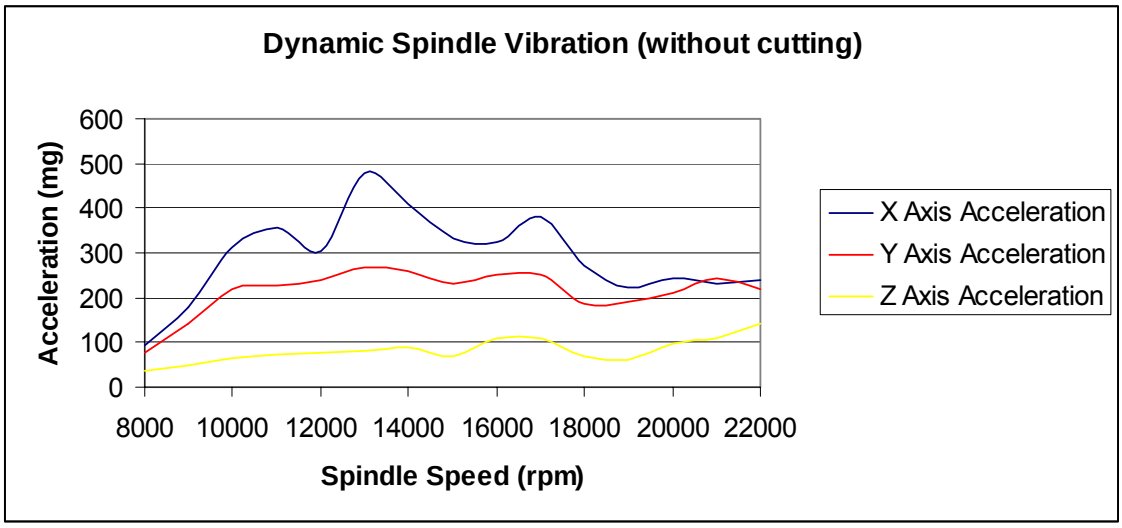

Figure 48. Acceleration of the three axis without cutting.

Chapter 7: Discussion

7.1 Contributions

At the end of this study we can conclude that relevant results were obtain that provide a precise and important view of the high speed milling process behavior. This these is not only useful to understand the milling process, but also to show an adequate methodology for future research in this topic.

From the acquisition system it was seen that different sensors were tested to be selected in the present study. Accelerometers and acoustic emission sensors were used in different positions giving interesting results. Acoustic emission sensors are widely used because of their high frequency range of operation, otherwise accelerometers are limited in this field. Acoustic emission sensors have a big disadvantage, more instrumentation or software processing is needed through the use of filters, due to their great affection by environmental noise. The use of AE sensors in machining plants may be impossible without filtering process to obtain just the process part of the signal. In the other hand, accelerometers are less sensitive and operate in lower frequencies, but resulted adequate for this study and helped obtain significant results. About the location of the sensors, in this study worked much better with the accelerometers located in the spindle head. Due to their low sensitivity, working with the accelerometers in the working table, resulted to be far from the process, and signals were not significant. The use of axial accelerometers give great advantages over a triaxial accelerometer because individual accelerometers can be adjusted in different positions along the z axis in order to obtain a better signal of the cutting process. The use of magnetic heads integrated to the case of the sensor may be good when experimenting with steel, because it can be placed directly in the material. This turns difficult when working with aluminums.

LabView resulted in an easy programming tool, which provide the researcher with many options and very little time spent. The use of data acquisition cards that have their own drivers for LabView versions made the acquisition system easy to use and to configure. When using several acquisition cards with

different speeds it is important to configure all cards in order to obtain always the same amount of data. Sometimes averaging may be use in order no to make the system slow and loose significant amount of data.

As shown in the results chapter several models were obtain to predict vibrations and surface roughness for each material. Some of them were not useful with very low prediction capability. For any aluminum the model with fz of 0.08 mm/t resulted not capable of giving a certain prediction. Several causes can be mentioned as the reason of such inefficiency, at first, the variability of the surface roughness throughout the different spindle speed is high, but still maintains a similar level. The model may give an idea of the level at may the real surface roughness result, but is not efficient following such variability. At second, the forces involved in the machining may be very not significant due to the low feed rate and the high spindle speed used. Such conditions may be the reason of maintaining almost the same level of Ra. For these reasons the models were not shown in chapter 6, but the information is available in Appendix I.

It is important to pay attention to the statistical analysis made before the regression analysis. Several statistic tools were used to validate all the analysis needed to obtain the models. The models obtained are shown in Table 12 with their corresponding parameters.

Material	*Model*	*Fz (mm/t)*	*Adj. R Square*	*Significant Parameters*
AL7075-T6	$Acc\,\mathrm{Re}\,s = -1556.44 + (0.448764 * S) - (2.89473E-05 * S^2) + (5.86818E-10 * S^3)$	---	*50%*	*-S- -S^2- -S^3-*
AL7075-T6	$Ra = -2.03638 + (0.0005969 * Vf) + (0.00525252 * Acc\,\mathrm{Re}\,s) - (8.00655E-07 * Vf * Acc\,\mathrm{Re}\,s)$	*0.18*	*38%*	*-Vf- -AccRes- -Vf*AccRes-*
AL6061-T6	$Acc\,\mathrm{Re}\,s = -2186.79161 - 2.1152E-13 * (ap * S)^3 + (0.582462 * S) - (3.7889E-05 * S^2) + (7.7859E-10 * S^3)$	---	*70%*	*-(ap*S)^3- -S- -S^2- -S^3-*

AL6061-T6	$Ra = -0.982117576 + (0.00049374 * Vf) + (0.003675913 * Acc\,\mathrm{Res}) - (6.85312E-07 * Vf * Acc\,\mathrm{Res})$	*0.18*	*47%*	*-Vf- -AccRes- -Vf*AccRes-*
1045 Steel	$Acc\,\mathrm{Res} = -30048.13 + (6.921679 * S) - (0.000515 * S^2) + (1.27E-08 * S^3)$	*---------*	*52%*	*-S- -S^2- -S^3-*
1045 Steel	$Ra = 2.847416667 - (0.001204779 * Vf)$	*0.065*	*27%*	*-Vf-*

Table 12. Models obtained with multiple regression analysis, and their corresponding parameters.

Observing the "Remaining Parameters" column at the right of the table, we can see that most of the parameters that constructs the model are the same depending on the predicted variable. In the case of the prediction of the resultant acceleration we can observe that the predominant factors are the spindle speed at first, second and third order. In the case of 6061-T6 aluminum the interaction between the spindle speed and the depth of cut resulted significant. It is important to mention that this interaction and others were also tested in the other models, but resulted insignificant to the prediction. The factor of depth of cut does not appear in most of the models, it resulted insignificant to any prediction. This can be seen in some graphs shown were the vibration level does not change with different depths of cut, it mostly remain at the same levels. In the other hand, the spindle speed resulted extremely important to the vibration prediction. This importance can also be seen in the statistical analysis made in the appendix I, were correlation analysis were made obtaining the spindle speed a medium-high factor and in the summary outputs of the regression analysis were the p-value of the factors where the spindle speed appear were very low. The issue of the not significant influence of the depth of cut in the results should be discussed carefully. As seen in literature, at higher depths of cut the process experiences higher cutting forces; then higher vibration levels are expected, but this did not appear in the results obtained. Any identified pattern is seen in the vibration graphs at different depths of cut. This phenomenon is the principal cause that most of the depths of cut parameters were eliminated from the models in the regression analysis. Without an specific answer to this behavior we can infer that:

- The depths of cut used in the experimentation are very low, that it has no influence in the surface roughness and the resultant acceleration levels. In the case of the aluminum the higher depth of cut used was 3.5 mm, being 12 the highest value permitted by the tool. In the case of steel the higher value was 0.8 mm being 10 mm the highest value possible.
- Literature establishes that higher forces are involved at higher depths of cut, such literature refers to conventional milling velocities, no information is found in High Speed Milling processes about the forces involved in the machining. It is possible to think that in HSM the affection of the depth of cut is almost null to the parameters of surface roughness and vibrations. Further studies are recommended to support these supposals.

One last contribution, and by the focus of this study, the most important, is the differentiation of the natural and ideal surface roughness level. In the previous chapter the theorical surface roughness was calculated and compared to the real surface roughness. The theorical R_a does not take into consideration any inaccuracies that may occur in the process, such as vibrations [Boothroyd and Knight, 2006]. With this comparison in Figure 49 we can see that the measured surface roughness is 3 or 4 times higher than the theorical model, this justifies the focus on the vibrations in the machining process measured in this study. Once analyzed this comparison we should think in selecting appropriate machining parameters to obtain a certain theorical surface roughness, taking into account that the inaccuracies of the process will grow up this value up to four times. The comparison was also useful to understand the spindle mechanical properties, which have a better development at certain values of spindle speed. For example analyzing the graphs of both aluminums at the values of 18000 and 19000 rpm we can observe that the R_a values are very low and near to the theorical ones. Then we can think of using such spindle speeds to obtain the lowest surface roughness possible.

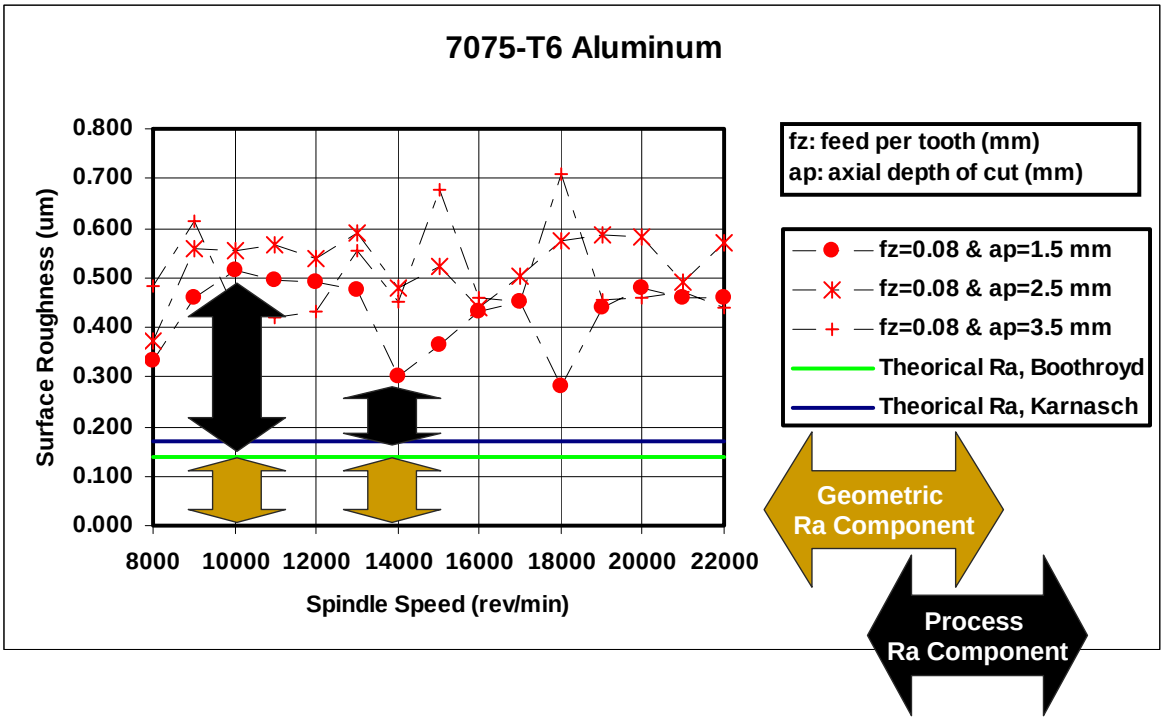

Figure 49. Comparison between theorical and real surface roughness.

7.2 Future Research

Further research must be done in obtaining these models taking into consideration different parameters involved in the process of end milling machining. Factors like different tools, different materials, tool wear, forces involved in the process, different process than grooving, etc, may be introduced in such models.

Different types of sensors may be tested in order to determine which are the most suitable ones from all the range of sensors to measure vibrations. Different locations of accelerometers must be tried to develop more effective monitoring systems.

As seen in figure 48 the dynamical behavior of the spindle may influence in the final surface roughness. As future work, studies can be made to determine optimal velocities to get the surfaces roughness expected. In this figure the vibration detected is due only to the mechanical and dynamical properties of the spindle. Subtracting this signal to the one measured in cutting conditions will give only the part of acceleration belonging to the process.

ITESM	Instituto Automática Industrial
DACs - CompuScope 1602 - MPI	**DACs** -CompuScope 1602 -MPI -DaqBoard 2000 and 2005
Amplifiers and Conditioners:	**Amplifiers and Conditioners:** -3 Kistler 5011 Amplifiers
Software: -LabView 7.1	**Software:** -LabView 7.1
Sensors: -3 IMI Accelerometers	**Sensors:** -3 Kistler Accelerometers -1 Triaxial accelerometers -1 Multicomponent force platform -2 AE Sensors

Table 13. Instrumentation comparison between the ITESM and the IAI in Spain.

Table 13 shows the instrumentation own by each research institute, the ITESM and the Industrial Automation Institute (IAI) in Spain. Further research and cooperation will be done due to the similarities in instrumentation.

BIBLIOGRAPHY

Abouelatta, O. and Mádl, J. "*Surface roughness prediction based on cutting parameters and tool vibration in turning operations*". Journal of Materials Processing Technology. 2001: 269-277.

Alique López, José Ramón and Haber Guerra, Rodolfo E. "*Automatización de los procesos de mecanizado a alta velocidad*". Automática e Instrumentación May 2004: 64-78.

Amaral, Ron and Chong Leonel. "*Surface Roughness*" December 2002: 2-20.

Anonymous. "*Using common sense with sensors*" Robotics World Spring 1997: 24-25.

Baek, D. K., Ko, T. J. and Kim, H.S. "*Optimization of federate in a face milling operation using a surface roughness model*". International Journal of Machine Tools and Manufacture. October 1999: 451-462.

Bird, John. Engineering Mathematics Pocket Book. Great Britain: Newnes, 2001.

Boothroyd G. and Knight W. Fundamentals of Machining and Machine Tools. USA: Taylor and Francis, 2006.

Brüel & Kjaer. "*Vibration Measurement and Analysis*" Brüel & Kjaer Sound and Vibration Measurement A/S. 1998.

Brüel & Kjaer. "*Vibration Transducers and Signal Conditioning*" Brüel & Kjaer Sound and Vibration Measurement A/S. 1998.

Chicala, Carlos. Adquisición de Datos, Medir para conocer y controlar. Argentina: Ed. Soluciones en Control S.R.L., 2004.

Dabade, U., Joshi, S. and Ramakrishnan, N. "*Analysis of surface roughness and chip cross-sectional area while machining with self-propelled round inserts milling cutter*". Journal of Materials Processing Technology. January 2002: 305-312.

Dornfeld, D. et al. "*Monitoring of Ultraprecision Machining Processes*" The International Journal of Advanced Manufacturing Technology. 2003: 571-578.

Edan, Yael, et al. "*Sensor economy principles and selection procedures*". IIE Transactions March 2000: 195-203.

Faasen, R. et al. "*Prediction of regenerative chatter by modelling and analysis of high-speed milling*" Machine tools and manufacture. March 2003: 1437-1446.

Franco, P., Estrems, M., and Faura, F. "*Influence of radial and axial runouts on surface roughness in face milling with round insert cutting tools*". International Journal of Machine Tools and Manufacture. February 2004: 1555-1565.

Gautschi, G. Piezoelectric Sensorics: Force, Strain, Pressure, Acceleration and Acoustic Emisión Sensors, Materials and Amplifiers. New York : Springer, 2003.

Haber, Rodolfo, et al. "*An investigation of tool-wear monitoring in a high-speed machining process*" Sensors and Actuators April 2004: 1-7.

Haber, Rodolfo and Alique Jose R. "*Intelligent process supervision for predicting tool wear in machining process*" Mechatronics November 2001: 825-849.

Insperger, T., et al. "*Multiple chatter frequencies in milling processes*" Journal of Sound and Vibration December 2001: 333-345.

Jiménez, Jose Emilio, et al. Nuevo método Analítico-Experimental para la identificación de los diagramas de lóbulos de estabilidad en fresado a alta velocidad. Madrid: Thesis, 2003.

King, Robert. Handbook of High Speed Machining Technology. New York: Chapman and Hall Advanced Industrial Technology Series, 1985.

Kosel, Tadej, et al. "*Intelligent location of two simultaneous active acoustic emission sources: Part I*" Aircraft Engineering and Aerospace Technology 2003: 11-17.

Kosel, Tadej, et al. "*Intelligent location of two simultaneous active acoustic emission sources: Part II*" Aircraft Engineering and Aerospace Technology 2003: 137-142.

Lee, et al. "*Simulation of surface roughness and profile in high-speed end milling*". Journal of Materials Processing Technology. 2001: 410-415.

Lee, Sang-Jin, et al. "A Study on Surface Integrities of High Speed Grinding with CBN Wheel in Mold Material". Journal of the Korean Society of Manufacturing Process Engineers. 2003: 5-13.

Lo, Ship-Peng. "*An adaptative-network based fuzzy inference system for prediction of workpiece surface roughness in end milling*". Journal of Materials Processing Technology. October 2001: 665-675.

Lopez Guerrero, F. Eugenio, et al. "*Caracterización de superficies maquinadas por medio de parámetros de rugosidad*" (Machined surface characterization through roughness parameters) March 2003: 62-68.

Lou, J. and Chen, J. "*In-Process Surface Roughness Recognition (ISRR) System in End-Milling Operations*" The International Journal of Advanced Manufacturing Technology 1999: 200-209.

Lou, Mike S., et al. "*Surface Roughness Prediction Technique For CNC End-Milling*". Journal of Industrial Technology November 1998: 1-6.

Mansour, A., Abdalla, H. and Meche, F. "*Surface roughness model for end milling: a semi-free cutting carbon casehardening steel (EN32) in dry conditionI*". Journal of Materials Processing Technology. October 2000: 183-191.

Mundo Electrónico. Transductores y medidores electrónicos. Barcelona: Marcombo Boixareu Editores, 1977.

Paimes Teixeira, Jorge. Fundamentos Físicos do Corte dos Metais. Lisboa: Edinova, 2001.

Peigne, et al. "*Impact of the cutting dynamics of small radial immersion milling operations on machined surface roughness*". International Journal of Machine Tools and Manufacture. November 2003: 1133-1142.

Peña, Daniel. Análisis de datos multivariantes. España: Ed. McGrawHill, 2002.

Perez, César. Técnicas Estadísticas con SPSS 12 Aplicaciones al análisis de datos. España: Ed. Prentice may, 2005.

Rodríguez, Ciro et al. "*Factores que afectan el acabado superficial en los procesos de mecanizado: Técnicas de Análisis y Modelos*" XXV Jornadas de Automática Industrial CEA-IFAC. September 2004: 75-82.

Savage, Mandara and Chen, Joseph. "*Multiple Regression-Based Multilevel In-Process Surface Roughness Recognition System in Milling Operations*". The Journal of Technology Studies. 28-34.

Savage, Mandara and Chen, Joseph. "*Effects of Tool Diameter Variations in On-Line Surface Roughness Recognition System*". Journal of Industrial Technology. August 1999: 1-7.

Schmitz, Tony L. "*Chatter recognition by a statistical evaluation of the synchronously sampled audio signal*" Journal of Sound and Vibration October 2002: 1-10.

Solís Venegas, Esteban. Generación del umbral de estabilidad para procesos de fresado a alta velocidad: planificación y optimización de parámetros tecnológicos de corte. Madrid: Tesis, 2003.

Suck Cho, Hyung Neural Network Applications to Manufacturing Processes: Monitoring and Control. Boca Raton: CRC Press, 2001.

Treviño, et al. Guide for Documented Research. México: Trillas, 1998.

Tsai, Yu-Hsuan, et al. "*An in-process surface recognition system based on neural networks in end milling cutting operations*" Machine tools and manufacture June 1997: 583-605.

Wang, Ming Yung and Chang, Hung Yen. "*Experimental study of surface roughness in slot end milling AL2014-T6*". International Journal of Machine Tools and Manufacture May 2003: 51-57.

Appendix A: Instrumentation

This appendix includes all relevant technical and configuration data of all the instrumentation used and mentioned in this these. This appendix will be divided to order datasheets by type of instrumentation. This division is presented as follow:

Appendix A.1: Data Acquisition Cards

- DaqBoard 2000 Series
- DBK 17
- Compuscope 1602

Appendix A.2: Sensors

- 8152B Kistler Acoustic Sensor
- 4370 Brüel & Kjaer Accelerometer
- 4371 Brüel & Kjaer Acceletometer

Appendix A.3: Amplifiers

- 5011 Kistler Amplifier

Appendix A.1: Data Acquisition Cards

DaqBoard/2000™ Series

16-Bit, 200-kHz PCI & CompactPCI® Data Acquisition Boards

Features

- Five DaqBoard/2000 series PCI boards and the DaqBoard/2001c CompactPCI® version are available
- 16-bit, 200-kHz A/D converter
- 8 differential or 16 single-ended analog inputs (software selectable per channel)
- Expandable up to 256 analog input channels, while maintaining 200 kHz (5 ∝s per channel) scan rate
- Up to four boards can be installed into one PC for up to 1024 analog input channels
- 100% digital calibration
- 512 location channel/gain FIFO, capable of scanning all channels, including 256 analog expansion channels and digital/counter channels, at 5 ∝s per channel
- DMA bus mastering for synchronous analog I/O, digital I/O, and counter inputs
- Trigger modes include analog, digital, and software, with <5 ∝s latency
- Virtually infinite pre-trigger buffer*
- Up to four 16-bit, 100-kHz analog outputs with infinite continuous waveform output capability*
- 40 digital I/O lines, can be scanned synchronously or asynchronously with analog inputs
- Digital I/O is expandable up to 272 lines, including optional isolation and relay closure
- Four counter/pulse input channels can be scanned synchronously or asynchronously with analog inputs
- Two timer/pulse output channels

Signal Conditioning Options

- Signal conditioning and expansion options for thermocouples, strain gages, accelerometers, isolation, RTDs, etc.—over 40 options in all

Software

- Includes support for Visual Basic®, C/C++, ActiveX/COM, Linux, LabVIEW®, MATLAB®, and DASYLab®
- Optional DaqView2000™ software package

* Limited only by available PC RAM and hard disk space

CompactPCI Versions Available!

The DaqBoard/2000 series plug-in boards provide cost-effective, high-speed data acquisition

The DaqBoard/2000™ series sets the price/performance benchmark for high-speed, multifunction plug-and-play data acquisition for PCI bus computers. The DaqBoard/2000 series hardware design offers all of the features normally found on significantly more expensive boards, including 16-bit, 200-kHz A/D, 100% digital calibration, bus mastering, two or four 16-bit, 100-kHz D/A converters, 40 digital I/O lines, four counters and two timers.

DaqBoard/2000 series is supported by a growing family of over 40 signal conditioning and expansion options, offering signal conditioning for thermocouples, RTDs, accelerometers, isolation, high-voltage, strain gages, and much more. Up to 528 channels of analog and digital I/O can be accessed using one DaqBoard/2000, while maintaining the 5 ∝s per channel update rate. Up to four DaqBoard/2000s can be installed into one PC.

Software support is the most extensive of any board, including comprehensive drivers and new ActiveX/COM-based programming tools for nearly every programming environment under Windows® 95 and higher. Included in this list are Visual Basic, C/C++, Linux, LabVIEW, MATLAB, and DASYLab. Also available is a suite of DaqView™ software options for *Out-of-the-Box*™ setup, acquisition, display, and analysis of acquired data—no programming required. DaqView2000™ combines DaqView, DaqViewXL™, and eZ-PostView™ in one software package for use with the DaqBoard/2000 series.

In total, the DaqBoard/2000 series sets the industry standard for plug-and-play PCI data acquisition.

PC Data Acquisition Hardware

tel: 440-439-4091 fax: 440-439-4093 192 sales@iotech.com www.iotech.com

DaqBoard/2000™ Series

General Information

DaqBoard/2000™ Series Selection Chart					
	Multifunction I/O			Digital I/O	Analog Output
Feature	/2001 & /2001c	/2000	/2005	/2002	/2004
Analog inputs (16 bit/200 kHz)	16	16	16	—	—
Analog outputs (16 bit/100 kHz)	4	2	—	—	4
Digital I/O	40	40	40	40	40
Freq./pulse I/O	6	6	6	6	6

Synchronous I/O for High-Speed Applications

The DaqBoard/2000 series sets a new standard with its ability to make analog measurements, read digital inputs, and read counter inputs, while synchronously generating up to four analog outputs and/or a 16-bit digital pattern output. Most other boards require CPU interaction to access I/O other than analog input, making it impossible to generate time-critical analog waveforms or digital patterns. With the DaqBoard/2000 series, the true power of today's PCI-based PCs can be unleashed.

The same synchronous features of the DaqBoard extend to its family of DBK signal conditioning and expansion options. Up to 256 analog input channels and 272 (256, P2 only) digital I/O channels can also be accessed synchronously to one another, with precise and deterministic channel-to-channel timing. Up to four DaqBoards can be installed in one PC, quadrupling the channel capacity to over 1000 analog input channels, 1000 digital I/O channels and 16 high-speed analog output channels.

Signal I/O

One 100-pin connector on the DaqBoard/2000 series provides access to all of the input and output signals. Unlike other multifunction boards that require multiple PC slots in order to access all of the I/O, careful design of the DaqBoard/2000 series accommodates all I/O using one cable, and utilizing a single PCI slot.

The 100-pin DaqBoard/2000 series I/O connector, **P4**, is logically divided into three sub-ports, P1, P2, and P3. **P1**, the analog input port, contains all of the analog input channels, as well as the sequencer control signals for accessing external analog input options. All analog expansion options attach to the P1 port. **P2**, the general purpose digital I/O port, can be used directly to control and monitor 24 digital I/O lines. P2 can also function as the digital I/O expansion port, whereby the 24 lines are exclusively used to control external digital DBK expansion options, for up to 256 lines of digital input or output. P3 contains an additional 16-bit digital I/O port, as well as the counter inputs, timer outputs, and analog outputs. Several options are available to provide easy user access to all of the I/O signals on P4.

Analog Input (P1)

The DaqBoard/2000 series has a 16-bit, 200-kHz A/D coupled with 16 single-ended, or 8 differential analog inputs. Thirteen software programmable ranges provide inputs from ±10V to ±156 mV full scale. Each channel can be software-configured for a different range, as well as for single-ended or differential, and unipolar or bipolar input. Beyond the 16 built-in analog inputs, the user can expand the DaqBoard/2000 series up to 256 analog inputs using external DBK signal conditioning and expansion options. As with the on-board channels, expansion channels are scanned at the same 5 ∝s/channel rate (200 kHz), and most are software-programmable for range. There is *no* speed penalty for scanning expansion channels versus built-in channels. The DBK expansion options offer a wide variety of signal measurements, including thermocouples, RTDs, strain gages, accelerometers, high voltage, isolation, current, and much more.

DaqBoard/2000™ Series

General Information

DaqBoard/2000, /2001, /2001c, and /2005 Block Diagram

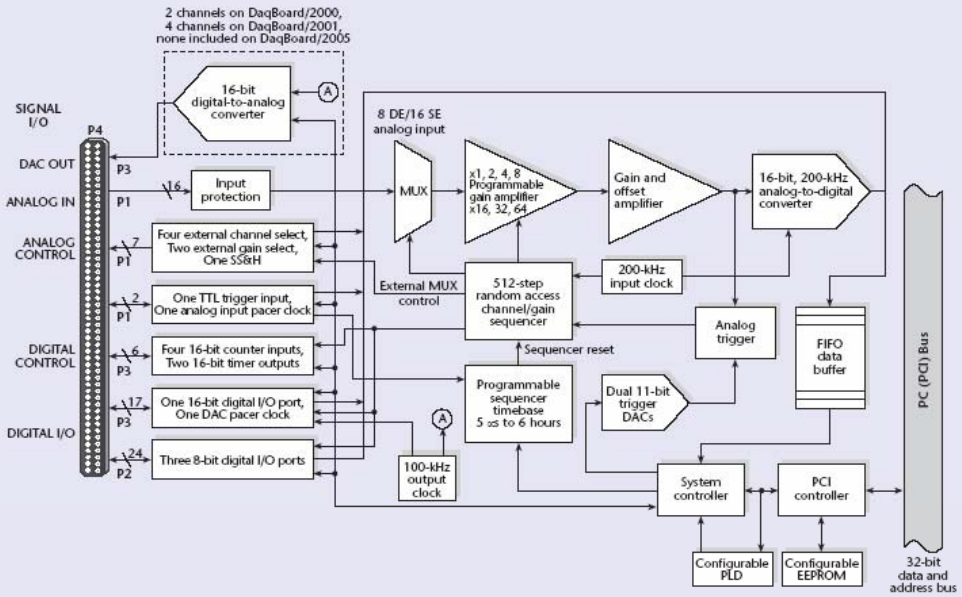

DaqBoard/2002 Block Diagram

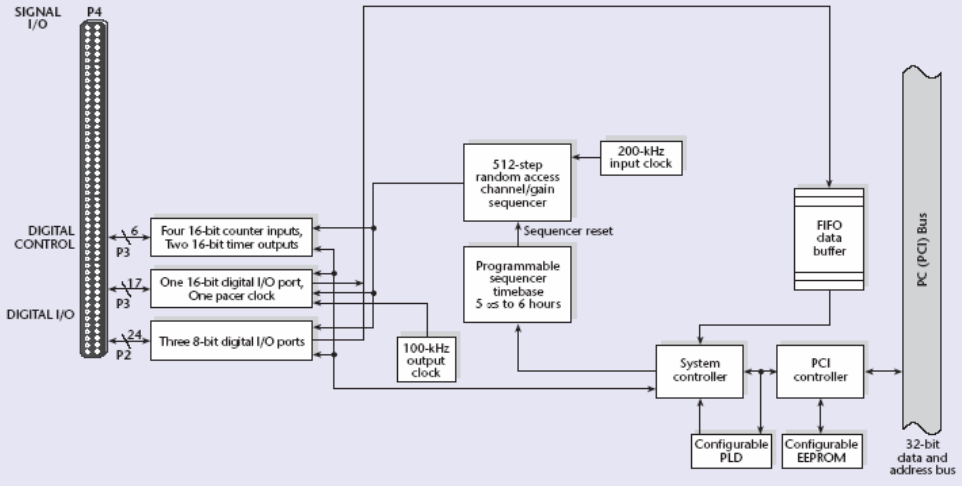

PC Data Acquisition Hardware

DaqBoard/2000™ Series

General Information

DaqBoard/2004 Block Diagram

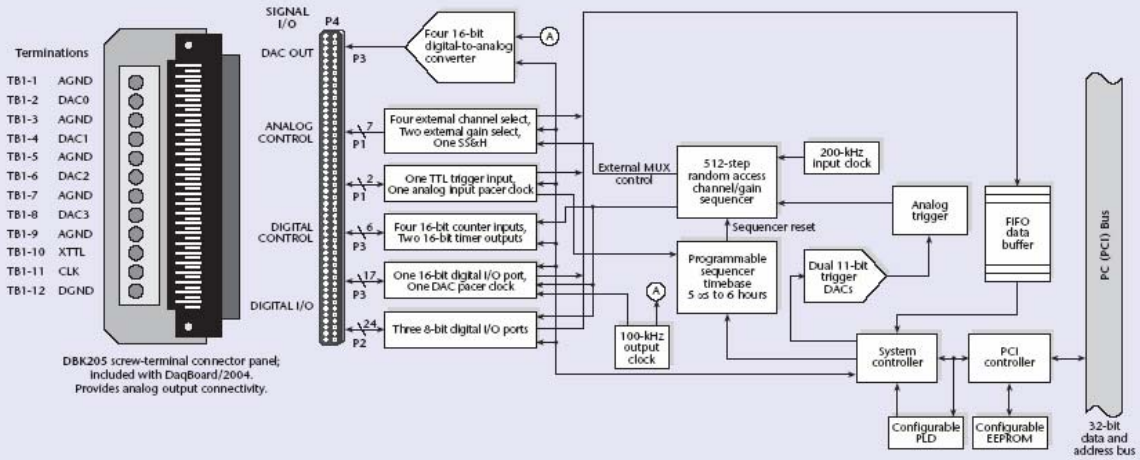

DaqBoard/2000™ Series

General Information

Scanning

The DaqBoard/2000 series has an on-board scan sequencer that permits the user to select any combination of up to 512 channel/range combinations. The sequencer scans all channels contained in the sequence at the fastest rate of 5 ∝s/channel, thereby minimizing the time-skew from channel-to-channel. The user can also set the time between scan groups, from 0 to 6 hours. In addition to scanning analog inputs, the sequencer can scan digital inputs and counter inputs.

Bus Mastering DMA

The DaqBoard/2000 series supports Bus Mastering DMA, which allows analog and digital/counter input data, as well as analog and digital output data to flow between the PC and the DaqBoard/2000 series without consuming valuable CPU time. The driver supplied with the DaqBoard/2000, as well as all other third-party software support such as MATLAB®, LabVIEW®, and DASYLab®, automatically utilize Bus Mastering DMA to efficiently conduct I/O from the PC to the DaqBoard.

Triggering

Triggering can be the most critical aspect of a data acquisition application. The DaqBoard/2000 series supports a full complement of trigger modes to accommodate any measurement situation.

Hardware Analog Triggering. Many data acquisition boards claim analog triggering, but rely on the PC to take readings and make a decision, which leads to uncertain and potentially long latencies. The DaqBoard/2000 series uses true analog triggering, whereby the trigger level programmed by the user sets an analog DAC, which is then compared in hardware to the analog input level on the selected channel. The result is analog trigger latency which is guaranteed to be less than 5 ∝s, significantly shorter than most data acquisition boards. Any analog channel can be selected as the trigger channel, including built-in or expansion channels. The user can program both the trigger level, as well as the edge (rising or falling).

Channel-Scanning Flexibility

The DaqBoard/2000 series offers a 512-location scan sequencer that allows you to select each channel and associated input amplifier gain at random. The sequencer circuitry circumvents a major limitation encountered with many plug-in data acquisition boards—a drastic reduction in the scan rate for external expansion channels. All DaqBoard/2000 series channels, including the 528 potential expansion channels, are scanned at 100K or 200 kHz (1 or 5 ∝s/channel), software programmable per channel. In addition, the digital and frequency inputs can be scanned using the same scan sequence employed for analog inputs, enabling the time correlation of acquired digital data to acquired analog data. The DaqBoard/2000 series permits each scan group, which can contain up to 512 channel/gain combinations, to be repeated immediately or at programmable intervals of up to 6 hours. Within each scan group, consecutive channels are measured at a fixed 5 ∝s/channel rate.

DaqBoard/2000 Series Scanning Example

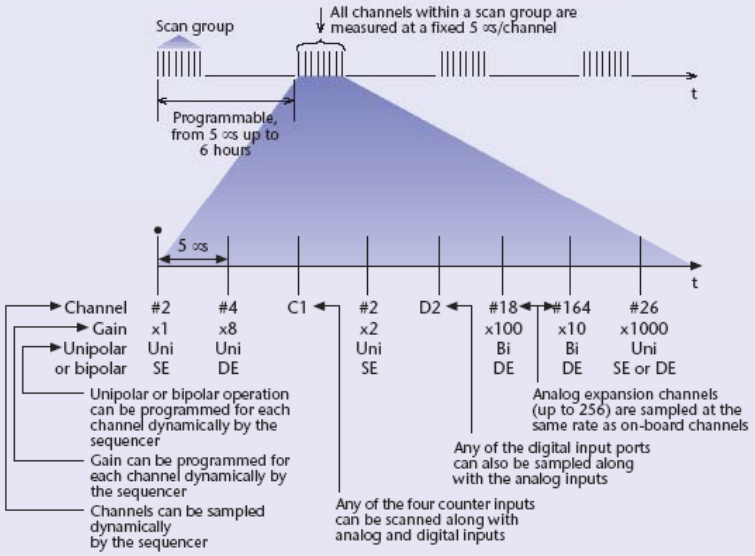

Digital and Pattern Triggering (P1). A separate digital trigger input line is provided, allowing TTL-level triggering, again with latencies guaranteed to be less than 5 ∝s. Both the logic levels (1 or 0), as well as the edge (rising or falling), can be programmed for the discrete digital trigger input.

Software-Based Triggering. Software-based triggering differs from the modes described above because the readings, analog, digital, or counter, are interrogated by the PC to detect the trigger event, not in the hardware as described above. The advantage of this mode is to permit triggering based on more complex situations, such as on a specific temperature, which was derived from the acquisition of at least two analog measurements, plus the calculation of the measured temperature using linearization algorithms.

The DaqBoard/2000 series also supports digital pattern triggering, whereby the user can designate any of the digital input ports as the trigger port. The programmed

DaqBoard/2000™ Series

General Information

digital pattern, including the ability to mask or ignore specific bits, is then compared to the actual input until a match is detected, after which the sequencer begins the scan sequence.

Triggering can also be programmed to occur when one of the counters reaches, exceeds, or is within a programmed level. Any of the built-in counter/totalizer channels can be programmed as a trigger source.

Normally software-based triggering results in long latencies from the time that a trigger condition is detected, until the actual capturing of data commences. However, the DaqBoard/2000 series circumvents this undesirable phenomenon by use of pre-trigger data. Specifically, when software-based triggering is employed, and the PC detects that a trigger condition has occurred, (which may be thousands of readings later than the actual occurrence of the signal), the DaqBoard driver automatically looks back to the location in memory where the actual trigger-causing measurement occurred. The acquired data that is presented to the user actually begins at the point where the trigger-causing measurement occurs. The latency in this mode is equal to one scan cycle.

Stop Trigger. Any of the software trigger modes described above can also be used to stop an acquisition. Thus an acquisition can be programmed to begin on one event, such as a temperature level, and then can stop on another event, such as a digital pattern.

Pre- and Post-Triggering Modes. Six modes of pre- and post-triggering are supported, providing a wide variety of options to accommodate any measurement requirement. When using pre-trigger, the user must use software-based triggering to initiate an acquisition.

No pre-trigger, post-trigger stop event. This, the simplest of modes, acquires data upon receipt of the trigger, and stops acquiring upon receipt of the stop-trigger event.

Fixed pre-trigger with post-trigger stop event. In this mode, the user specifies the number of pre-trigger readings to be acquired, after which, acquisition continues until a stop-trigger event occurs.

No pre-trigger, infinite post-trigger. No pre-trigger data is acquired in this mode. Instead, data is acquired beginning with the trigger event, and is terminated when the operator issues a command to halt the acquisition.

Fixed pre-trigger with infinite post-trigger. The user specifies the amount of pre-trigger data to acquire, after which the system continues to acquire data until the program issues a command to halt acquisition.

Variable pre-trigger with post-trigger stop event*. Unlike the previous pre-trigger modes, this mode does not have to satisfy the pre-trigger number of readings before recognizing the trigger event. Thus the number of pre-trigger readings acquired is variable and dependent on the time of the trigger event relative to the start. In this mode, data continues to be acquired until the stop trigger event is detected.

Variable pre-trigger with infinite post trigger*. This is similar to the mode described above, except that the acquisition is terminated upon receipt of a command from the program to halt the acquisition.

Calibration

Every range on the DaqBoard/2000 series is calibrated from the factory using a digital calibration method. This method works by storing a correction factor for each range on the DaqBoard/2000 series at the time of calibration. Whenever a particular range is selected, the appropriate calibration constant is automatically applied to a compensating DAC, thereby calibrating the specific range. The result is that readings generated by the A/D are already calibrated, and do not require additional processing.

This is significantly better than other boards, that merely adjust the readings in software after they are transferred to the PC. That method has the disadvantage of reducing the dynamic range of the A/D, and can adversely affect the speed at which the PC can obtain a calibrated reading.

The DaqBoard/2000 series also has a user-cal mode, whereby the user can adjust the calibration of the board in their system, without destroying the factory calibration supplied with the board. This is accomplished by having 2 distinct calibration tables in the DaqBoard/2000 series on-board EPROM, one which contains the factory cal, and the other which is available for user calibration.

Analog Output (P3)

DaqBoard/2000, /2001, & /2004 Only

Two or four 16-bit, 100-kHz analog output channels are built into the DaqBoard/2000 series, with an output from –10V to +10V. These outputs are entirely separate from the D/As which are used to determine analog trigger level (some data acquisition board suppliers confusingly refer to trigger D/As as if they are available to the user). Through the use of Bus Mastering DMA, each D/A output can continuously output a waveform, which can be read from PC RAM or a file on the hard disk. In addition, a program can asynchronously output a value to either of the D/As for non-waveform applications, presuming that the D/A is not already being used in the waveform output mode. Additional low-speed D/A channels can be added to the DaqBoard through the use of the DBK2 analog output option card.

When used to generate waveforms, the D/As can be clocked in several different modes. Each D/A can be separately selected to be clocked from one of the sources described below.

Asynchronous Internal Clock. The on-board programmable clock can generate updates ranging from 1.5 Hz to 100 kHz, independent of any acquisition rate.

Synchronous Internal Clock. The rate of analog output update can be synchronized to the acquisition rate derived from 100 kHz to once every 5.96 hours.

Asynchronous External Clock. A user-supplied external input clock can be used to pace the D/A, entirely independent of analog inputs.

Synchronous External Clock. A user-supplied external input clock can pace both the D/A and the analog input.

* Driver support only

DaqBoard/2000™ Series

General Information

Digital Pattern Generation (P3)

The DaqBoard/2000 series supports digital pattern generation via Bus Mastering DMA on the 16-bit high-speed digital I/O port. In the same manner as Analog Output, the digital pattern can be read from PC RAM or a file on the hard disk. Digital pattern generation is clocked in the same four modes as described above with analog output*.

Digital Inputs and Outputs (P2, P3)

Forty TTL-level digital I/O lines are included in the DaqBoard/2000 series. They are divided into three 8-bit ports (P2) and one 16-bit port (P3). The P2 ports can be programmed in 8-bit groups as either input or output. The 16-bit P3 port can be programmed as all inputs or all outputs. Ports programmed as inputs can be part of the scan group and scanned along with other analog and digital input channels, or can be asynchronously accessed via the PC at any time, including when a scanned acquisition is occurring.

In addition, the P2 ports can be expanded up to 256 digital I/O lines using external DBK digital options. These options are available as TTL-level I/O, relay output, or optically isolated input and output. Whenever expansion digital I/O is attached to the DaqBoard/2000 series, the P2 I/O lines are no longer user-programmable, and are instead used to communicate with the digital expansion options.

Counter Inputs (P3)

Four 16-bit counters are built into the DaqBoard/2000, each capable of counting up to 65,536 TTL-level transitions. Each of the four counters will accept frequency inputs up to 10 MHz, and can be configured for pulse count or totalize mode. The counters can also be cascaded, allowing over four billion counts to be accumulated. As with all other inputs to the DaqBoard/2000 series, the counter inputs can be read asynchronously under program control, or synchronously as part of an analog and digital scan group.

* When digital pattern generation is used, one of the analog output channels is limited to asynchronous output mode

DaqBoard/2000 Series Signal Conditioning & Expansion Options

Product	Description	Capacity	Page
DBK1	16-connector BNC interface module	16 connectors	116
DBK2	D/A voltage-output card	4 channels	117
DBK4	Dynamic signal-input card	2 channels	118
DBK5	Current output card	4 channels	120
DBK7	Frequency-to-voltage input card	4 channels	122
DBK8	High-voltage input card	8 channels	124
DBK9	RTD measurement card	8 channels	125
DBK10	Expansion-card enclosure module	3 cards	126
DBK11A	Screw-terminal card	40 terminals	127
DBK15	Universal current/voltage input card	16 channels	128
DBK16	Strain gage measurement card	2 channels	130
DBK17	Simultaneous sample and hold card	4 channels	132
DBK18	Low-pass filter card	4 channels	134
DBK20	Digital I/O card (screw-terminal connectors)	48 channels	136
DBK21	Digital I/O card (male DB37 connectors)	48 channels	136
DBK23	Optically isolated digital-input module	24 channels	137
DBK24	Optically isolated digital-output module	24 channels	139
DBK25	Relay output card	8 channels	141
DBK30A	Rechargeable battery/excitation module	14.4 or 28.8 VDC	142
DBK32A	Auxiliary power supply card	±15 VDC @ 500 mA	143
DBK40	BNC interface module	18 connectors	145
DBK41	Analog expansion enclosure module	10 cards	146
DBK42	5B isolated signal-conditioning module	16 channels	148
DBK43A	Strain gage module	8 channels	150
DBK44	5B isolated signal conditioning card	2 channels	152
DBK45	SS&H card with low-pass filter	4 channels	154
DBK50	Isolated high-voltage input module	8 channels	156
DBK51	Isolated low-voltage input module	8 channels	156
DBK55	Frequency-to-voltage input module	8 channels	158
DBK60	3-slot expansion module w/customizable panels	3 cards	160
DBK65	Transducer interface module	8 channels	162
DBK70	Vehicle network interface module	16 channels	164
DBK80	Differential voltage input card with excitation output	16 channels	169
DBK81	TC/mV card with screw-terminal connections	7 channels	170
DBK82	TC/mV card with screw-terminal connections	14 channels	170
DBK83	TC/mV card with external screw-terminal Pod and 3 ft. cable	14 channels	170
DBK84	TC/mV module with mini TC connector jacks	14 channels	170
DBK85	Differential voltage input module	16 channels	172
DBK200	Adapter board for analog inputs	P1	199
DBK201	Panel-mount adapter board with three (DBK) expansion ports	P1, P2, P3	199
DBK202	Screw-terminal adapter board, solder locations for user-supplied resistors and R/C networks, with three expansion ports	120 terminals, P1, P2, P3	200
DBK203	Same as DBK202 adapter board with a rugged metal enclosure	120 terminals, P1, P2, P3	200
DBK206	Adapter board with removable screw-terminals with three expansion ports	120 terminals, P1, P2, P3	177
DBK207	5B-isolated analog input signal conditioning board with two expansion ports	P1 (2)	178
DBK207/CJC	Same as DBK207 plus on-board, cold-junction compensation; two expansion ports	P1 (2)	178
DBK208	Opto-22® signal conditioning board for isolated (solid-state-relay) digital I/O, with two P2 digital I/O expansion ports	P2 (2)	180
DBK209	Same as DBK201 but rack and DIN-rail mountable with optional kits	P1, P2, P3	199
DBK210	Isolated high-density digital I/O board	32 channels	182

Timer Outputs (P3)

Two 16-bit timer outputs are built into the DaqBoard/2000, each capable of generating different square waves with a programmable frequency range from 16 Hz to 1 MHz.

Multiple DaqBoards per PC

All of the features described for the DaqBoard/2000 can be replicated with up to four DaqBoard/2000s (PCI and cPCI) installed in the same PC. The serial number on each DaqBoard/2000 is used to differentiate one from another, and a user-selected name can be assigned to each board for easy program documentation. Thus, with four boards installed along with DBK expansion options, over 1,000 analog input channels and over 1,000 digital I/O channels could be accessed from one PC. When multiple boards are installed, all boards can be operated synchronously.

DBK17™

4-Channel Simultaneous Sample & Hold Card

Compatibility: ✓ LogBook ✓ DaqBook ✓ DaqLab ✓ DaqScan ✓ DaqBoard/2000 Series

Features

- Provides four input channels with simultaneous sample and hold
- Features a separate instrumentation amplifier and input stage for each channel
- One system accepts up to 64 DBK17 cards for a total of 256 simultaneously sampled inputs
- All channels sampled within 100 ns of one another

The DBK17™ simultaneous sample and hold* card allows IOtech's data acquisition systems to capture multiple input channels concurrently in order to eliminate channel-to-channel time skewing. Each DBK17 provides four channels of differential voltage input. The 16 analog input channels of the data acquisition systems can each accept up to four DBK17 cards, for a total of 256 analog input channels with simultaneous sampling. When multiple DBK17 cards are in use, all channels on all cards are sampled at the same instant.

Each of the DBK17's four channels features an instrumentation amplifier with switch-selectable gains of x1, 10, 100, 200, and 500. Each channel is also equipped with a location for a user-selected gain resistor, allowing you to select a custom gain up to x500. Each of the instrumentation amplifier input stages are followed by separate sample-and-hold stages whose outputs are connected to an output multiplexer stage. You can connect up to four DBK17s to one analog input channel.

The DBK17 is equipped with BNC input connectors. Its differential inputs are equipped with switchable 100K bias resistors referenced to analog common.

See DBK45 for SS&H plus low-pass filter

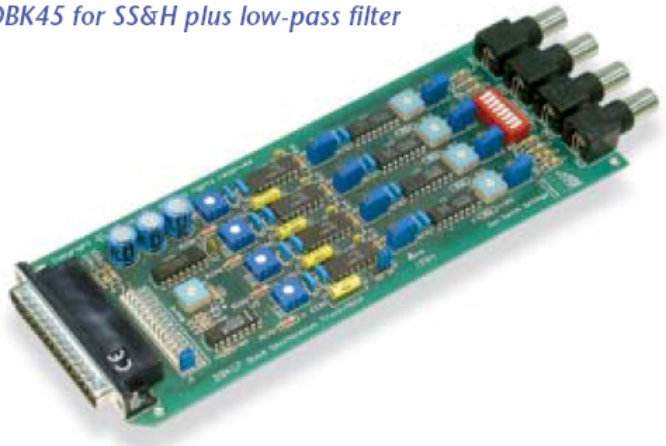

The DBK17 allows systems to capture multiple input channels simultaneously

DBK17 Simultaneous Sample & Hold Card Block Diagram

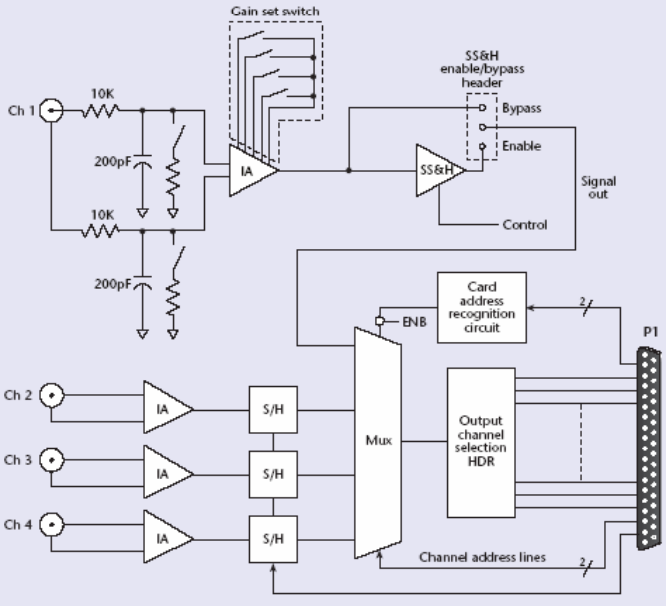

Note: Ch 1 is typical of Ch 2, Ch 3, and Ch 4

* In systems incorporating DBK products with SS&H, the per-channel rate is [Maximum sample rate/(n + 1)], where n=number of channels

PC Data Acquisition Hardware

DBK17™

Specifications & Ordering Information

Specifications

Connector: DB37 male, mates with P1*; BNC connectors provided for signal inputs
Number of Channels: 4
Number of Cards Addressable: 64
Input Type: Differential
Voltage Input Ranges:
0 to ±5 VDC
0 to ±500 mVDC
0 to ±25 mVDC
0 to ±10 mVDC
For Custom Gains:

$$R_{user} = \frac{40{,}000}{Gain\text{-}1} - 80 \quad (Ohms)$$

Input Amplifier Slew Rate: 12 V/∝s min
Acquisition Time: 0.6 ∝s (10V excursion to 0.1%); 0.7 ∝s (10V excursion to 0.01%)
Channel-to-Channel Aperture Uncertainty: 50 ns
Output Droop Rate: 0.1 ∝V/∝s
Bandwidth: 72.4 kHz
Input Gains: x1, 10, 100, 200, 500, and user determined up to 500
Input Offset Voltage: [500 + 5000/G] ∝V max (nullable)
Input Offset Drift: [±5 + 100/G] ∝V/°C max
Input Bias Current: 100 pA max
Input Offset Current: 50 pA max
Input Impedance: 5 x 10^{12} Ohms parallel with 6 pF
Switchable Bias Resistors: 100K each to analog common
Gain Errors:

x1	±0.04% max
x10	±0.1% max
x100	±0.2% max
x200	±0.4% max
x500	±1.0% max

Gain vs. Temperature:

x1	±20 ppm/°C max
x10	±20 ppm/°C max
x100	±40 ppm/°C max
x200	±60 ppm/°C max
x500	±100 ppm/°C max

Non-Linearity:

x1	±0.015% FS max
x10	±0.015% FS max
x100	±0.025% FS max
x200	±0.025% FS max
x500	±0.045% FS max

Common-Mode Rejection:

x1	70 dB min
x10	87 dB min
x100	100 dB min
x200	100 dB min
x500	100 dB min

Note: For simultaneous sample and hold with anti-alias filter, see DBK45.

Power Consumption: 905 mW

Ordering Information

Description	Part No.
4-channel simultaneous sample and hold card	DBK17

Cables

For use with DBK10, use CA-37-x ribbon cable, or contact factory of additional cabling options
For use with DBK60 or LogBook360, no cable is required (except from DBK60 or LogBook/360 to the A/D mainframe)
For use with no enclosure, use CA-37-x where x is the number of DBK devices attached
For use with DaqLab series (internal slots), use CA-255-2T with one board, or CA-37-2 for use with two DBK cards (or contact factory for additional cabling options)

For complete information on accessories and cables, visit **www.iotech.com/acc**

Related Products

LogBook	p. 75
DaqBook	p. 89
DaqLab	p. 103
DaqScan	p. 108
DBK10	p. 126
DBK41	p. 146
DBK45	p. 154
DBK60	p. 160
DaqBoard/2000 Series	p. 192

* Attachment to the DaqBoard/2000 series requires a DBK200, DBK201, DBK202, DBK203, DBK205, or DBK209 adapter

CompuScope 1602

Ultra-fast waveform digitizer card for PCI bus

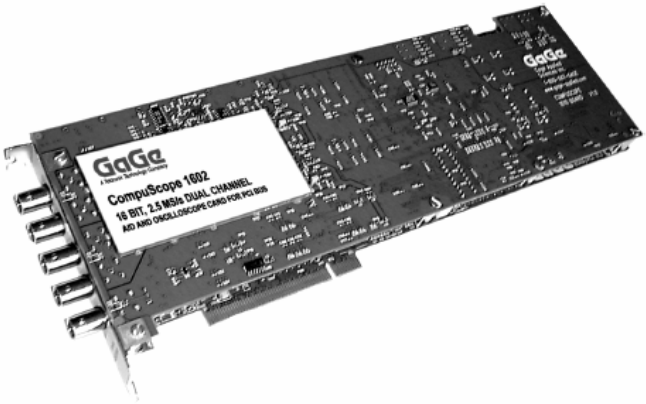

Lower cost alternative for high precision measurements.

FEATURES

- 16 bit, 2.5 MS/s A/D sampling on two simultaneous channels
- Differential or single-ended inputs
- Up to 1 GigaSamples of on-board acquisition memory
- 75 dB signal to noise ratio
- Multi-card systems of up to 16 simultaneous channels at 2.5 MS/s
- Fast data transfer rate to system RAM
- GageScope compatible
- SDKs for C/C++, MATLAB, LabVIEW

APPLICATIONS

Non-destructive testing
Military & Aerospace
Communications & wireless
Electro-optic
Radar
Laser
High energy physics
Embedded digitizer

GaGe
www.gage-applied.com

COMPUSCOPE 1602

A CompuScope 1602 card for PCI bus can simultaneously sample two analog signals at speeds up to 2.5 MS/s with 16 bit resolution and store the data in the on-board memory.

16 BIT 2.5 MS/S SAMPLING

CompuScope 1602 uses state-of-the-art data conversion technology to provide dual-channel simultaneous sampling rate of 2.5 MS/s with 16 bit resolution. Each channel has its own ADC chip, eliminating the need for multiplexing the inputs.

DIFFERENTIAL INPUTS

Differential inputs allow the user to fully exploit the 16-bit A/D of the CompuScope 1602. Differential input circuitry automatically eliminates noise picked up by the signal and its reference. With over 80 dB CMRR (Common Mode Rejection Ratio) for low frequency inputs, differential inputs eliminate any ground loop problems.

Single-ended inputs are also available through a simple software command. This command simply connects the negative input of the differential pair to zero volts, allowing single-ended operation.

HIGH IMMUNITY TO DIGITAL NOISE

In order to isolate the high-frequency analog circuitry from PCI bus–related digital electronics, a two-board piggyback configuration is used. This allows maximum separation of analog and digital grounds, thereby providing high immunity to digital noise.

MEMORY DEPTH

CompuScope 1602 is available with memory depths of 1M, 4M, 8M, 64M, 256M, 512M and 1G (16-bit samples). This memory can be used as a circular buffer for storage of pre- and post-trigger data.

Memory is divided equally between the two input channels, i.e. a 1 Meg board provides 512 Ksamples of memory per channel.

The data stored in the CompuScope 1602 memory can be transferred to the system RAM for post-processing, display or storage to hard disk without any interface bus (no GPIB bus required).

FLEXIBLE TRIGGERING

CompuScope 1602 features flexible, oscilloscope-like analog triggering.

An analog comparator provides triggering from any one of the two input channels, from an external signal or from software.

In addition to the trigger source, trigger level and slope are also selectable by software, making the trigger system similar to traditional oscilloscopes.

BUILT-IN DECIMATION FILTER

CompuScope 1602 uses a unique architecture to provide 16 bit resolution. The input signal is over-sampled by a factor of 8 and the resulting data stream is fed into an on-chip decimation filter and error-correction circuitry which enhances the effective resolution and dynamic range by eliminating high frequency noise and by providing the lower order bits of the digital output.

EXTERNAL CLOCK UPGRADE

An external clock upgrade can be ordered if A/D sampling must be coherent with a system clock. The external clock must be 8 times faster than the required sample rate, i.e. if 1 MS/s sampling is required, external clock must be 8 MHz.

The External Clock must be a TTL signal with a maximum frequency of 20 MHz and minimum frequency of 8 kHz.

The rise and fall times of the clock signal must be better than 8 ns for proper operation at the peak sample rates. A minimum pulse width of 22.5 ns must be respected.

MULTIPLE RECORD

Even though the PCI bus allows very fast data throughput to system RAM, there may still be applications in which data bursts cannot be off-loaded either due to very fast trigger repeat frequency or due to software limitations.

Multiple Recording allows CS1602 to capture data on successive triggers and stack it in the on-board memory. Up to 4,194,304 triggers can be captured in multiple record mode.

Once the CompuScope 1602 finishes capturing a Multiple Record segment, the trigger circuitry is automatically re-armed within 5 sample clock cycles to start looking for the next trigger - with no software intervention.

MULTI-CARD SYSTEMS

A Multi-Card system, comprised of one Master and up to 7 Slave CS1602 boards, can be ordered from the factory if the user wants to capture more than two channels with a common clock and trigger. A board-to-board interconnect is supplied with the system. This interconnect carries all the signals needed for proper synchronization. Refer to the detailed spec for available configurations for different memory models.

GageScope can then display all channels from these boards on the same screen.

ORDERING INFORMATION

Hardware & Upgrades

CompuScope 1602-1M	162-001-001
CompuScope 1602-4M	162-001-002
CompuScope 1602-8M	162-001-003
CompuScope 1602-64M	162-001-004
CompuScope 1602-256M	162-001-005
CompuScope 1602-512M	162-001-006
CompuScope 1602-1G	162-001-007
CS1602 Memory Upgrade Charge	162-181-200
External Clock Upgrade	162-181-004
Master Multi-Card Upgrade	162-181-006
Slave Multi-Card Upgrade	162-181-007

GageScope Software

GageScope: Lite Edition	included
GageScope: Standard Edition *(with Purchase of CompuScope Hardware)*	300-100-351
GageScope: Professional Edition *(with Purchase of CompuScope Hardware)*	300-100-354

Software Development Kits (SDKs)

Gage SDK Pack on CD	200-113-000
CompuScope SDK for C/C++	200-200-101
CompuScope SDK for MATLAB	200-200-102
CompuScope SDK for LabVIEW	200-200-103

All Upgrades performed at the factory.

COMPUSCOPE 1602 SPECIFICATIONS

SYSTEM REQUIREMENT

PCI-based computer with at least one free full length PCI slot, 128 MB RAM, 50 MB hard disk and SVGA video.

SIZE

Plugs into 1 full length PCI Slot, 13" x 4.1"

Memory Depth:	Board Width occupies:
1M	1 full length slot
4M and 8 M	2 full length slots
64M, 256M	3 full length slots
512M, 1G	3 full length slots

POWER (IN WATTS)

Memory	+5 V	
	Worst	Typical
1 M	25.0	17.5
4 M	28.0	20.5
8 M	28.0	20.5
64 M	30.0	21.5
256 M	32.5	23.5
512 M	32.5	23.5
1 G	32.5	23.5
- 5V		
	Worst	Typical
All Models	0.0	0.0
+12 V		
	Worst	Typical
All Models	0.0	0.0
-12 V		
	Worst	Typical
All Models	0.0	0.0

CHANNELS A & B

Inputs per card: 2 differential inputs

Impedance: 1 MΩ, 35 pF or 50 Ω, software selectable

Coupling: AC or DC

Resolution: 16 bits

A/D Type: Monolithic, 16 bit oversampling with decimation filter

Analog Bandwidth: DC to 4 MHz (DC) 10 Hz to 4 MHz (AC) DSP FIR filter limits the signal bandwidth to Nyquist Frequency

Full Scale Single-Ended Input Range: ±500mV, ±1V, ±2V, ±5V, ±10V

Common Mode Input Voltage: ±7.5V (DC+peak AC)max

Common Mode Rejection Ratio: 80 dB at 60 Hz

Absolute Max. Amplitude: 1 MΩ Impedance: ±15 Volts (continuous) 50 Ω Impedance: ±5 Volts (continuous) ±15 Volts (for 1 ms duration)

DC Accuracy relative to Full Scale Input: ±0.5% of full scale input

Sampling Rate: MS/s: 2.5, 1 kS/s: 500, 200, 100, 50, 20,10, 5, 2, 1

Protection: 1 MΩ: Diode Clamped 50 Ω: No protection

Connector: 2 BNCs per input

DYNAMIC PARAMETERS

Measured using 98 KHz sine wave input at 2.5 MS/s with amplitude of 95% of full scale on the ±1V range. Typical values listed below:

SNR: 75 dB

SFDR: 77 dB

SINAD: 74 dB

THD: -76 dB

ENOB: 12.15 bits

ACQUISITION MEMORY

Data Storage: In on-board memory

Memory Depth: 1M, 4M, 8M, 64M, 256M, 512M, 1G

Max. Depth: Up to half on-board memory per channel

TRIGGERING

of Trigger Inputs: 2 per card

Trigger Source: CH A, CH B, Ext or Software

Input combination: Wired-OR

Type: Analog triggering

Sensitivity: ±20% of full scale

Level Accuracy: ±10% of full scale

Slope: Positive or Negative, software selectable

Post Trigger Data: 64 points minimum in single record acquisition. 128 points minimum in multiple record acquisition. Can be defined with 64 point resolution.

EXTERNAL TRIGGER

Impedance: 1 MΩ, 30 pF

Input Type: Single-ended analog

Amplitude: Absolute Max ±15V

Voltage Range: ±1V and ±5V

Bandwidth: 10 MHz

Connector: BNC

EXTERNAL CLOCK (OPTIONAL)

Max. Freq.: 20 MHz, max. using 8x decimation filter.

Min. Freq.: 8 kHz

Signal Level: TTL

Required Duty Cycle: 50% ±5% at 20 MHz

MULTIPLE RECORD

Pre-trigger Data: 20 points

Record Length: 128 points minimum. Can be defined with a 64 point resolution

Max # of Triggers: 4,194,304

MULTI-CARD SYSTEMS

Operating Mode: Master/Slave or Multiple Independent

Number of Cards in:

- Master/Slave Mode:
  - 1M models: 2, 4, 6 or 8 cards
  - 4M & 8M models: 2, 3 or 4 cards
  - 64M and higher models: 2 or 3 cards
- Multiple Ind.: Limited by backplane

OPERATING SYSTEMS

Windows 95/98/ME/NT*/2000/XP

*version 4, SP3 or higher

ELECTROMAGNETIC COMPATIBILITY

CE Compliant

EC Council Directive 89/336/EEC

EN 61326 Class A

IEC 61000-4-2 Electrostatic Discharge (Perf.Crit.B)
IEC 61000-4-3 RF Electromagnetic Field (Perf.Crit.A)
IEC 61000-4-4 Electrical Fast Transient/Burst (Perf.Crit. B)
IEC 61000-4-5 Power Surge (Perf.Crit.B)
IEC 61000-4-6 Conducted RF (Perf.Crit.A)
IEC 61000-4-11 Voltage Dips & Interruptions (Perf.Crit B)
EN 61000-3-2 AC Power Line Harmonics Emissions

AS/NZS 2064

Australian emissions standard for Industrial, Scientific & Medical Equipment

Compliance demonstrated on a single card configuration

WARRANTY

One year parts and labor

All specifications subject to change without notice

Specification Last Updated: February 2003

Appendix A.2: Sensors

Acceleration - AAS

KISTLER
measure. analyze. innovate.

Piezotron®

Type 8152B...

Acoustic Emission Sensor

Piezotron Acoustic Emission Sensor with an integral impedance converter for measuring acoustic emission (AE) above 50 kHz in machine structures. With its small size it mounts easily near the source of emission to optimally capture the signal. The sensor has a very rugged welded housing (degree of protection IP 65 PUR or IP 67 Viton). The small sensor is easily mounted nearly everywhere; an M6 or 1/4-28 bolt is all that is needed.

- High sensitivity and wide frequency range
- Inherent highpass-characteristic
- Insensitive to electric and magnetic noise fields
- Robust, for industrial use (IP65 (PUR), IP67 (Viton))
- Ground isolated: Prevents ground loops
- Conforming to CE

Description

The Piezotron AE Sensor consists of the sensor housing, the piezoelectric sensing element and the built-in impedance converter. The sensing element, made of piezoelectric ceramic, is mounted on a thin steel diaphragm. Its construction determines the sensitivity and frequency response of the sensor. The coupling surface of the diaphragm welded into the housing is slightly protruding to measure the AE signals. Thus a precisely defined coupling force results when mounting. This assures a constant and reproducible coupling for the AE transmission. The sensing element is acoustically isolated from the housing by design and therefore well protected against external noise. The Kistler AE sensors feature a very high sensitivity for surface (Rayleigh) and longitudinal waves over a broad frequency range. Type 8152B1... covers 50 ... 400kHz and Type 8152B2... covers 100 ... 900 kHz. A miniature impedance converter is built into the Piezotron AE Sensor, giving an output low-impedance voltage signal. The AE Piezotron Coupler Type 5125B1, is used to supply power to the sensor and for signal processing. Special highly insulating and low noise connecting cables are not required.

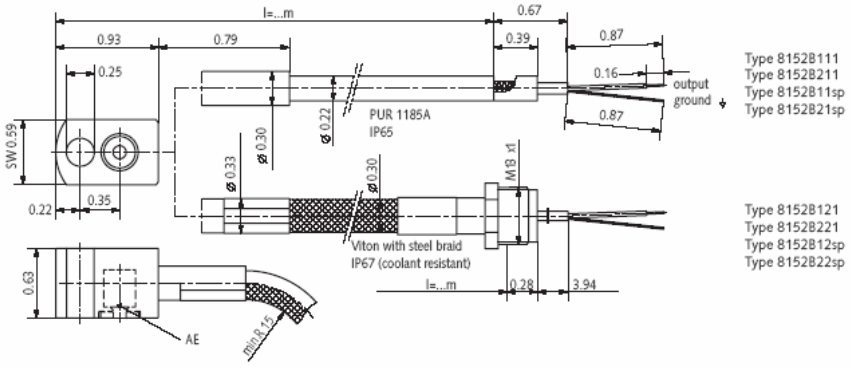

8152B_000-204a-03.05

Acoustic Emission Sensor, Type 8152B...

KISTLER
measure. analyze. innovate.

Technical Data

Type	Units	8152B111 8152B121	8152B11sp 8152B12sp	8152B211 8152B221	8152B21sp 8152B22sp
Sensitivity	dBref 1V/(m/s)	57	57	48	48
Frequency Range ±10dB	kHz	50 ... 400	50 ... 400	100 ... 900	100 ... 900
Environmental:					
Shock Limit (0.5ms pulse)	gpk	2000	2000	2000	2000
Temperature Range Operating	°F	-40 ... 140	-40 ... 140	-40 ... 140	-40 ... 140
Output:					
Bias nom.	VDC	2.2	2.2	2.5	2.5
Impedance	Ω	<10	<10	<10	<10
Voltage full scale	V	±2	±2	±2	±2
Current	mA	2	2	4	4
Source:					
Voltage (Coupler)	VDC	5 ... 36	5 ... 36	5 ... 36	5 ... 36
Constant Current	mA	3 ... 6	3 ... 6	3 ... 6	3 ... 6
Construction:					
Sensing Element	type	ceramic	ceramic	ceramic	ceramic
Housing/Base	material	stainless steel	stainless steel	stainless steel	stainless steel
Sealing-housing/connector	type	hermetic	hermetic	hermetic	hermetic
Weight (without cable)	grams	29	29	29	29

1 g = 9.80665 m/s², 1 inch = 25.4 mm, 1 gram = 0.03527 oz, 1 lbf-in = 0.1129 Nm

Application

The AE Sensor is especially well suited for measuring AE above 50 kHz in the surface of metallic components or structures. Such AE results from plastic deformation of materials, crack formation and growth, fracturing or friction. Application examples are monitoring of processes, tools and machines in metal cutting as well as forming operations. Thanks to its rugged construction and the tightly welded housing this sensor can operate under severe environmental conditions.

Ordering Key

8152B □

Variants	
PUR, 5m (50 ... 400kHz)	111
PUR, 0.3 ... 10m (50 ... 400kHz)	11sp
PUR, 5m (100 ... 900kHz)	211
PUR, 0.3 ... 10m (100 ... 900kHz)	21sp
Viton, 2m (50 ... 400kHz)	121
Viton, 0.3 ... 3m (50 ... 400kHz)	12sp
Viton, 2m (100 ... 900kHz)	221
Viton, 0.3 ... 3m (100 ... 900kHz)	22sp

Accessories Included	Type
• mounting screw, 1/4-28 x 1in	431-0500-001
• mounting screw, M6 x 25mm	431-0497-001

Optional Accessories	Type
• Magnetic clamp	8443B
• Piezotron AE coupler	5125B

8152B_000-204a-03.05

KISTLER
measure. analyze. innovate.

Mounting

The AE Sensor is simply mounted with an M6-1/4 screw or a magnetic clamp Type 8443B onto the surface of the structure. A minimum tightening torque is sufficient for a reproducible and constant coupling. The smoother the mounting surface, the better the result. The use of a highly viscous grease (e.g. silicone grease) between the coupling surfaces is recommended.

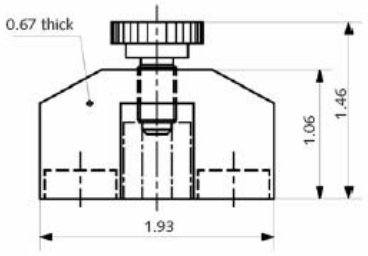

Type 8443B Magnetic clamp

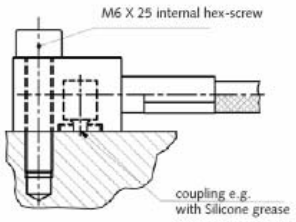

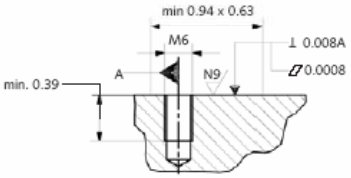

Mounting AE-Sensor

8152B_000-204a-03.05

KISTLER
measure. analyze. innovate.

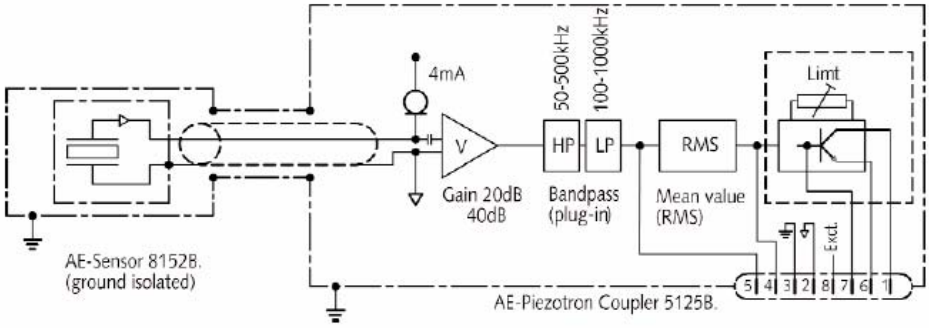

Frequenzgang / Réponse en fréquence / Frequency response

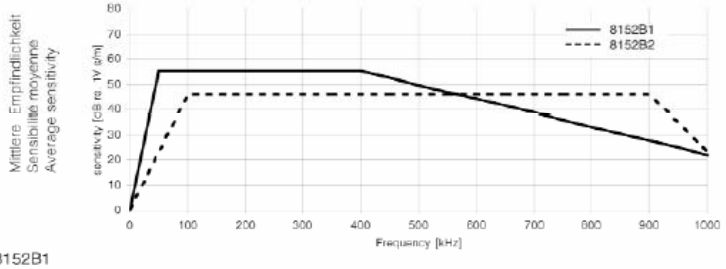

Type 8152B1

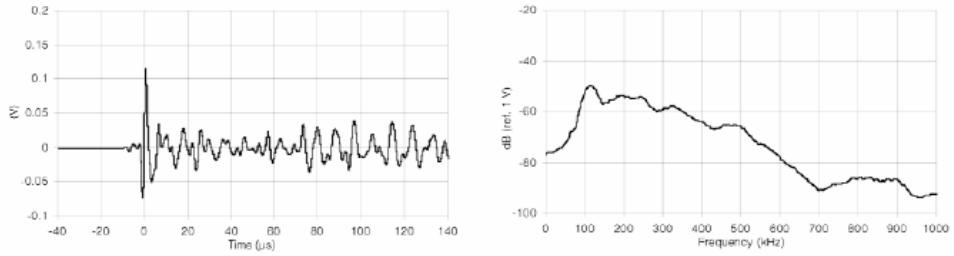

Type 8152B2

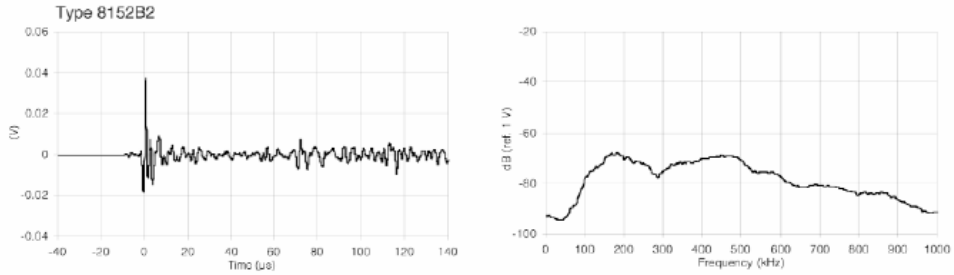

8152B_000-204a-03.05

PRODUCT DATA

Piezoelectric Accelerometer
Charge Accelerometer — Type 4370, 4370 S and 4370 V

FEATURES

- General purpose
- High sensitivity
- Low-level, low-frequency measurements

Description

Type 4370 is a piezoelectric, DeltaShear®, Unigain® accelerometer with top connector. Type 4370 features 10–32 UNF receptacle for output connection and can be mounted on the object by means of a 10–32 UNF threaded steel stud.

Characteristics

This piezoelectric accelerometer may be treated as a charge source. Its sensitivity is expressed in terms of charge per unit acceleration (pC/g).

The DeltaShear design involves three piezoelectric elements and three masses arranged in a triangular configuration around a triangular centre post. The ring prestresses the piezoelectric elements to give a high degree of linearity. The charge is collected between the housing and the clamping ring. The piezoelectric element used is a PZ 23 lead zirconate titanate element. The housing material is stainless steel.

Calibration

The sensitivity given in the calibration chart has been measured at 159.2 Hz and an acceleration of 10 g. For 99.9% confidence level, the accuracy of the factory calibration is ±2%.

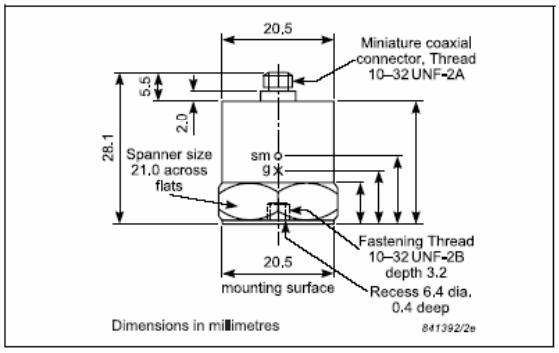

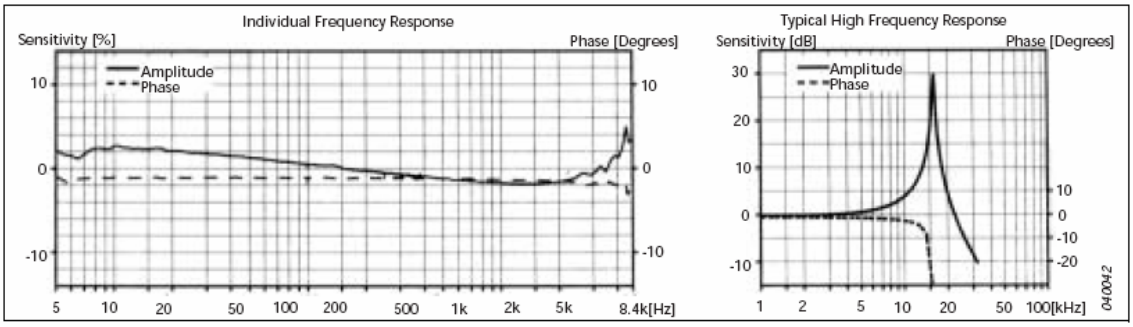

Brüel & Kjær

Specifications – Charge Accelerometer Type 4370, 4370 S and 4370 V

	Units	4370/4370 S	4370 V
Dynamic Characteristics			
Charge Sensitivity (@ 159.2 Hz)	pC/g	98 ± 2%	98 ± 15%
Frequency Response		See typical Amplitude Response	
Mounted Resonance Frequency	kHz	16	
Amplitude Response ±10% [1]	Hz	0.1 to 4800	
Transverse Sensitivity	%	<4	
Transverse Resonance Frequency	kHz	10	
Electrical Characteristics			
Min. Leakage Resistance @ 20°C	GΩ	≥20	
Capacitance	pF	1200	
Grounding		Signal ground connected to case	
Environmental Characteristics			
Temperature Range	°C (°F)	–74 to 250 (–101 to 482)	
Humidity		Welded	
Max. Operational Sinusoidal Vibration (peak)	g pk	2000	
Max. Operational Shock (± peak)	g pk	2000	
Base Strain Sensitivity	Equiv. g/μ strain	0.003	
Thermal Transient Sensitivity	Equiv. g/°C (g/°F)	0.002 (0.011)	
Magnetic Sensitivity (50 Hz–0.03 Tesla)	g/T	0.1	
Physical Characteristics			
Dimensions		See outline drawing	
Weight	gram (oz.)	54 (1.89)	
Case Material		Stainless steel	
Connector		10–32 UNF	
Mounting		10–32 UNF × 5 mm threaded hole	

[1] Low-end response of the transducer is a function of its associated electronics

Ordering Information

Type 4370 includes the following accessories:
- Carrying box
- Calibration chart
- AO 0038: Low noise cable fitted with 10–32 connectors, 1.2 m
- 10–32 UNF threaded steel stud. Length 12.7 mm

Type 4370 S includes the following accessories:
- Carrying box
- Calibration chart
- AO 0038: Low noise cable fitted with 10–32 connectors, 1.2 m
- 10–32 UNF threaded steel stud. Length 12.7 mm
- UA 0078: Accessory box including:
  - Cementing stud, 10–32 UNF
  - EP610 input adaptor, TNC to 10–32 UNF microdot
  - Mounting magnet, 10–32 UNF thread
  - Case of beeswax
  - Insulating disk
  - Insulating stud
  - Steel stud 10–32 UNF × ½"
  - Tools

Type 4370V includes the following accessories:
- Carrying box
- Calibration chart
- 10–32 UNF threaded steel stud. Length 12.7 mm

OPTIONAL ACCESSORIES
- AO 0038: 260°C Teflon® low-noise cable, 10–32 UNF, length 1.2 m (4 ft)
- AO 0122: 250°C, reinforced super low noise cable, 10–32, 3 m (10 ft)
- AO 0231: 260°C Teflon low-noise cable, 10–32 UNF/TNC, length 3 m (10 ft)
- AO 1382: Teflon low noise cable, double screened 10–32, 1.2 m (4 ft)
- DB 0544: 10–32 UNF Round tip
- JJ 0207: 2-pin TNC/10–32 UNF plug adaptor
- JP 0162: 10–32 UNF to TNC connector adaptor
- QA 0013: Hexagonal key for 10–32 UNF studs
- QA 0029: Tap for 10–32 UNF thread
- UA 0559: Mechanical filter for Accelerometer
- UA 0641: Extension Connector, 10–32 UNF/TNC (only top connector accelerometer)
- UA 0642: Mounting magnet and 2 insulating discs
- UA 0866: Cement stud 10–32 UNF 0.14 mm (set of 25)
- YG 0150: Steel stud 10–32/10–32 with flange
- YJ 0216: Beeswax for mounting
- YP 0080: Probe with sharp tip
- YP 0150: 10–32 UNF insulated stud. Length 12.7 mm
- YQ 2960: 0–32 UNF threaded steel stud. Length 12.7 mm
- YQ 2962: 0–32 UNF threaded steel stud. Length 7.62 mm

BP 2035 – 11 04/04 Rosendahls Bogtrykkeri

PRODUCT DATA

Piezoelectric Accelerometer
Charge Accelerometer — Type 4371, 4371 S and 4371 V

FEATURES

- General purpose
- High sensitivity
- High frequency
- Vibration testing

Description

Type 4371 is a piezoelectric, DeltaShear®, Unigain® accelerometer with side connector. Type 4371 features 10–32 UNF receptacle for output connection and can be mounted on the object by means of a 10–32 UNF threaded steel stud.

Characteristics

This piezoelectric accelerometer may be treated as a charge source. Its sensitivity is expressed in terms of charge per unit acceleration (pC/g).

The DeltaShear design involves three piezoelectric elements and three masses arranged in a triangular configuration around a triangular centre post. The ring prestresses the piezoelectric elements to give a high degree of linearity. The charge is collected between the housing and the clamping ring. The piezoelectric element used is a PZ 23 lead zirconate titanate element. The housing material is titanium.

Calibration

The sensitivity given in the calibration chart has been measured at 159.2 Hz and an acceleration of 10 g. For 99.9% confidence level, the accuracy of the factory calibration is ±2%.

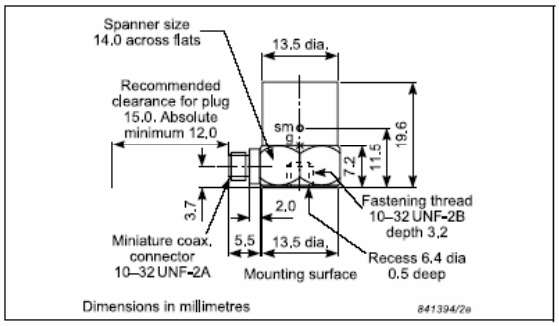

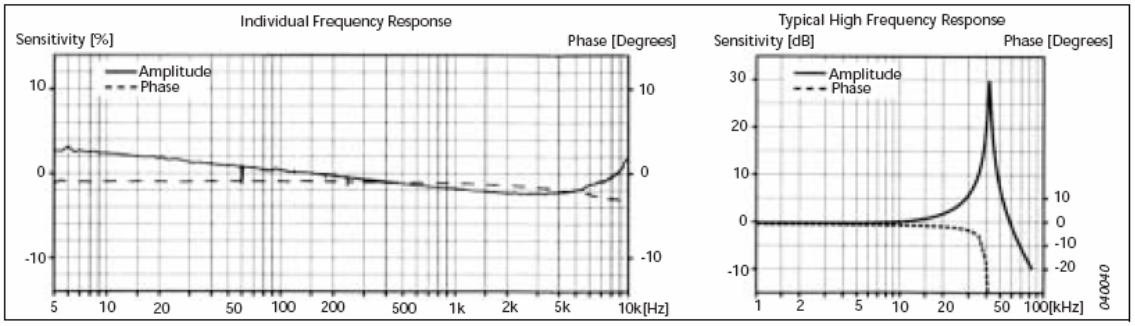

Brüel & Kjær

Specifications – Charge Accelerometer Type 4371, 4371 S and 4371 V

	Units	4371/4371 S	4371 V
Dynamic Characteristics			
Charge Sensitivity (@ 159.2 Hz)	pC/g	9.8 ± 2%	9.8 ± 15%
Frequency Response		See typical Amplitude Response	
Mounted Resonance Frequency	kHz	42	
Amplitude Response ±10% [1]	Hz	0.1 to 12600	
Transverse Sensitivity	%	<4	
Transverse Resonance Frequency	kHz	15	
Electrical Characteristics			
Min. Leakage Resistance @ 20°C	GΩ	≥20	
Capacitance	pF	1200	
Grounding		Signal ground connected to case	
Environmental Characteristics			
Temperature Range	°C (°F)	–74 to 250 (–101 to 482)	
Humidity		Welded, sealed	
Max. Operational Sinusoidal Vibration (peak)	g pk	6000	
Max. Operational Shock (± peak)	g pk	20000	
Base Strain Sensitivity	Equiv. g/μ strain	0.002	
Thermal Transient Sensitivity	Equiv. g/°C (g/°F)	0.004 (0.022)	
Magnetic Sensitivity (50 Hz–0.03 Tesla)	g/T	0.4	
Physical Characteristics			
Dimensions		See outline drawing	
Weight	gram (oz.)	11 (0.39)	
Case Material		Titanium	
Connector		10–32 UNF	
Mounting		10–32 UNF × 3.2 mm threaded hole	

[1] Low-end response of the transducer is a function of its associated electronics

Ordering Information

Type 4371 includes the following accessories:
- Carrying box
- Calibration chart
- AO 0038: Low noise cable fitted with 10–32 connectors, 1.2 m
- 10–32 UNF threaded steel stud. Length 12.7 mm

Type 4371 S includes the following accessories:
- Carrying box
- Calibration chart
- AO 0038: Low noise cable fitted with 10–32 connectors, 1.2 m
- 10–32 UNF threaded steel stud. Length 12.7 mm
- UA 0078: Accessory box including:
  - Cementing stud, 10–32 UNF
  - EP610 input adaptor, TNC to 10–32 UNF microdot
  - Mounting magnet, 10–32 UNF thread
  - Case of beeswax
  - Insulating disk
  - Insulating stud
  - Steel stud 10–32 UNF × ½"
  - Tools

Type 4371 V includes the following accessories:
- Carrying box
- Calibration chart
- 10–32 UNF threaded steel stud. Length 12.7 mm

OPTIONAL ACCESSORIES
- AO 0038: 260°C Teflon® low-noise cable, 10–32 UNF, length 1.2 m (4 ft)
- AO 0122: 250°C, reinforced super low noise cable, 10–32, 3 m (10 ft)
- AO 0231: 260°C Teflon low-noise cable, 10–32 UNF/TNC, length 3 m (10 ft)
- AO 1382: Teflon low noise cable, double screened 10–32, 1.2 m (4 ft)
- DB 0544: 10–32 UNF Round tip
- JJ 0207: 2-pin TNC/10–32 UNF plug adaptor
- JP 0162: 10–32 UNF to TNC connector adaptor
- QA 0013: Hexagonal key for 10–32 UNF studs
- QA 0029: Tap for 10–32 UNF thread
- UA 0559: Mechanical filter for Accelerometer
- UA 0642: Mounting magnet and 2 insulating discs
- UA 0866: Cement stud 10–32 UNF 0.14 mm (set of 25)
- YG 0150: Steel stud 10–32/10–32 with flange
- YJ 0216: Beeswax for mounting
- YP 0080: Probe with sharp tip
- YP 0150: 10–32 UNF insulated stud. Length 12.7 mm
- YQ 2960: 0–32 UNF threaded steel stud. Length 12.7 mm
- YQ 2962: 0–32 UNF threaded steel stud. Length 7.62 mm

HEADQUARTERS: DK-2850 Nærum · Denmark · Telephone: +45 4580 0500
Fax: +45 4580 1405 · www.bksv.com · info@bksv.com

Australia (+61) 2 9889-8888 · Austria (+43) 1 865 74 00 · Brazil (+55) 11 5188-8166
Canada (+1) 514 695-8225 · China (+86) 10 680 29906 · Czech Republic (+420) 2 6702 1100
Finland (+358) 9-755 950 · France (+33) 1 69 90 71 00 · Germany (+49) 421 17 87 0
Hong Kong (+852) 2548 7486 · Hungary (+36) 1 215 83 05 · Ireland (+353) 1 807 4083
Italy (+39) 0257 68061 · Japan (+81) 3 3779 8671 · Republic of Korea (+82) 2 3473 0605
Netherlands (+31) 318 55 9290 · Norway (+47) 66 77 11 55 · Poland (+48) 22 816 75 56
Portugal (+351) 21 47 11 453 · Singapore (+65) 377 4512 · Slovak Republic (+421) 25 443 0701
Spain (+34) 91 659 0820 · Sweden (+46) 8 449 8600 · Switzerland (+41) 1 880 7035
Taiwan (+886) 2 2502 7255 · United Kingdom (+44) 14 38 739 000 · USA (+1) 800 332 2040

Local representatives and service organisations worldwide

Brüel & Kjær

BP 2036 – 11 04/04 Rosendahls Bogtrykkeri

Appendix A.3: Amplifiers

Measure & Analyze – MCA

KISTLER

1 ... 4

Ladungsverstärker
Amplificateur de charge
Charge Amplifier

5011B...

Der netzbetriebene, mikroprozessorgesteuerte, einkanalige Ladungsverstärker Typ 5011B wandelt die von piezoelektrischen Sensoren abgegebene Ladung in proportionale Spannung um.

Hauptsächlicher Einsatzbereich ist das Messen mechanischer Grössen, z.B. Druck, Kraft oder Beschleunigung.

Wesentliche Merkmale des Gerätes sind die kontinuierliche Einstellbarkeit des Messbereichs von ±10 bis ±999'000 pC und die komfortable Einstellung der Parameter über eine zweizeilige LC-Anzeige. Die eingegebenen Werte bleiben auch bei einer Netzunterbrechung erhalten.

L'amplificateur de charge type 5011B monocanal, alimenté par secteur et commandé par microprocesseur transforme la charge électrique engendrée d'un capteur piézoélectrique en une tension proportionelle.

Cet amplificateur est essentiellement utilisé pour mesurer de grandeurs mécaniques, par exemple de pressions, de forces ou d'accélérations.

Les principales caractéristiques de cet appareil sont le réglage continu de la plage de mesure de ±10 à ±999'000 pC ainsi que le réglage des paramètres par l'intermédiaire d'un affichage à cristaux liquides à deux chiffres. En cas de coupure du courant, les paramètres restent mémorisés.

The mains-operated, microprocessor controlled one-channel charge amplifier Type 5011B converts the electrical charge yielded by piezoelectric sensors into a proportional voltage signal.

This amplifier serves mainly to measure mechanical quantities, e.g. pressure, force or acceleration.

The main features of the instrument are its continuous measuring range adjustment facility from ±10 to ±999'000 pC and convenient adjustment of the parameters with a two-line LC display. The values entered are retained in the event of an interruption in the power supply.

- Grosser Messbereich
  Gamme de mesure étendue
  Large measuring range
- Weiter Frequenzbereich
  Gamme de fréquence étendue
  Wide frequency range
- Automatische Nullpunktkorrektur
  Correction automatique du zéro
  Automatic zero correction
- Tiefpassfilter und Zeitkonstante einstellbar
  Possibilité de réglage du filtre passe-bas et des constantes de temps
  Adjustable low-pass filter and time constant
- Optimale Anpassung an das Messproblem durch verschiedene Optionen und Modifikationen
  Adaptation optimale aux conditions de mesure par le biais de différentes options et modifications
  Various options and modifications provide optimum adaptation to the measuring problem
- CE - konform
  Conforme au CE
  Conforming to CE

Als Option ist eine eingebaute IEEE-488 Parallel-Schnittstelle oder eine serielle Schnittstelle RS-232C erhältlich. Damit können alle Einstellwerte eingegeben bzw. abgefragt werden. Messdaten-Übertragung ist nicht möglich.

L'appareil est disponible en option avec une interface parallèle de type IEEE-488 incorporée ou une interface sérielle de type RS-232C. Ces interfaces permettent l'entrée ou l'appel de toutes les valeurs de consigne. Un transfert des données de mesure n'est pas possible.

A built-in IEEE-488 parallel interface or a serial RS-232C interface is available as an option. This enables all set values to be entered or queried. Transmission of data measured is not possible.

Mit der Zusatzbezeichnung ...Y38 hat das Gerät zusätzlich einen Kalibriereingang und ist auch für den Anschluss von Niederimpedanz-Sensoren (Piezotronsystem, ICP) geeignet.

Sous la référence 5011B complétée de ...Y38, cet amplificateur est équipé en supplément d'une entrée d'étalonnage, il a été par ailleurs modifié de manière à permettre le branchement de capteurs de basse impédance (système Piezotron, ICP).

The additional designation ...Y38 indicates that the instrument also has a calibration input and is modified for the connection of low-impedance sensors (Piezotron system, ICP).

Die Abmessungen des Gerätes sind nach DIN genormt, es kann in einem Tischgehäuse eingebaut oder ohne Gehäuse zum Einbau in ein Racksystem geliefert werden.

Les dimensions de l'appareil sont conformes aux normes DIN. Il peut être livré dans un boîtier de table ou sans boîtier pour montage en rack.

The instrument dimensions are DIN standardized and it can be supplied in a table-mounted case or a case for mounting in a rack system.

Prinzip: Messen ohne Rechnen

- Sensorempfindlichkeit einstellen
- Anzeige-Massstab wählen
- Sensorempfindlichkeit und Massstab werden angezeigt
- Am Signalausgang angeschlossene Anzeigegeräte (Schreiber, Oszilloskop...) auf z.B. 1 V/Einheit (1 V/cm) einstellen
- Die Anzeige erfolgt gemäss des eingestellten Anzeige-Massstabs direkt in mechanischen Einheiten

Principe: Mesurer sans calcul

- Régler la sensibilité du capteur
- Sélectionner l'échelle d'affichage
- La sensibilité du capteur et l'échelle s'affichent
- Régler l'instrument d'affichage (enregistreur, oscilloscope...) branché sur la sortie du signal sur 1 V/unité (1 V/cm) par exemple
- L'affichage s'effectue alors directement en unités mécaniques conformément à l'échelle préalablement sélectionnée

Principle: Measurement without Calculation

- Set sensor sensitivity
- Select display scale
- Sensor sensitivity and scale are displayed
- Set the signal output of the indicator device connected (recorder, oscilloscope...), for example to 1 V/unit (1 V/cm)
- The display appears directly in mechanical units according to the display scale selected

5011B_000-296m-11.04

Kistler Instrumente AG Winterthur, CH-8408 Winterthur, Switzerland, Tel. (052) 224 11 11 Kistler Instrument Corp., Amherst, NY 14228-2171, USA, Phone (716) 691-5100

2

Technische Daten	Données techniques	Technical Data		
Grundgerät	*Appareil de base*	*Basic unit*		
Messbereich, für 10 V FS	Gamme de mesure, pour à 10 V FS	Measuring range, for 10 V FS	pC	±10 ... 999'000
Sensorempfindlichkeit	Sensibilité du capteur	Sensor sensitivity	pC/M.U.	0,01 ... 9990
Modifikation Y38, zusätzlich (M.U. = Mechanische Einheiten)	Modification Y38, en supplément (M .U. = unités mécaniques)	Modification Y38, in addition (M.U. = Mechanical)	mV/M.U.	0,01 ... 9990
Massstab	Echelle	Scale	M.U./V	0,001 ... 9'990'000
Ausgangsspannung	Tension de sortie	Output voltage	V	±10
Ausgangsstrom, max. (kurzschlusssicher)	Courant de sortie, maximal (protégé contre les court-circuits)	Output current, max. (short-circuit protected)	mA	±5
Ausgangswiderstand	Impédance de sortie	Output impedance	Ω	10
Frequenzbereich (–3dB, Filter "OFF")	Gamme de fréquence (–3dB, Filter "OFF")	Frequecy limit (–3dB, Filter "OFF")	kHz	≈ 0 ... 200
Tiefpassfilter	Filtre passe-bas	Low-pass filter		
obere Grenzfrequenz -3dB Butterworth 2-pol., 8-stufig (10, 30, 100...)	Seuil de fréquence supérieur -3dB Butterworth à 2 pôles, à 8 étages (10, 30, 100...)	upper cutoff frequency -3dB Butterworth, 2 pol., 8 stages (10, 30, 100...)	kHz (%)	0,01 ... 30 (±10)
Zeitkonstante (Hochpassfilter)	Constante de temps (filtre passehaut)	Time constant (high-pass filter)		
Long	*Long*	*Long*	-	DC-Mode
Medium ($T=R_g \cdot C_g$)	*Medium* ($T=R_g \cdot C_g$)	*Medium* ($T=R_g \cdot C_g$)	s	1 ... 10'000
Short ($T=R_g \cdot C_g$)	*Short* ($T=R_g \cdot C_g$)	*Short* ($T=R_g \cdot C_g$)	s	0,01 ... 100
Fehler	Erreur	Error		
<±100 pC FS (max./typ.)	<±100 pC FS (max./typ.)	<±100 pC FS (max./typ.)	%	<±3 / <±2
≥±100 pC FS (max./typ.)	≥±100 pC FS (max./typ.)	≥±100 pC FS (max./typ.)	%	<±1 / <±0,5
Linearität	Linéarité	Linearity	% FS	<±0,05
Ausgangsstörsignal 9,99 pC/V (1 pC/V)	Interférence à la sortie 9,99 pC/V (1 pC/V)	Output interference 9,99 pC/V (1 pC/V)	mV_{rms}	<0,5 (<1,5)
			mV_{pp}	<4 (<8)
Störsignal durch Eingangskabel-kapazität	Interférence due à la capacité d'entrée du câble	Interference due to cable capacitance	pC_{rms}/pF	$<2 \cdot 10^{-5}$
Drift bei 25 °C	Dérive à 25 °C	Drift at 25 °C	pC/s	<±0,07
Allgemeine Daten	*Caractéristiques générales*	*General Data*		
Betriebstemperaturbereich	Gamme de température de service	Operating temperature range	°C	0 ... 50
Anschlüsse	Connexions	Connections		
Messeingang / Signalausgang	Entrée de mesure/Sortie du signal	Measuring input / signal output	BNC negativ	
Fernsteuerung (Operate, Overload, ...)	Télécommande (Operate, Overload, ...)	Remote control (Operate, Overload, ...)	Buchse 6-pol DIN 45322	
Netzstecker	Fiche secteur	Power plug	IEC 320 C 14	
Konformität mit EG-Richtlinien	Conformité à la Directive CE	Conformity to EC Directive		
Sicherheit	Sécurité	Safety	EN 61010-1	
EMV - Störaussendung	CEM Emission	EMC Interference Emission	EN 50081-1 / EN 50081-2	
EMV - Störimmunität	CEM Immunité	EMC Interference Immunity	EN 50082-1 / EN 50082-2	
Netzanschluss, umschaltbar (Schutzklasse I)	Réseau, commutable (Classe de protection I)	Mains, switchable (Protection class I)	V AC (%)	230/115 (-22/+15)
			Hz (VA)	48 ... 62 (20)
Spannung zwischen Schutz- und Messerde	Tension entre terre de protection et terre de mesurage	Voltage between protection and measuring ground	V_{rms}	<50
Abmessungen	Dimensions	Dimensions		
mit Tischgehäuse Typ 5747A1	Boîtier de table type 5747A1	with table-mount. case Type 5747A1	mm	ca. 94x151x195
ohne Tischgehäuse	sans boîtier	without case	mm	70,9x128,7x169,5
Frontplatte, gemäss DIN 41494 (Teil 5)	Platine avant, conforme à la norme DIN 41494 (Partie 5)	Front panel according to DIN 41494 (Part 5)	HE/TE	3 /14
Gewicht (inkl. IEEE-488 oder RS-232C)	Poids (IEEE-488 ou RS-232C incl.)	Weight (incl. IEEE-488 or RS-232C)	kg	≈2
Modifikation Y38 (Piezotron- und Kalibrier-Eingang, umschaltbar)	*Modification Y38 (entrée Piezotron et entrée d'étalonnage, commutable)*	*Modification Y38 (Piezotron and calibration input, switchable)*		
Anschluss	Connexion	Connection	BNC negativ	
Als Piezotron-Eingang:	Entrée Piezotron:	As Piezotron input:		
Stromversorgung für Piezotronsensor	Alimentation en courant pour capteur Piezotron	Power supply for Piezotron sensor	mA (%)	4,3 (±10)
Als Kalibrier-Eingang:	Entrée d'étalonnage:	As calibration input:		
Kalibrierkondensator eingebaut	Condensateur d'étalonnage incorporé	Calibration capacitor built in	pF (%)	1000 (±0,5)
Empfindlichkeit Kalibr. Eingang	Sensibilité de l'entrée d'étalonnage	Sensitivity calib. input	pC/mV (%)	1 (±0,5)
Eingangsspannung	Tension d'entrée	Input voltage	V	≤±30

5011B_000-296m-11.04

Funktion
(siehe Funktionsschema)

Das zu messende Ladungssignal (Charge Input) wird dem invertierenden Verstärker (OP1) zugeführt, der sich durch hohe innere Verstärkung und extrem hohe Eingangsisolation auszeichnet. OP1 ist mit Cg kapazitiv gegengekoppelt und wirkt dadurch als Integrator für die zu messende Ladung. Der Kapazitätswert von Cg bestimmt dabei den Ladungsmessbereich nach der Näherungsformel Q = Cg • U1.

Fonctionnement
(voir schéma de fonctionnement)

Le signal de charge à mesurer (Charge Input) est acheminé à l'amplificateur inverseur (OP1). Cet amplificateur se distingue par une haute amplification interne et par un isolement d'entrée extrêmement élevé. OP1 est monté en contre-réaction avec le condensateur Cg et fonctionne de ce fait comme circuit d'intégration pour la charge à mesurer. La valeur de la capacité de Cg détermine la plage de mesure de la charge selon la formule d'approximation Q = Cg • U1.

Function
(see function diagram)

The charge signal to be measured (Charge Input) is fed to the inverting amplifier (OP1), which features high internal gain and extremely high input insulation. OP1 is negativ feedback to Cg and thus acts as an integrator for the charge to be measured. The Cg capacitance determines the charge measuring range according to the approximation formula Q = Cg • U1.

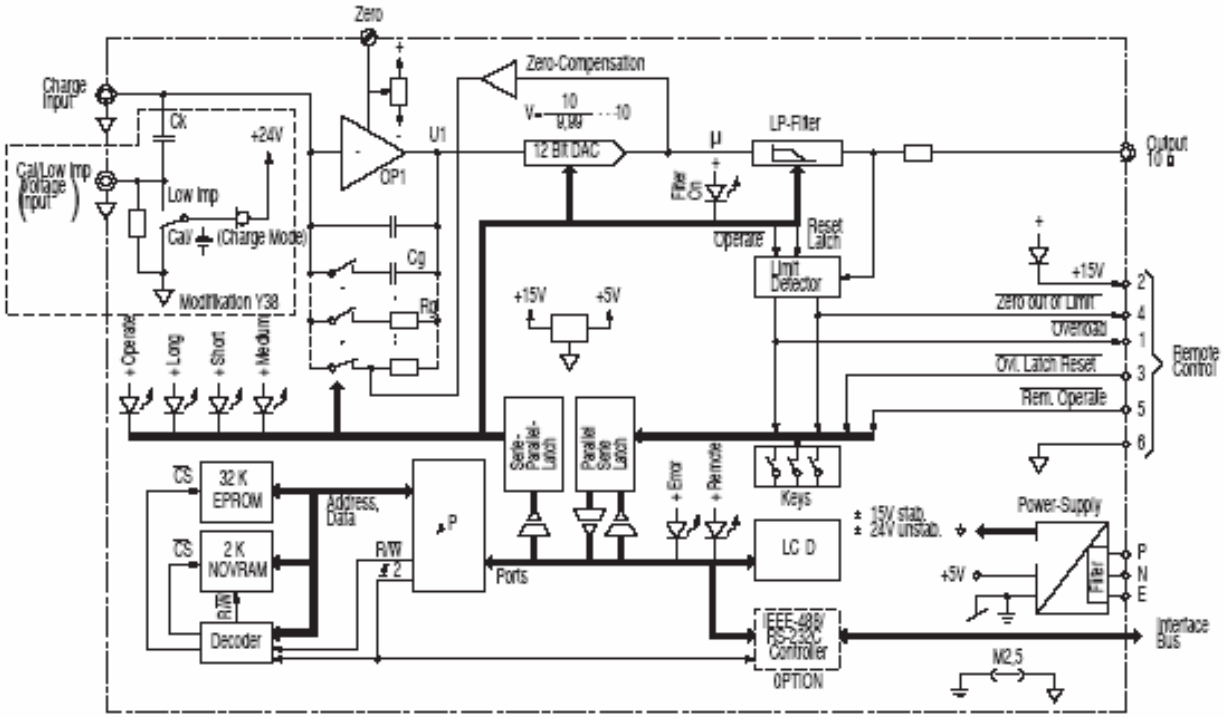

Am Ausgang von OP1 erscheint dann eine der Ladung und damit der mechanischen Messgrösse proportionale Spannung U1.

Wenn es sich um eine rein-dynamische Messung handelt, kann parallel zum Bereichskondensator Cg einer der beiden Zeitkonstantenwiderstände Rg eingeschaltet sein. Damit werden Driftprobleme, wie sie bei quasistatischen Messungen auftreten können, vermieden.

Ein Relaiskontakt im Gegenkopplungszweig von OP1 dient dazu, den Bereichskondensator Cg zu entladen und damit das Gerät für eine neue Messung vorzubereiten (Reset-Funktion, U1 → 0). Eine eventuell verbleibende Nullpunktabweichung wird von einer spezeiten Schaltung (Zero-Compensation) im Reset-Zustand kompensiert. Mit einem digitalen Spannungsteiler (12 Bit DAC) wird das Spannungssignal U auf den vom Gerät berechneten Wert gebracht.

Das in 8 Stufen einstellbare Tiefpassfilter (LP-Filter) erlaubt eine Reduktion der oberen Grenzfrequenz, falls die Applikation dies erfordert.

Eine 8-Bit Mikroprozessorschaltung (µP) steuert und überwacht das gesamte Gerät. Die Software ist in einem EPROM gespeichert, die Einstellwerte in einem batteriegepufferten NOVRAM.

Über die Fernsteueranschlüsse (Remote Control) sind, ohne optionelle Schnittstelle, folgende Funktionen möglich:

- Umschaltung Reset/Operate
- Overload-Signal zurücksetzen
- Anzeige: Overload
- Anzeige: Zero out of Limit

Das modifizierte Gerät 5011BxxY38 hat zusätzlich einen BNC-Signaleingang für Piezotronsensoren (Low Imp./Cal.), einen Umschalter "Low Imp./ Cal.", eine 4,3 mA Stromquelle sowie einen 1 nF Kalibrierkondensator. Dieser Kondensator dient einerseits der Umsetzung des Spannungssignals eines Piezotronsensors in ein Ladungssignal, andererseits kann mit Hilfe einer externen Spannungsquelle die Kalibrierung des Gerätes überprüft werden.

A la sortie d'OP1 apparaît alors une tension U1 proportionnelle à la charge et donc à la grandeur mécanique à mesurer.

S'il s'agit d'une mesure purement dynamique, l'une des deux résistances de la constante de temps Rg peut être montée en parallèle avec le condensateur de plage Cg. Ceci permet d'éviter les problèmes de dérive du type de ceux susceptibles d'apparaître dans les mesures quasi-statiques.

Le contact d'un relais monté sur le circuit de contre-réaction d'OP1 sert à la décharge du condensateur de plage Cg et donc à la préparation de l'appareil pour une nouvelle mesure (fonction Reset, U1 → 0). Une éventuelle déviation résiduelle du point zéro est compensée par un circuit spécial (compensation du zéro) à l'état Reset. Un diviseur de tension numérique (convertisseur analogique/numérique à 12 bits) porte le signal de tension U à la valeur calculée par l'appareil.

Un filtre passe-bas réglable sur 8 positions permet une réduction du seuil supérieur de fréquence lorsque l'application l'exige.

Un microprocesseur à 8 bits (µP) assure la commande et la surveillance de l'instrument. Le logiciel est enregistré sur un EPROM, les valeurs de consigne sur un NOVRAM à batterie-tampon.

La télécommande (Remote Control) permet - sans interface optionnelle - d'assurer les fonctions suivantes :

- Commutation Reset/Operate
- Remise à 0 du signal Overload
- Affichage : Overload
- Affichage : Zero out of Limit

L'appareil modifié de type 5011BxxY38 est doté par ailleurs d'une entrée de signal BNC pour capteurs Piezotron (Low Imp./Cal.), d'un commutateur "Low Imp./Cal.", d'une source de courant de 4,3 mA ainsi que d'un condensateur d'étalonnage de 1 nF. Ce condensateur sert à la conversion du signal de tension des capteurs Piezotron en un signal de charge. Il permet d'autre part le contrôle de l'étalonnage de l'appareil à l'aide d'une source de tension externe.

A voltage U1 then appears at the output of OP1 proportional to the charge and thus to the mechanical measurand.

When a purely dynamic measurement is involved, one of the two time constant resistors Rg can be connected in parallel with the range capacitor Cg. This avoids problems of drift such as can occur in quasi-static measurements.

A relay contact in the negative feedback branch of OP1 is used to discharge the range capacitor Cg thereby preparing the instrument for a new measurement (Reset function, U1 → 0). Any remaining zero deviation is compensated by a special circuit (zero compensation) in the Reset condition. The voltage signal U is brought to the value calculated by the instrument with a digital voltage divider (12 bit DAC).

The adjustable 8-stage low-pass filter (LP filter) allows a reduction in the upper frequency limit if this is required by the application.

An 8 bit microprocessor circuit (µP) controls and monitors the entire instrument. The software is stored in an EPROM; the set values in a battery-backed NOVRAM.

The following functions are available through the remote control connections (Remote Control) without optional interface:

- Reset/Operate switching
- Reset overload signal
- Display: Overload
- Display: Zero out of Limit

The modified version of the instrument 5011BxxY38 also has a BNC signal input for Piezotron sensors (Low Imp./Cal.), a selector Low Imp./Cal., a 4,3 mA current source and a 1 nF calibration capacitor. This capacitor is used on the one hand to convert the voltage signal of a Piezotron sensor to a charge signal, and on the other hand the instrument calibration can be checked using an external voltage source.

5011B_000-295m-11.04

Option: Parallele Schnittstelle IEEE-488 Typ 5605A

Standardisierte Schnittstelle, mit IEC-625-1 elektrisch kompatibel, zur Fernein-stellung und -abfrage sämtlicher Parameter. Messdaten werden nicht übertragen.

Option: Interface parallèle IEEE-488 Type 5605A

Interface standardisée, compatible électrique-ment avec IEC-625-1 pour le réglage et l'appel à distance de tous les paramètres. Les données de mesure ne sont pas transmises.

Option: Parallel Interface IEEE-488 Type 5605A

Standardized interface with IEC 625-1 electrically compatible for remote control and checking of all parameters. Measured data are not transmitted.

Technische Daten | **Données techniques** | **Technical Data**

Verwendeter Standard	Standard utilisé	Standard used	IEEE-488-1978
Abstand zwischen 2 Geräten	Distance entre 2 appareils	Distance between 2 instruments	max. 2 m
Maximallänge des Bus	Longueur maximale du bus	Maximum bus length	20 m
Maximale Anzahl Geräte am Bus	Nombre maximal d'appareils sur le bus	Maximum number of instruments on the bus	15
Adressbereich	Domaine d'adressage	Address range	0 ... 30
Funktionen	Fonctions	Functions	Listener, Talker

Option: Serielle Schnittstelle RS-232C Typ 5611A

Standardisierte Schnittstelle, zur Fernein-stellung und -abfrage sämtlicher Parameter. Messdaten werden nicht übertragen.

Option: Interface sérielle RS-232C Type 5611A

Interface standardisée pour réglage et appel à distance de tous les paramètres. Les données de mesure ne sont pas transmises.

Option: Serial Interface RS-232C Type 5611A

Standardized interface for remote control and checking of all parameters. Measured data not transmitted.

Technische Daten | **Données techniques** | **Technical Data**

Verwendeter Standard	Standard utilisé	Standard used	RS-232C resp. V24
Maximallänge des Kabels	Longueur maximale du câble	Maximum cable length	20 m (2500 pF)
Baudraten	Vitesse de transfert en bauds	Baud rates	50, 110, 250, 300, 600, 1200, 2400, 4800
Anzahl Datenbit	Nombre de bit d'information	Number of data bit	7 oder / ou / or 8
Anzahl Stoppbit	Nombre de bit d'arrêt	Number of stop bit	1 oder / ou / or 2
Parität	Parité	Parity	ohne, gerade od. ungerade sans, pair ou unpair without, even or odd
Software-Protokoll	Protocole du logiciel	Software protocol	XON/XOFF nicht zulässig / pas permis / not allowed

Bestellbezeichnung | **Références** | **Order Designation**

Ladungsverstärker	Amplificateur de charge	Charge Amplifier		Type 5011B □ □
ohne Tischgehäuse	Sans boîtier de table	Without table-mounted case		0
mit Tischgehäuse	Avec boîtier de table	With table-mounted case		1
ohne Schnittstelle	Sans interface	Without interface		0
mit Parallel-Schnittstelle	Avec interface parallèle	With parallel interface	IEEE-488 (Type 5605A)	1
mit serieller Schnittstelle	Avec interface sérielle	With serial interface	RS-232C (Type 5611A)	2

Obige Bestellbezeichnung kann durch Modifikationen ergänzt sein. Zur Zeit sind folgende Modifikationen erhältlich:

...Y26 Ladungsverstärker auf 115 V AC Netzspannung eingestellt (Netzspannungsumschaltung anwenderseits jederzeit möglich).

...Y38 Ladungsverstärker, zusätzlich mit Piezotroneingang und Kalibriereingang.

Beispiel Typ 5011B10Y26Y38
Das ist ein Ladungsverstärker vom Grundtyp 5011B mit Gehäuse, ohne eingebaute Schnittstelle, auf 115 V AC Netzspannung eingestellt, mit zusätzlichem Piezotron- und Kalibriereingang.

La référence ci-dessus peut être complétée par des extensions. Actuellement les extensions suivantes sont disponibles :

...Y26 Amplificateur de charge réglé sur une tension secteur de 115 V AC (possibilité de commutation de la tension secteur à tout moment par l'utilisateur).

...Y38 Amplificateur de charge, avec entrée Piezotron et entrée d'étalonnage.

Exemple: type 5011B10Y26Y38
Il s'agit d'un amplificateur de charge de type 5011B avec boîtier, sans interface incorporée, réglé sur une tension secteur de 115 V AC, doté en supplément d'une entrée Piezotron et d'étalonnage.

Above order designation can be supplemented by modifications. At present, the following modifications are available:

...Y26 Charge amplifier set to 115 V AC power supply (supply voltage setting can be changed by the user at any time).

...Y38 Charge amplifier additionally with Piezotron input and calibration input.

Example: Type 5011B10Y26Y38
This is a charge amplifier of the basic type 5011B with case, without integral interface, set to 115 V AC supply with additional Piezotron and calibration input.

Zubehör | **Accessoires** | **Accessories**

- Anschlusskabel für Fernsteuerung, Länge 5 m, Typ 1455A5 (Datenblatt 15.016)
- Fernsteuerkästchen Typ 5663 (Datenblatt 13.5663)
- Stecker für Fernsteueranschluss, Typ 1564, 6-polig, nach DIN 45322 (Datenblatt 15.016)
- RS-232C Kabel, Länge 3 m, mit "Hardwired-Handshake" DB-25 P/DB-9S: Typ 1475A3
- RS-232C Adapter DB-9 P/DB-25 S: Typ 1469

- Câble de connexion pour télécommande, 5 m de longueur, type 1455A5 (fiche technique 15.016)
- Coffret de télécommande, type 5663 (fiche technique 13.5663)
- Fiche pour connexion de la télécommande, type 1564, à 6 pôles, selon DIN 45322 (fiche technique 15.016)
- RS-232C câble, 3 m de longueur, avec "Hard-wired-Handshake" DB-25 P/DB-9S: type 1475A3
- RS-232C Adaptor DB-9 P/DB-25 S: Type 1469

- Connecting cable for remote control, length 5 m, Type 1455A5 (Data Sheet 15.016)
- Remote control box Type 5663 (Data Sheet 13.5663)
- Connector for remote control connection, Type 1564, 6-pole, per DIN 45322 (Data Sheet 15.016)
- RS-232C cable, length 3 m, with Hardwired-Handshake DB-25 P/DB-9S: Type 1475A3
- RS-232C Adaptor DB-9 P/DB-25 S: Type 1469

5011B_000-29/6m-11.04

Appendix B: Amplifiers configuration

One Kistler 5011 amplifier was used for each accelerometer signal. The accelerometers were installed in the spindle head. The configuration of these amplifiers is simple and will be explained next.

The microprocessor inside the charge amplifier 5011 converts the electrical charge yielded by the piezoelectric transducers into a proportional voltage signal. The configuration of such amplifiers contains several data that must be introduced.

Measuring range

This means the electrical charge which, corresponding to the menu settings of the [Transducer Sensitivity T] and of the [Scale S], gives a voltage of 10 V at the output. According to the transducer sensitivity, the measuring range in mechanical units used in practice can be inferred.

The front panel of the amplifier does not show the measuring range but the Scale in Mechanical Units/V for a given Transducer Sensitivity [pC/Mechanical Unit].

Transducer sensitivity

[T Transducer Sensitivity (pC/Mechanical Unit)]

This is the coefficient for the conversion of mechanical units into electrical charge. The numerical value is given in the calibration sheet delivered with the transducer.

Low Pass filter

A low-pass filter with Butterworth characteristic switchable in 8 stages is connected following the DAC stage. The filter setting allows to adjust the upper cutoff frequency of the measuring system to the specific application.

Time constant

The time constant τ, with which the stationary measuring signal drops, is given by the product of the selected range capacitor C_g and the selected time constant resistor R_g paralleling it:

$$\tau = R_g \bullet C_g$$

The longest time constants in the different ranges are given when in the setting [Long] the resistor R_g is determined by the insulation resistance of the particular range capacitor.

Next figure shows the frontal panel of such amplifiers:

Figure 50. Charge amplifier front panel of a Kistler 5211.

The configuration used for the three axes is described in Table 14:

Axis	X	Y	Z
Transducer Sensitivity	1.00 E2	1.00 E2	1.00 E3
Scale	1.00 E0	1.00 E0	1.00 E0
Low Pass Filter	Off	Off	Off
Time Constant	Short	Short	Short

Table 14. Amplifiers configuration.

The transducer sensitivity corresponds to the sensitivity that appears in the data sheet of the sensor. The scale means that 1 V will be measured with each G detected. Low pass filters were set off and an automatic short time constant was configured.

Appendix C: Multisensor Acquisition Platform

A Multisensor Acquisition Platform was developed to obtain signals and data from different sensors, such as accelerometers, acoustic emission and CNC variables. The base software used was LabView from National Instruments, which has a completely graphical programming language. In this appendix, it will be explained with detail the acquisition software used during the experimentation phase.

LabView version 7.1 is the latest of National Instruments, this software permits the manipulation of acquisition cards easily, allowing to use the VIs already made and purchased together with the acquisition cards. This VIs permits the user to configure everything related with the acquisition of data and the way they are displayed graphically. These VIs will be next explained in order to understand when the complete program diagram is shown. As it was explained before three main acquisition cards will be used: a CompuScope 1602, and two Daqboards (2000 and 2005). The CompuScope will be acquiring signal from two acoustic emission sensors, and the Daqboards will be used to get data from the accelerometers installed in the milling machine. A fourth card, developed by Siemens will permit to get information, not from sensors, but from the process itself, such as actual feed rate, actual spindle speed, axis position, etc. this card is named MPI.

Due to its graphical manner of programming, LabView uses colors to distinguish between different type of terminal data, float, integer, array, etc. Next figure contains the description of each of this type of data with its corresponding color.

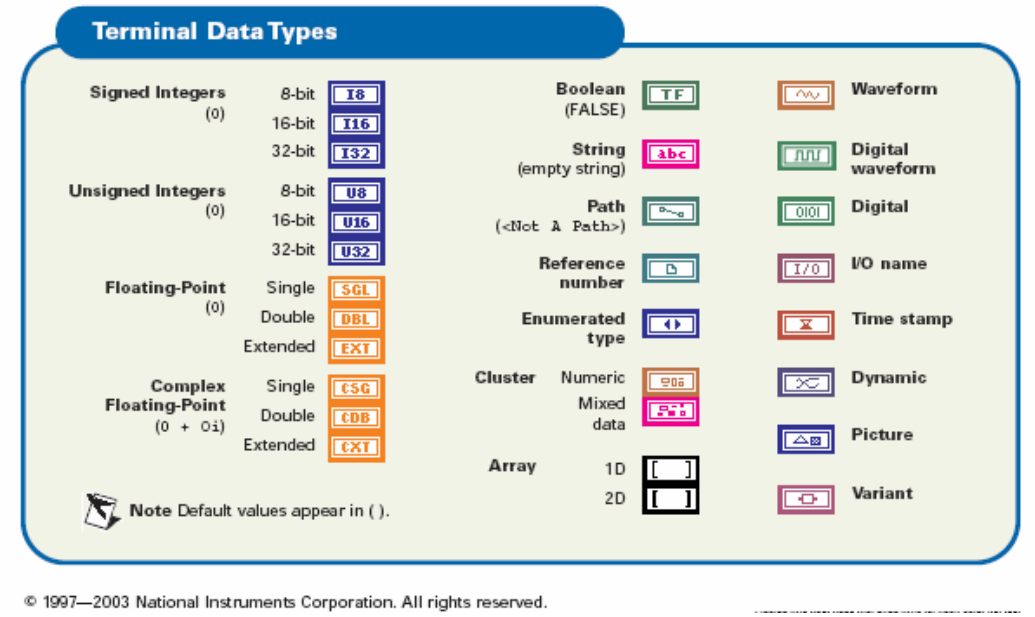

Figure 51. Terminal data types of LabView. Graphic obtained from National Instruments documentation [LabView Help].

To describe the VIs used to interact with the acquisition cards the next figures are used. Each of them has all its possible connections and its proper type of data. After each figure a brief explanation of the purpose of each connection.

VI Name: **CScope**

Acquisition card: **CompuScope 1602**

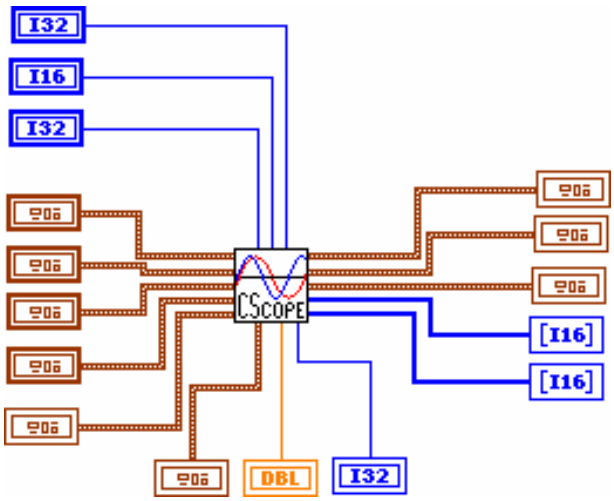

Figure 52. CScope subVi connection scheme.

- **Trigger Timeout.** This input admits a quantity of time to be wait before the beginning of acquisition.
- **Board Number.** A board number must be defined when using several boards in the same CPU.
- **Compuscope Mode.** Indicates the mode in which the compuscope card will function, as differential or absolute.
- **Capture Configuration.** Capture mode configuration.
- **Input Configuration.** Input of configuration.
- **Trigger Configuration.** Trigger activation.
- **Transfer Request.** Input to activate transfer of data.
- **Transferred.** Indicator of the amount of date transferred.
- **PPS.** Indicates the points per second acquired.
- **Volts.** Indicates the value acquire in volts.
- **Status.** Indicates the status of the acquisition.
- **Capture Mode.** Indicator of capture mode.
- **Input Mode.** Indicator of input mode.
- **Trigger Mode.** Indicator of trigger mode.
- **Data A.** Channel A output.
- **Data B.** Channel B output.

VI Name: **DAQ Basic**

Acquisition card: **DaqBoard 2000 and 2005**

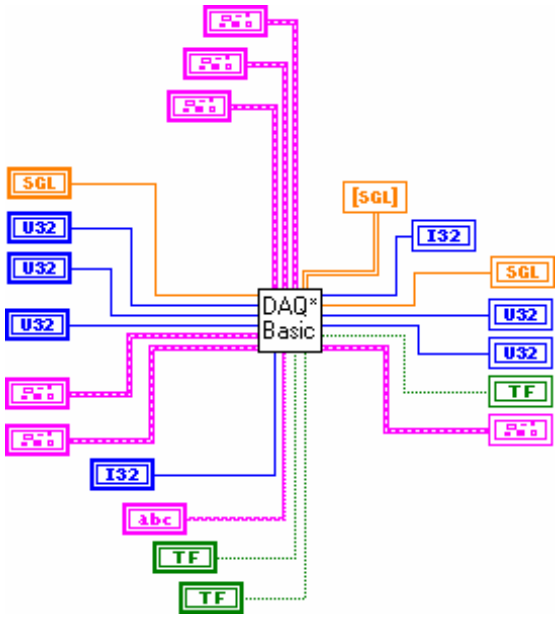

Figure 53. DAQBasic subVi connection scheme.

- **DBK Configuration.** In this section the selection of which channels to acquire is made. Four possible channels can be selected.
- **Scaling Array In.** Input of the signal coming from other card, such as a DBK17.
- **Scan Configuration.** Scan configuration input.
- **Scan Frequency (Hz).** Input that controls the frequency at which the card is acquiring information.
- **Total Scans to Acquire 0 = Infinite Acquisition.** A finite number of scans can be set in this input. If 0 then the acquisition is infinite.
- **Scan Count to Process per VI Iteration.** Indicates how the counter should be held compared with the iterations of the loop.
- **Pacing Control.** Input for pacing control.
- **Device Name.** Indicates the name of the board, such as it is in the control panel. Useful when using several boards in one CPU.
- **Error In.** Error input, passage when there is a block before.
- **Iteration.** Indicates the current number of iteration of the acquisition.

- **Calibration File Name.** When a calibration file name exists it can be introduced via this input.
- **Stop Button.** Control to stop the acquisition.
- **Loop Control.** Input for loop control.
- **Scaled Output.** Output of information.
- **Device Handle Out.** Indicates the name of the device in use.
- **Actual Rate (Hz).** Indicates the actual rate in hertz.
- **Scans Buffered.** Indicates the number of scans buffered in the card memory.
- **Scans Read.** Indicates the number of scans read.
- **Acquisition On.** Indicates the status of the acquisition.
- **Error Out.** Output of the error signal.

VI Name: **DBK 17 Conf**

Acquisition card: **DaqBoard 2000 and 2005**

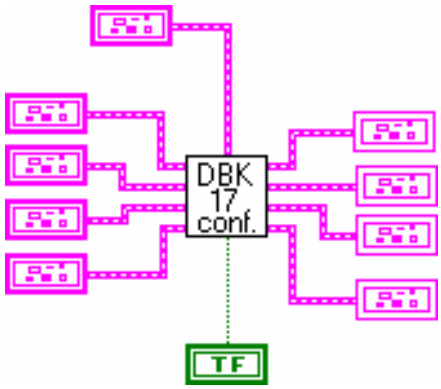

Figure 54. DBK17 subVi connection scheme.

- **DBK17 Settings.** In this section the selection of which channels to acquire is made. Four possible channels can be selected.
- **Scan Settings In.** Configuration of scan settings.

- **Scaling Array.** Input of the array coming from the card.
- **DBK Configuration.** Configuration parameters, selection of channels.
- **Error Cluster In.** Input of error signal.
- **Base Unit Voltage.** Functioning voltage range selection.
- **Scan Settings Out.** Indicator of current scan settings.
- **Scaling Array Out.** Data output.
- **DBK Configuration Out.** Indicator of current configuration.
- **Error Cluster Out.** Output of error signal.

Appendix D: MPI

The Siemens MPI (Multi point interface) card functions the same way as an acquisition card. The difference is that is specially for siemens products applications. In the case of the machining center, it works with a open architecture controller. This type of control is designed to facilitate the inclusion and exclusion of signals related to the machine and the process.

This way, using this card we are able to read real time many variables available from the machine and the milling process. Variables used in this these such as, spindle speed, feed rate and depth of cut were obtained simultaneously with this device, which was configured and manage through LabView. The velocity of acquisition goes from 9.6 Kbits/s to 12 Mbits/s. Each variable uses words of 32 bits. So reading only one variable we may be able to sample at a velocity of 375KHz.

Figure 55. CP5512 MPI photo.

Appendix E: Materials specifications

In this section is presented some properties related to the three materials used for testing: 7075-T6 aluminum, 6061-T6 and 1045 Steel. The information was obtained from the supplier.

7075-T6 aluminum

Composition:

Si: 0.40	Fe: 0.50	Cu: 1.2-2.0	Mn: 0.30	Mg: 2.1-2.9
Zn: 5.1-6.1	Ti: Zr0.20	Cr: 0.18-0.28	Other: 0.15	

Breakage Charge (N/mm^2): 280

Mechanical Elastic limit (N/mm^2): 150

Enlargement (%): 10

Elastic Module (N/mm^2): 72000

Specific Weight (Kg/dm^3): 2.80

Brinell Hardness HB: 145

6061-T6 aluminum

Composition:

Si: 0.721	Fe: 0.408	Cu: 0.1-0.4	Mn: 0.109	Mg: 0.937
Zn: 0.176	Ti: 0.051	Pb: 0.002	Cr: 0.072	

Breakage Charge (N/mm^2): 310

Mechanical Elastic limit (N/mm^2): 270

Enlargement (%): 13

Elastic Module (N/mm^2): 69500

Specific Weight (Kg/dm^3): 2.70

Brinell Hardness HB: 95

1045 Steel (SAE)

Composition:

C: 0.43-0.50 Mn: 0.60-0.90 P max: 0.040 S max: 0.050 Si max: 0.20-0.35

Traction Resistance (Kg/mm^2): 60

Mechanical Elastic limit (Kg/mm^2): 38

Enlargement (%): 16

Reduction Area (%): 40

Brinell Hardness HB: 220

Appendix F: End mill tools

Next images show the Karnasch catalog information used in the selection of parameters. For aluminum the tool 30.6215 was used and the 30.6472 for steel.

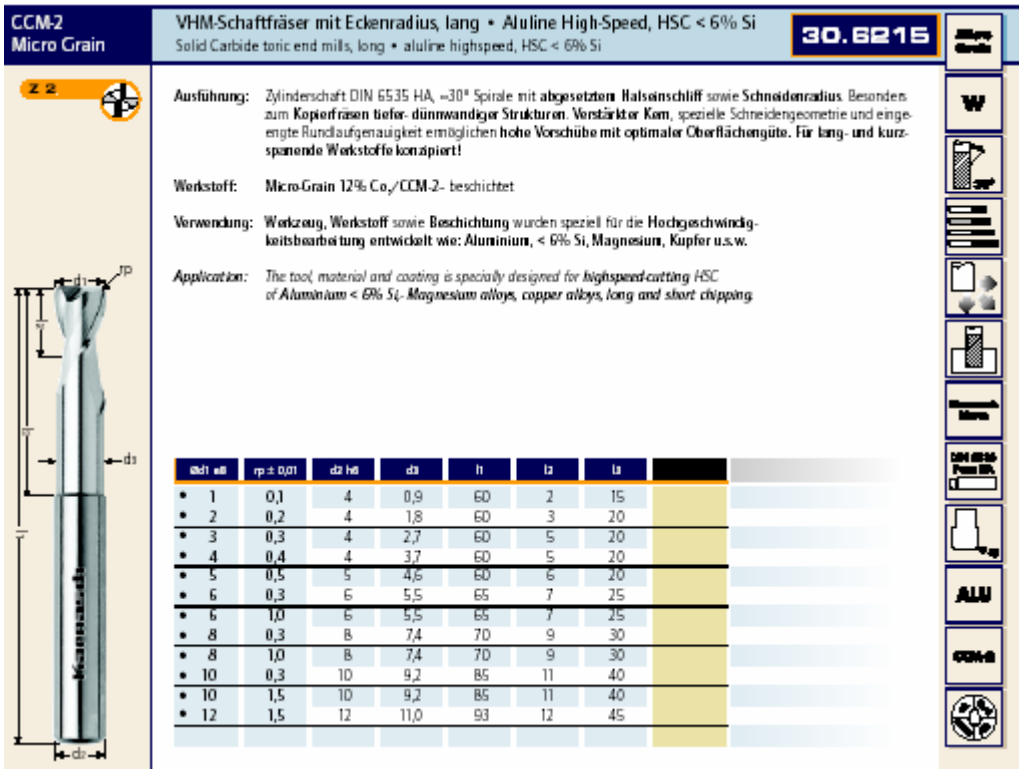

Ød1 e8	rp ± 0,01	d2 h6	d3	l1	l2	l3
• 1	0,1	4	0,9	60	2	15
• 2	0,2	4	1,8	60	3	20
• 3	0,3	4	2,7	60	5	20
• 4	0,4	4	3,7	60	5	20
• 5	0,5	5	4,6	60	6	20
• 6	0,3	6	5,5	65	7	25
• 6	1,0	6	5,5	65	7	25
• 8	0,3	8	7,4	70	9	30
• 8	1,0	8	7,4	70	9	30
• 10	0,3	10	9,2	85	11	40
• 10	1,5	10	9,2	85	11	40
• 12	1,5	12	11,0	93	12	45

Figure 56. 30.6215 tool datasheet [Karnasch tool catalog].

For the 30.6215 the tool used is a 2 teeth and 12 mm diameter end mill. As seen in the picture, the radius is of 1.5 mm. This tool is specially designed for high speed milling, the dimensions can be seen in the image above. Next image helped choosing the correct feed rates, this due to the limitations that it has in the feed per tooth of 0.08 to 0.18 mm/tooth. The maximum depth of cut is defined as ap=<1xd, which means that it can be introduced 12 mm of depth. In this case the depth of cut is independent of the material hardness.

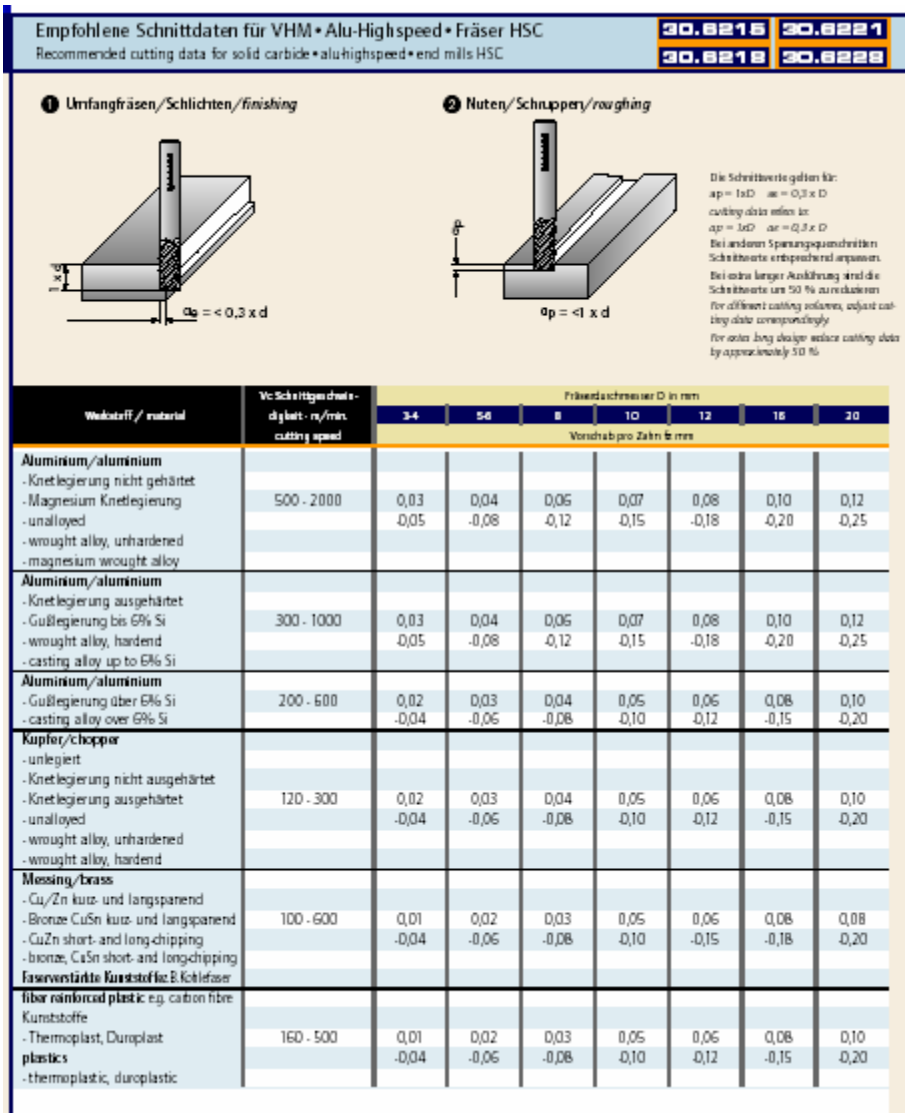

Empfohlene Schnittdaten für VHM • Alu-Highspeed • Fräser HSC
Recommended cutting data for solid carbide • alu-highspeed • end mills HSC

30.6215 30.6221
30.6218 30.6228

❶ Umfangfräsen/Schlichten/*finishing*

❷ Nuten/Schruppen/*roughing*

Die Schnittwerte gelten für:
ap = 1xD ae = 0,3 x D
cutting data refers to:
ap = 1xD ae = 0,3 x D
Bei anderen Spanungsquerschnitten Schnittwerte entsprechend anpassen.
Bei extra langer Ausführung sind die Schnittwerte um 50 % zu reduzieren.
For different cutting volumes, adjust cutting data correspondingly.
For extra long design reduce cutting data by approximately 50 %.

Werkstoff / material	Vc Schnittgeschwindigkeit - m/min. cutting speed	Fräserdurchmesser D in mm						
		3-4	5-6	8	10	12	16	20
		Vorschub pro Zahn fz mm						
Aluminium/aluminium								
- Knetlegierung nicht gehärtet								
- Magnesium Knetlegierung	500 - 2000	0,03	0,04	0,06	0,07	0,08	0,10	0,12
- unalloyed		-0,05	-0,08	-0,12	-0,15	-0,18	-0,20	-0,25
- wrought alloy, unhardened								
- magnesium wrought alloy								
Aluminium/aluminium								
- Knetlegierung ausgehärtet								
- Gußlegierung bis 6% Si	300 - 1000	0,03	0,04	0,06	0,07	0,08	0,10	0,12
- wrought alloy, hardend		-0,05	-0,08	-0,12	-0,15	-0,18	-0,20	-0,25
- casting alloy up to 6% Si								
Aluminium/aluminium								
- Gußlegierung über 6% Si	200 - 600	0,02	0,03	0,04	0,05	0,06	0,08	0,10
- casting alloy over 6% Si		-0,04	-0,06	-0,08	-0,10	-0,12	-0,15	-0,20
Kupfer/chopper								
- unlegiert								
- Knetlegierung nicht ausgehärtet								
- Knetlegierung ausgehärtet	120 - 300	0,02	0,03	0,04	0,05	0,06	0,08	0,10
- unalloyed		-0,04	-0,06	-0,08	-0,10	-0,12	-0,15	-0,20
- wrought alloy, unhardened								
- wrought alloy, hardend								
Messing/brass								
- Cu/Zn kurz- und langspanend								
- Bronze CuSn kurz- und langspanend	100 - 600	0,01	0,02	0,03	0,05	0,06	0,08	0,08
- CuZn short- and long-chipping		-0,04	-0,06	-0,08	-0,10	-0,15	-0,18	-0,20
- bronze, CuSn short- and long-chipping								
Faserverstärkte Kunststoffe z.B. Kohlefaser								
fiber reinforced plastic e.g. carbon fibre								
Kunststoffe								
- Thermoplast, Duroplast	160 - 500	0,01	0,02	0,03	0,05	0,06	0,08	0,10
plastics		-0,04	-0,06	-0,08	-0,10	-0,12	-0,15	-0,20
- thermoplastic, duroplastic								

Figure 57. 30.6215 tool datasheet [Karnasch tool catalog].

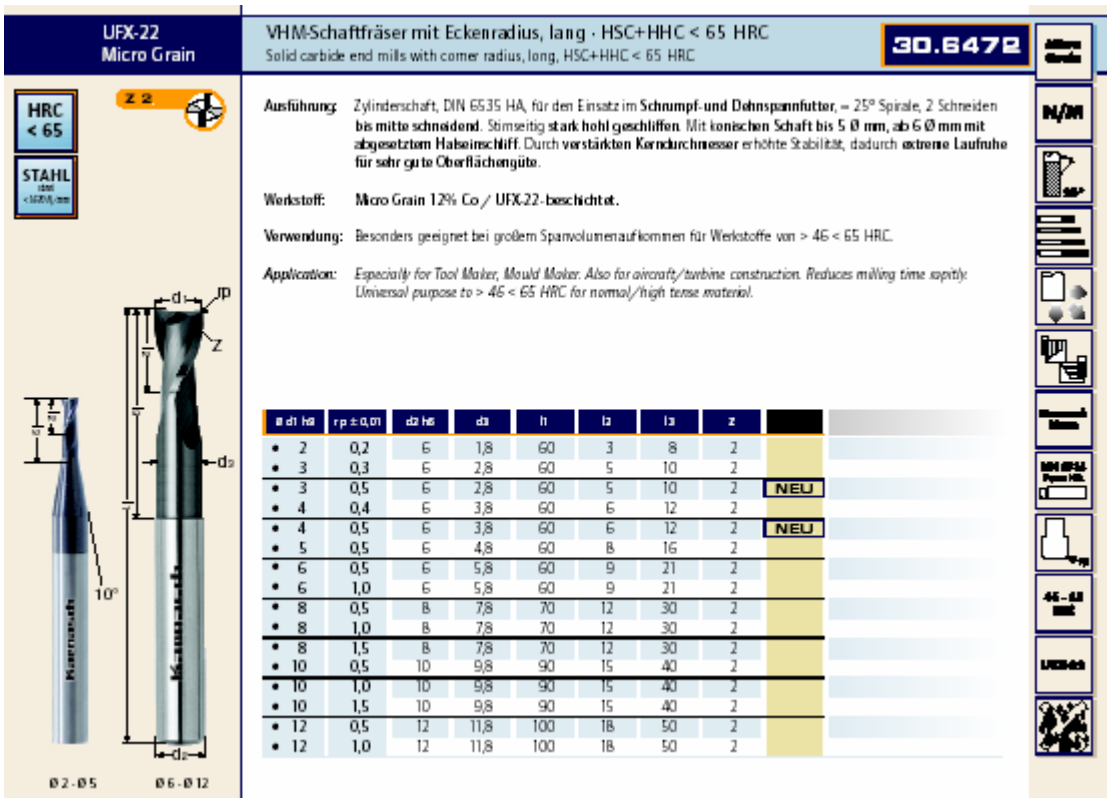

Figure 58. 30.6472 tool datasheet [Karnasch tool catalog].

Figure 58 shows the tool characteristics of the 30.6472 used for steel machining. It is important to notice that in order to keep the same nose radius which is an important factor affecting surface roughness, it was necessary to choose an 8 mm diameter tool. Keeping a 12 mm diameter tool means to lower the radius to at least 1.0 mm, which could affect the measurements. The dimensional properties can be seen in the picture above. Below, the table to consider the limits of feed rates is shown. Differently from aluminum, this tool must consider the hardness of steel. For our case, the 1045 Steel used for experimentation has a Brinnel hardness of 220 which is equal to 730 N/mm^2. This way, the second section data of the table was used, this section has the machining parameter optimum for steels below 1600 N/mm^2 of Hardness. This table shows that fz must be 0.065 mm/tooth and the range of spindle speed must be 11000 and 15000 rpm.

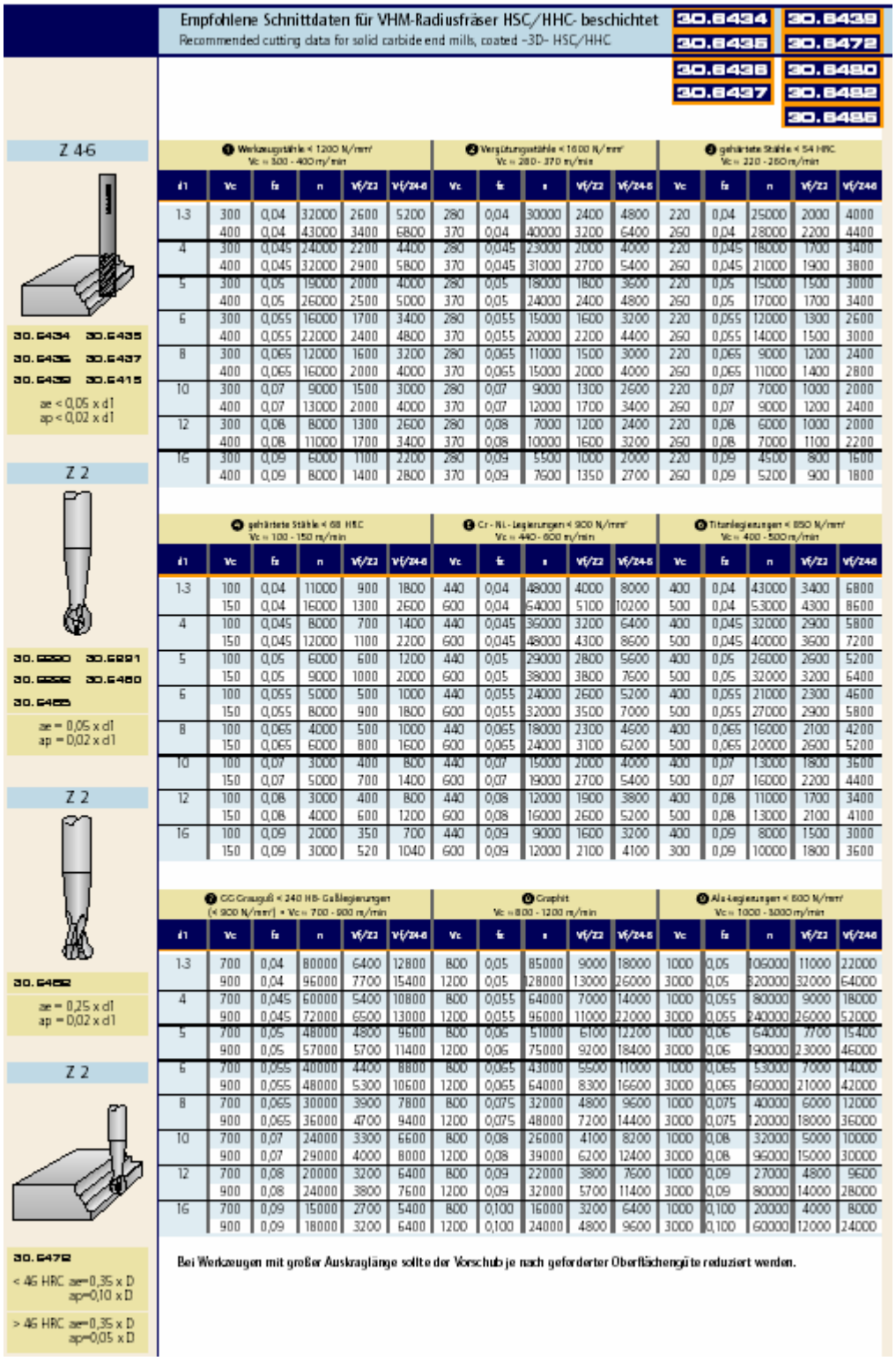

Empfohlene Schnittdaten für VHM-Radiusfräser HSC/HHC- beschichtet
Recommended cutting data for solid carbide end mills, coated -3D- HSC/HHC

30.6434 30.6439 30.6435 30.6472 30.6438 30.6480 30.6437 30.6482 30.6485

Z 4-6

30.6434 30.6435 30.6436 30.6437 30.6439 30.6415

ae < 0,05 x d1
ap < 0,02 x d1

d1	❶ Werkzeugstähle < 1200 N/mm² Vc = 300 - 400 m/min					❷ Vergütungsstähle < 1600 N/mm² Vc = 280 - 370 m/min					❸ gehärtete Stähle < 54 HRC Vc = 220 - 260 m/min				
	Vc	fz	n	Vf/Z2	Vf/Z4-6	Vc	fz	n	Vf/Z2	Vf/Z4-6	Vc	fz	n	Vf/Z2	Vf/Z4-6
1-3	300	0,04	32000	2600	5200	280	0,04	30000	2400	4800	220	0,04	25000	2000	4000
	400	0,04	43000	3400	6800	370	0,04	40000	3200	6400	260	0,04	28000	2200	4400
4	300	0,045	24000	2200	4400	280	0,045	23000	2000	4000	220	0,045	18000	1700	3400
	400	0,045	32000	2900	5800	370	0,045	31000	2700	5400	260	0,045	21000	1900	3800
5	300	0,05	19000	2000	4000	280	0,05	18000	1800	3600	220	0,05	15000	1500	3000
	400	0,05	26000	2500	5000	370	0,05	24000	2400	4800	260	0,05	17000	1700	3400
6	300	0,055	16000	1700	3400	280	0,055	15000	1600	3200	220	0,055	12000	1300	2600
	400	0,055	22000	2400	4800	370	0,055	20000	2200	4400	260	0,055	14000	1500	3000
8	300	0,065	12000	1600	3200	280	0,055	11000	1500	3000	220	0,065	9000	1200	2400
	400	0,065	16000	2000	4000	370	0,055	15000	2000	4000	260	0,065	11000	1400	2800
10	300	0,07	9000	1500	3000	280	0,07	9000	1300	2600	220	0,07	7000	1000	2000
	400	0,07	13000	2000	4000	370	0,07	12000	1700	3400	260	0,07	9000	1200	2400
12	300	0,08	8000	1300	2600	280	0,08	7000	1200	2400	220	0,08	6000	1000	2000
	400	0,08	11000	1700	3400	370	0,08	10000	1600	3200	260	0,08	7000	1100	2200
16	300	0,09	6000	1100	2200	280	0,09	5500	1000	2000	220	0,09	4500	800	1600
	400	0,09	8000	1400	2800	370	0,09	7600	1350	2700	260	0,09	5200	900	1800

Z 2

30.6250 30.6291 30.6252 30.6480 30.6455

ae = 0,05 x d1
ap = 0,02 x d1

d1	❹ gehärtete Stähle < 68 HRC Vc = 100 - 150 m/min					❺ Cr - Ni - Legierungen < 900 N/mm² Vc = 440 - 600 m/min					❻ Titanlegierungen < 850 N/mm² Vc = 400 - 500 m/min				
	Vc	fz	n	Vf/Z2	Vf/Z4-6	Vc	fz	n	Vf/Z2	Vf/Z4-6	Vc	fz	n	Vf/Z2	Vf/Z4-6
1-3	100	0,04	11000	900	1800	440	0,04	48000	4000	8000	400	0,04	43000	3400	6800
	150	0,04	16000	1300	2600	600	0,04	64000	5100	10200	500	0,04	53000	4300	8600
4	100	0,045	8000	700	1400	440	0,045	36000	3200	6400	400	0,045	32000	2900	5800
	150	0,045	12000	1100	2200	600	0,045	48000	4300	8600	500	0,045	40000	3600	7200
5	100	0,05	6000	600	1200	440	0,05	29000	2800	5600	400	0,05	26000	2600	5200
	150	0,05	9000	1000	2000	600	0,05	38000	3800	7600	500	0,05	32000	3200	6400
6	100	0,055	5000	500	1000	440	0,055	24000	2600	5200	400	0,055	21000	2300	4600
	150	0,055	8000	900	1800	600	0,055	32000	3500	7000	500	0,055	27000	2900	5800
8	100	0,065	4000	500	1000	440	0,055	18000	2300	4600	400	0,065	16000	2100	4200
	150	0,065	6000	800	1600	600	0,055	24000	3100	6200	500	0,065	20000	2600	5200
10	100	0,07	3000	400	800	440	0,07	15000	2000	4000	400	0,07	13000	1800	3600
	150	0,07	5000	700	1400	600	0,07	19000	2700	5400	500	0,07	16000	2200	4400
12	100	0,08	3000	400	800	440	0,08	12000	1900	3800	400	0,08	11000	1700	3400
	150	0,08	4000	600	1200	600	0,08	16000	2600	5200	500	0,08	13000	2100	4100
16	100	0,09	2000	350	700	440	0,09	9000	1600	3200	400	0,09	8000	1500	3000
	150	0,09	3000	520	1040	600	0,09	12000	2100	4100	300	0,09	10000	1800	3600

Z 2

30.6452

ae = 0,25 x d1
ap = 0,02 x d1

d1	❼ GG Grauguß < 240 HB- Gußlegierungen (< 900 N/mm²) + Vc = 700 - 900 m/min					❽ Graphit Vc = 800 - 1200 m/min					❾ Alu-Legierungen < 600 N/mm² Vc = 1000 - 3000 m/min				
	Vc	fz	n	Vf/Z2	Vf/Z4-6	Vc	fz	n	Vf/Z2	Vf/Z4-6	Vc	fz	n	Vf/Z2	Vf/Z4-6
1-3	700	0,04	80000	6400	12800	800	0,05	85000	9000	18000	1000	0,05	106000	11000	22000
	900	0,04	96000	7700	15400	1200	0,05	128000	13000	26000	3000	0,05	320000	32000	64000
4	700	0,045	60000	5400	10800	800	0,055	64000	7000	14000	1000	0,055	80000	9000	18000
	900	0,045	72000	6500	13000	1200	0,055	96000	11000	22000	3000	0,055	240000	26000	52000
5	700	0,05	48000	4800	9600	800	0,06	51000	6100	12200	1000	0,06	64000	7700	15400
	900	0,05	57000	5700	11400	1200	0,06	75000	9200	18400	3000	0,06	190000	23000	46000
6	700	0,055	40000	4400	8800	800	0,065	43000	5500	11000	1000	0,065	53000	7000	14000
	900	0,055	48000	5300	10600	1200	0,065	64000	8300	16600	3000	0,065	160000	21000	42000
8	700	0,065	30000	3900	7800	800	0,075	32000	4800	9600	1000	0,075	40000	6000	12000
	900	0,065	36000	4700	9400	1200	0,075	48000	7200	14400	3000	0,075	120000	18000	36000
10	700	0,07	24000	3300	6600	800	0,08	26000	4100	8200	1000	0,08	32000	5000	10000
	900	0,07	29000	4000	8000	1200	0,08	39000	6200	12400	3000	0,08	96000	15000	30000
12	700	0,08	20000	3200	6400	800	0,09	22000	3800	7600	1000	0,09	27000	4800	9600
	900	0,08	24000	3800	7600	1200	0,09	32000	5700	11400	3000	0,09	80000	14000	28000
16	700	0,09	15000	2700	5400	800	0,100	16000	3200	6400	1000	0,100	20000	4000	8000
	900	0,09	18000	3200	6400	1200	0,100	24000	4800	9600	3000	0,100	60000	12000	24000

Z 2

30.6472

< 46 HRC ae=0,35 x D
ap=0,10 x D

> 46 HRC ae=0,35 x D
ap=0,05 x D

Bei Werkzeugen mit großer Auskraglänge sollte der Vorschub je nach geforderter Oberflächengüte reduziert werden.

Figure 59. 30.6472 tool datasheet [Karnasch tool catalog].

Appendix G: Stability Lobes

An important factor that influenced the Parameter Selection with which the machining experiments were done, it's the Stability Lobes Test. During a machining process different types of vibrations affect the quality of parts. These vibrations could be classified in machine vibrations and process vibrations. Machine vibrations are greatly influenced by its mechanical structure, for such situation, it is pretty difficult to establish the influence of the machine vibrations because each machine is different from other. For the purpose of this work, it was sought to find the influence of process vibrations in the surface quality of parts.

During the experimentation phase it is important to be sure that the variations in vibrations were originated by the process dynamic. But it is not enough to keep making changes in parameters because every process has its limits, most limits are establish by the type of tool that it is used. Not respecting these limits will affect vibration measuring considerably, and results and experimentation will get out of control, giving non representative results in surface finish such as the chatter phenomena. The Stability Lobes Test helped keeping some of these process parameters inside their limits.

One of these parameters is the depth of cut. The resulting graphs of spindle speed versus depth of cut gives an idea of which values to use to avoid entering into chatter zones.

Figure 60 shows the resultant graph from the stability lobe analysis made to the aluminum tool 30.6215, the one used for all aluminum samples. Over the graph, the points displayed shows samples machined to test the graph reliability. The red dots show the first appearance of chatter phenomenon. It can be seen that incrementing spindle speed helps to avoid the appearance of chatter, contrary to what is done in practice.

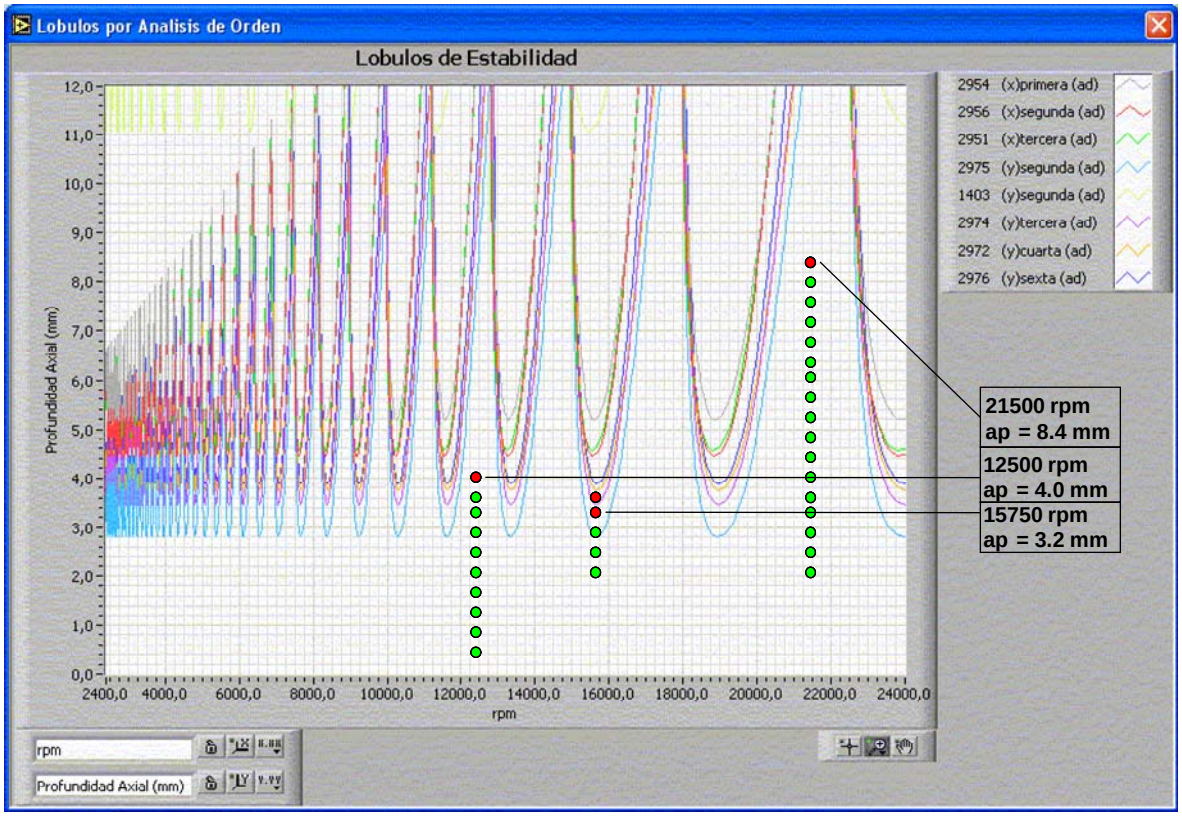

Figure 60. 30.6215 stability lobes test results.

Appendix H: Numeric control program

```
%_N_LUIS_MPF
;$PATH=/_N_MPF_DIR
N100 def real largo=180
N200 def real ancho=100
N300 def real Ppz=1.5
N400 def real Ppzincremental=0
N500 def real EspesorP=2
N600 def real RPM=19000
N700 def real RPMin=1000
N800 def real Ndientes=2
N900 def int radio=6
N1000 def real avance=100
N1100 def real desplazamiento
N1200 g0 G54 G90 X=-radio y =radio z10
N1300 desplazamiento=(radio*2)+EspesorP
N1400 ancho=ancho+(desplazamiento*2)+(radio*2)
N1500 g0 x= ic(desplazamiento) y =ic (desplazamiento)
N1600 Pasada:
N1700 avance=0.18*Ndientes*rpm
N1800  f=avance s=RPM m3 t1 d1
N1900 g0 g90 z0
N2000 g1 g90 z=-Ppz
N2100 Ppz=Ppz+Ppzincremental
N2200 g1 g90 y=ic (-ancho)
N2300 g0 g90 z10
N2400 g0 g90 x= ic (desplazamiento)y = ic (ancho)
N2500 largo=largo-desplazamiento
N2600 RPM=RPM+RPMin
N2700 if rpm>22000 gotof fin
N2800 if largo>=0 gotoB pasada
N2900 fin:
N3000 g0 g90 z150 m5
N3100 m30
```

Appendix I: Regression Analysis

In this appendix is shown the statistical analysis of the data acquired during the experimentation phase. The results were obtained by following the methodology shown in Chapter 5. Two models for each material used are presented. All the analysis was made with statistical software such as Excel and Minitab.

7075-T6 aluminum

Before making any statistical analysis we must be sure that the data obtained comes from a normal distribution. To know this a Q-Q Plot is used. Considering that every groove corresponds to a different population, only a few populations are observed considering that all the rest will behave the same way. For this case the populations of 8000, 9000, 10000, and 11000 rpm are considered at a depth of cut of 2.5 mm.

S	ap	AccX	AccY	AccZ	Accres
8000	2.5	274.9639	294.9977	61.73744	407.9709
8000	2.5	327.717	336.534	62.97292	473.94
8000	2.5	305.425	312.3153	67.70732	442.0515
8000	2.5	357.6453	315.8831	72.02195	482.5758
8000	2.5	302.6569	301.3028	74.75993	433.5593
8000	2.5	306.5148	325.4015	79.65374	454.0729
8000	2.5	322.7692	291.3466	72.67231	440.8447
8000	2.5	345.3597	333.6159	75.04767	486.0093

k	x	Prob	Percentil
1	407.9709	0.0625	411.3163
2	473.94	0.1875	428.7384
3	442.0515	0.3125	439.466
4	482.5758	0.4375	448.3919
5	433.5593	0.5625	456.8642
6	454.0729	0.6875	465.7901
7	440.8447	0.8125	476.5177
8	486.0093	0.9375	493.9398
Media	452.6281	EstDev	26.92862

S	ap	AccX	AccY	AccZ	Accres
9000	2.5	419.6972	382.0999	90.46776	574.7438
9000	2.5	395.0355	388.8202	90.86229	561.6851
9000	2.5	379.8686	397.9725	94.08898	558.1532
9000	2.5	366.6721	396.656	129.355	555.4432
9000	2.5	443.2393	343.1709	118.6923	572.988
9000	2.5	431.3663	392.1161	117.8958	594.7531
9000	2.5	402.4514	359.2772	114.2731	551.4576

k	x	Prob	Percentil
1	574.7438	0.071429	545.0723
2	561.6851	0.214286	555.1676
3	558.1532	0.357143	561.5451
4	555.4432	0.5	567.032
5	572.988	0.642857	572.5189
6	594.7531	0.785714	578.8964
7	551.4576	0.928571	588.9917
Media	567.032	EstDev	14.98716

S	ap	AccX	AccY	AccZ	Accres
10000	2.5	459.6312	434.3472	69.19349	636.1651
10000	2.5	498.9308	423.5333	85.78532	660.0542
10000	2.5	520.5565	423.4266	81.15994	675.9113
10000	2.5	522.0495	387.3838	76.19123	654.528
10000	2.5	477.3919	408.9936	70.92659	632.621
10000	2.5	528.9029	379.9702	84.10112	656.6495
10000	2.5	491.5361	375.2152	77.94806	623.2737

k	x	Prob	Percentil
1	636.1651	0.071429	621.5177
2	660.0542	0.214286	633.9025
3	675.9113	0.357143	641.7263
4	654.528	0.5	648.4576
5	632.621	0.642857	655.1888
6	656.6495	0.785714	663.0127
7	623.2737	0.928571	675.3974
Media	648.4576	EstDev	18.38604

Table 15. Data of populations observed to obtain the Q-Q Plot.

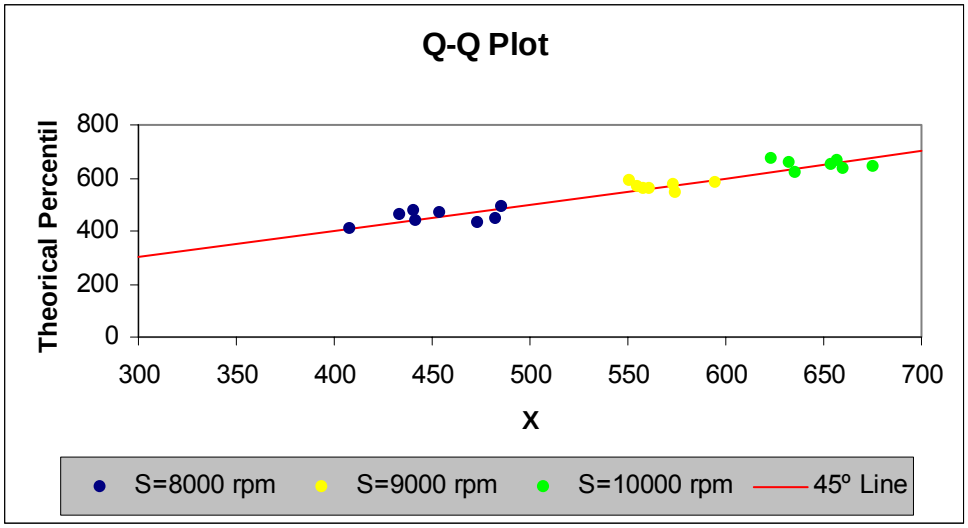

Figure 61. Q-Q Plot graph for 7075-T6 aluminum that shows statistical evidence of a normal distribution of the data.

As it can be seen in the Q-Q Plot in Figure 61, the data is almost adjusted to the 45º line marked in red. This means that there is enough statistical evidence that the data follows a normal distribution. To build this plot, the tables shown are needed to be developed; where the k value is an index given to each data, the x column is the data being analyzed, in this case the resultant acceleration value. The probability column is a value calculated with equation 3:

$$\Pr ob = \frac{k - 0.5}{n} \qquad \text{(Equation 3)}$$

Where n is the number of samples. In the other hand the percentile is calculated with the inverse distribution function of that probability.

Once we are sure that it follows a normal distribution the next step is the correlation analysis. The correlation analysis is performed to identify those parameters which have a strong linear correlation.

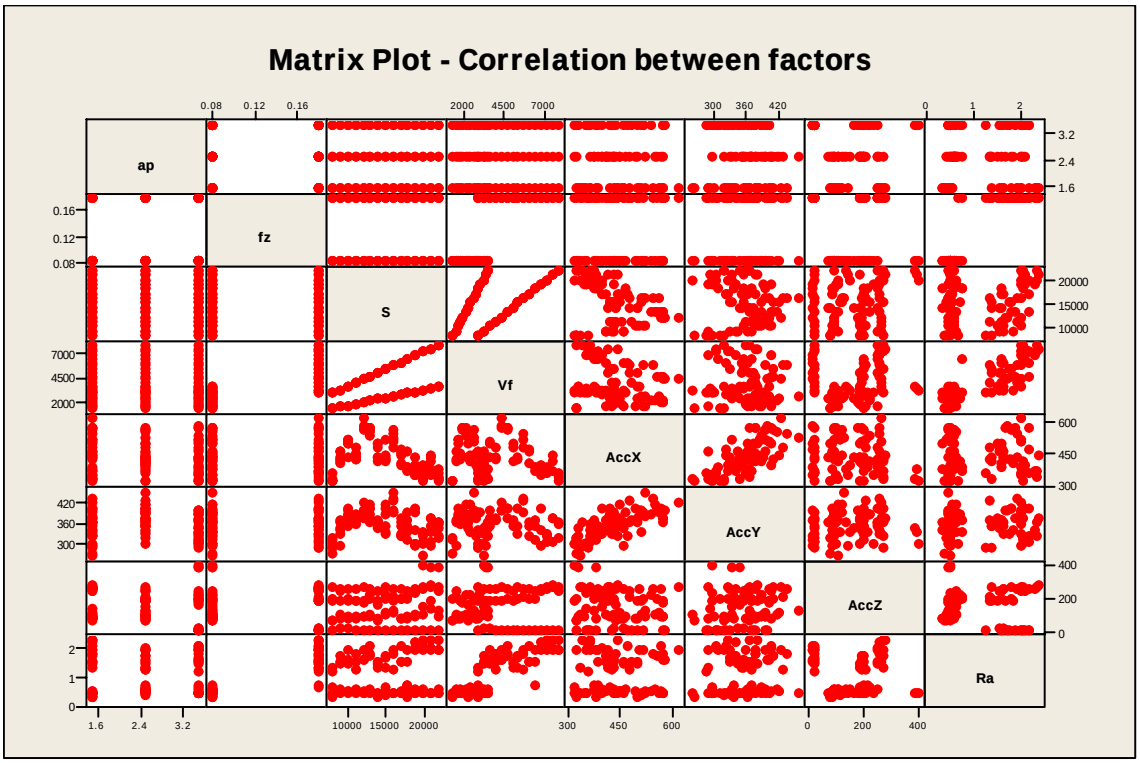

Figure 62. Matrix Plot with the correlation of all factors for 7075-T6 aluminum. The distribution of points suggests if there is linear correlation between factors.

In the Matrix plot shown in Figure 62, most of the interactions seem not to follow a linear correlation, except AccX with AccY. To visualize the previous graph in numbers, the next matrix shows the correlation factor and the p-value. The p-value has an inversely proportional function than the correlation factor. As smaller the p-value a higher correlation may be seen.

	ap	fz	S	Vf	AccX	AccY	AccZ
fz	-0.000						
	1.000						
S	0.000	-0.000					
	1.000	1.000					
Vf	-0.000	0.780	0.584				
	1.000	0.000	0.000				
AccX	-0.082	-0.003	-0.360	-0.212			
	0.441	0.979	0.000	0.045			
AccY	-0.056	0.043	-0.132	-0.026	0.732		
	0.603	0.688	0.217	0.808	0.000		
AccZ	-0.210	0.074	0.184	0.143	-0.133	0.150	
	0.047	0.487	0.082	0.179	0.211	0.157	
Ra	-0.008	0.917	0.155	0.839	0.021	0.083	0.089
	0.938	0.000	0.145	0.000	0.845	0.437	0.406

Cell Contents: Pearson correlation
P-Value

Table 16. Correlation matrix between factor for 7075-T6 aluminum.

After the correlation analysis it can be seen in its results, that the models to be developed must contain factors and interactions with higher orders. There is not such an statistical tool which permits to know at what approximate order is the interaction behaving. For such reason the regression analysis must be done several times, testing different factors and interactions at different exponential orders. The importance of these factors and interactions is reflected in the p-value, which appears in the summary output of a regression analysis. The p-value is the probability of the coefficient to be cero. In this case, al regression analysis was done with a confidence level of 95%, with this level all factors and interactions with a p-value below 0.05 must remain in the final equation, and those above 0.05 must be eliminated from the equation without considerably affecting the efficiency of the model.

Three regression models were obtained from the Table 17 which shows all the date acquired for 7075-T6 aluminum. The first model uses all the variables which are related to geometrical aspects, such as depth of cut and spindle speed. With this variables a model capable of predicting the resultant acceleration was developed. The resultant acceleration is calculated with the square root of the sum

of squares of AccX, AccY and AccZ. The results of these regression analysis can be seen in Table 17.

The third and fourth models are related with the prediction of the surface roughness. In this model, only the factors and interactions related with forces were used. These parameters are the resultant acceleration, the feed per tooth and the feed rate. The third model is obtained with the data corresponding to a constant feed per tooth of 0.08 mm/t. And the fourth model correspond to a feed per tooth of 0.18 mm/t. This separation of models is due to a very different level in the surface roughness obtained in both feed per tooth values. This difference can be seen in appendix J, where all graphs of vibrations are presented.

ap	S	fz	Vf	AccX	AccY	AccZ	Ra	ap	S	fz	Vf	AccX	AccY	AccZ	Ra
1.5	8000	0.08	1280	322.9836	264.6408	7.21106	0.333333	1.5	8000	0.18	2880	335.3953	288.1363	26.74513	1.363333
1.5	9000	0.08	1440	458.1532	289.0002	8.051256	0.46	1.5	9000	0.18	3240	430.1181	330.3544	26.21568	1.606667
1.5	10000	0.08	1600	518.9045	383.0225	8.868199	0.513333	1.5	10000	0.18	3600	505.1689	400.8165	26.33364	2.02
1.5	11000	0.08	1760	454.8676	359.0664	8.61278	0.496667	1.5	11000	0.18	3960	436.4135	377.2245	26.00003	1.896667
1.5	12000	0.08	1920	575.1447	375.8943	9.265032	0.49	1.5	12000	0.18	4320	617.4536	422.556	26.6319	2.003333
1.5	13000	0.08	2080	573.4816	366.86	9.548791	0.476667	1.5	13000	0.18	4680	568.867	405.768	25.6898	2.17
1.5	14000	0.08	2240	499.3571	362.4721	7.731466	0.3	1.5	14000	0.18	5040	478.101	367.6481	24.97529	1.543333
1.5	15000	0.08	2400	512.6368	333.4595	11.02932	0.363333	1.5	15000	0.18	5400	421.9626	409.7809	27.02763	1.8
1.5	16000	0.08	2560	563.6839	395.2877	12.06425	0.433333	1.5	16000	0.18	5760	543.6734	435.3446	25.39893	1.906667
1.5	17000	0.08	2720	442.1657	322.6457	8.359547	0.45	1.5	17000	0.18	6120	458.518	362.026	25.31828	1.61
1.5	18000	0.08	2880	381.4991	337.4934	7.963874	0.28	1.5	18000	0.18	6480	385.1456	355.4486	24.56918	1.573333
1.5	19000	0.08	3040	344.764	300.3602	9.561539	0.44	1.5	19000	0.18	6840	363.7758	340.8323	25.46904	2.316667
1.5	20000	0.08	3200	335.5193	260.6044	10.5407	0.48	1.5	20000	0.18	7200	364.616	324.537	27.06016	2.34
1.5	21000	0.08	3360	351.2223	292.9833	13.7412	0.46	1.5	21000	0.18	7560	444.2373	379.1908	27.71312	2.386667
1.5	22000	0.08	3520	326.8642	319.35	9.012942	0.46	1.5	22000	0.18	7920	342.3534	367.2903	27.25068	2.363333
2.5	8000	0.08	1280	324.3972	317.0876	7.353242	0.373333	2.5	8000	0.18	2880	319.1328	297.8251	18.67082	0.65
2.5	9000	0.08	1440	409.9985	368.8411	10.44175	0.556667	2.5	9000	0.18	3240	407.5967	340.1717	19.1352	1.836667
2.5	10000	0.08	1600	496.0289	404.6883	7.94334	0.553333	2.5	10000	0.18	3600	497.5247	379.0797	18.69581	1.5
2.5	11000	0.08	1760	419.9038	387.9358	8.939624	0.566667	2.5	11000	0.18	3960	424.6749	369.2741	19.07393	1.326667
2.5	12000	0.08	1920	565.8299	396.0475	8.925196	0.536667	2.5	12000	0.18	4320	574.4059	402.3842	18.87713	1.653333
2.5	13000	0.08	2080	552.8311	416.5961	10.18788	0.59	2.5	13000	0.18	4680	558.236	408.4145	19.90369	1.78
2.5	14000	0.08	2240	436.6798	364.1634	7.082542	0.48	2.5	14000	0.18	5040	414.9527	350.9904	18.64304	1.363333
2.5	15000	0.08	2400	445.4502	420.9124	12.19452	0.523333	2.5	15000	0.18	5400	428.4512	353.3633	19.84495	1.363333
2.5	16000	0.08	2560	521.1131	456.4221	12.71514	0.44	2.5	16000	0.18	5760	477.1421	429.0175	20.88364	1.34
2.5	17000	0.08	2720	448.3955	375.7706	8.570837	0.503333	2.5	17000	0.18	6120	409.0293	352.0681	19.65901	1.57
2.5	18000	0.08	2880	464.3979	393.5576	9.139698	0.573333	2.5	18000	0.18	6480	371.6223	369.7736	19.99495	0.706667
2.5	19000	0.08	3040	430.9332	392.2561	10.30524	0.586667	2.5	19000	0.18	6840	396.2677	405.9067	25.0187	2.086667
2.5	20000	0.08	3200	394.7084	334.2005	15.02718	0.583333	2.5	20000	0.18	7200	383.678	329.6733	25.37283	2.006667
2.5	21000	0.08	3360	432.2923	354.1016	18.62155	0.49	2.5	21000	0.18	7560	415.1653	376.9077	26.85214	2.03
2.5	22000	0.08	3520	374.6668	364.7483	13.31421	0.57	2.5	22000	0.18	7920	359.7353	360.2925	24.95084	2.003333
3.5	8000	0.08	1280	322.7061	312.5776	20.07648	0.483333	3.5	8000	0.18	2880	357.4156	285.9607	15.54738	1.226667
3.5	9000	0.08	1440	426.0039	362.8304	24.71182	0.613333	3.5	9000	0.18	3240	461.1834	344.2188	17.36347	1.55
3.5	10000	0.08	1600	517.9505	388.5594	20.51378	0.43	3.5	10000	0.18	3600	428.4174	353.1667	18.08879	1.636667
3.5	11000	0.08	1760	433.2508	370.2688	18.53527	0.42	3.5	11000	0.18	3960	480.251	368.5724	14.35087	1.556667
3.5	12000	0.08	1920	574.6946	400.8702	17.41858	0.43	3.5	12000	0.18	4320	578.1194	398.5637	13.12936	1.69
3.5	13000	0.08	2080	537.258	386.3606	22.00518	0.553333	3.5	13000	0.18	4680	574.1353	378.4443	15.85583	1.89
3.5	14000	0.08	2240	435.7082	348.7415	16.29785	0.45	3.5	14000	0.18	5040	496.6699	371.6943	11.17496	1.596667
3.5	15000	0.08	2400	417.6299	386.3435	22.19054	0.676667	3.5	15000	0.18	5400	425.1352	330.9027	14.60531	1.75
3.5	16000	0.08	2560	507.6872	403.2848	18.87615	0.46	3.5	16000	0.18	5760	514.4378	396.6893	13.79333	1.993333
3.5	17000	0.08	2720	395.2219	325.9574	19.90866	0.453333	3.5	17000	0.18	6120	471.3322	320.7718	11.83514	2.183333
3.5	18000	0.08	2880	386.9477	335.0373	21.13413	0.71	3.5	18000	0.18	6480	382.0322	307.4482	11.89892	2.036667
3.5	19000	0.08	3040	348.4013	297.2878	23.36727	0.456667	3.5	19000	0.18	6840	348.245	290.6954	13.09495	2.013333
3.5	20000	0.08	3200	317.3128	296.5488	39.95786	0.46	3.5	20000	0.18	7200	354.5638	301.8654	15.61592	2.153333
3.5	21000	0.08	3360	381.1077	331.3357	39.18652	0.47	3.5	21000	0.18	7560	363.4788	303.9339	16.67517	2.1
3.5	22000	0.08	3520	327.8863	346.9028	38.77339	0.44	3.5	22000	0.18	7920	319.7032	316.7823	14.88996	2.026667

Table 17. Data used for regression analysis for 7075-T6 aluminum.

SUMMARY OUTPUT

Regression Statistics	
Multiple R	0.728922418
R Square	0.531327892
Adjusted R Square	0.509272734
Standard Error	56.65208718
Observations	90

ANOVA

	df	*SS*	*MS*	*F*	*Significance F*
Regression	4	309274.6052	77318.6513	24.09086757	2.42386E-13
Residual	85	272804.0135	3209.458982		
Total	89	582078.6187			

	Coefficients	*Standard Error*	*t Stat*	*P-value*	*Lower 95%*	*Upper 95%*
Intercept	-1556.444671	288.2991352	-5.398714324	5.98514E-07	-2129.660578	-983.2287637
(ap*S)^3	-0.000581598	0.000468535	-1.241310213	0.217905895	-0.001513171	0.000349976
S	0.450218919	0.062960055	7.150866005	2.80053E-10	0.325037464	0.575400374
S^2	-2.89473E-05	4.36338E-06	-6.634138909	2.87653E-09	-3.76228E-05	-2.02717E-05
S^3	5.86818E-10	9.66333E-11	6.072632341	3.41463E-08	3.94685E-10	7.78951E-10

Table 18. Regression summary output for the resultant acceleration prediction in 7075-T6 aluminum.

SUMMARY OUTPUT

Regression Statistics	
Multiple R	0.723071202
R Square	0.522831963
Adjusted R Square	0.506186567
Standard Error	56.82994949
Observations	90

ANOVA

	df	*SS*	*MS*	*F*	*Significance F*
Regression	3	304329.307	101443.1023	31.41000331	8.3068E-14
Residual	86	277749.3117	3229.643159		
Total	89	582078.6187			

	Coefficients	*Standard Error*	*t Stat*	*P-value*	*Lower 95%*	*Upper 95%*
Intercept	-1556.444671	289.204266	-5.381817814	6.28712E-07	-2131.363712	-981.5256292
S	0.448764925	0.063146791	7.106694116	3.26082E-10	0.323233262	0.574296587
S^2	-2.89473E-05	4.37708E-06	-6.613375856	3.03415E-09	-3.76486E-05	-2.02459E-05
S^3	5.86818E-10	9.69367E-11	6.05362665	3.59838E-08	3.94115E-10	7.79522E-10

Table 19. Second regression summary output for the resultant acceleration prediction in 7075-T6 aluminum.

The first regression analysis shown for this material helps to understand how to select only the factors that have a considerable weight in the equation. In the very last part of the table, at the left we have the factors that are being studied. The next column at the right of the factors we have the coefficients, which are the ones that must be placed in the equation and multiply the factor. Other important column is the p-value, factors with a p-value over 0.05 must be eliminated and the regression analysis must be done again. In this analysis the interaction $(ap*S)^3$ shows little or none influence. The factor is eliminated from the analysis and the second table shows the analysis with the remaining factors. Once having very low p-values we can construct our model with the coefficients shown. For the resultant acceleration prediction for 7075-T6 aluminum the model ends as follows:

$$Acc\,\mathrm{Re}\,s = -1556.44 + (0.448764 * S) + (-2.89473E-05 * S^2) + (5.86818E-10 * S^3)$$

Figure 63, Figure 64, and Figure 65 show the predicted resultant acceleration compared to the real resultant acceleration. Results are presented in a graph for each depth of cut, 1.5, 2.5 and 3.5 mm.

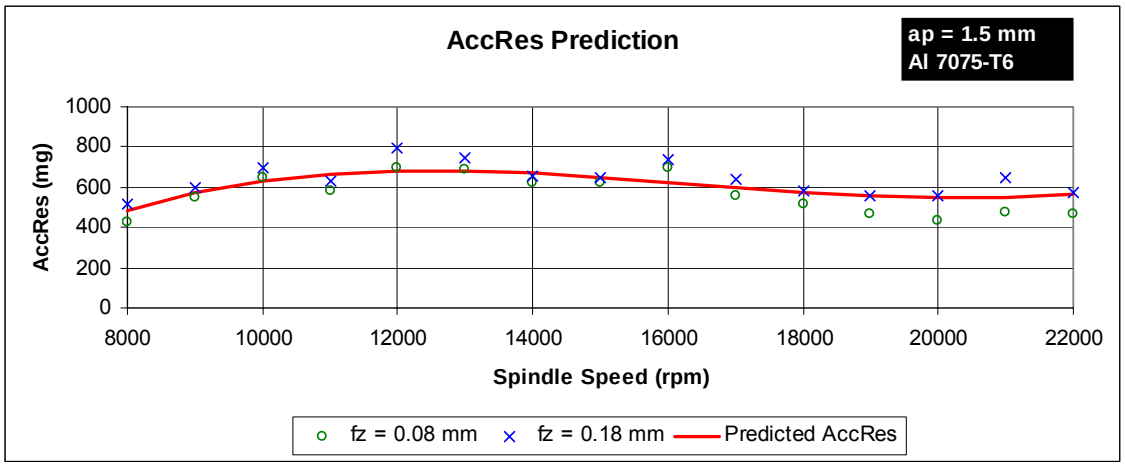

Figure 63. Resultant acceleration model response for 7075-T6 aluminum and ap = 1.5 mm.

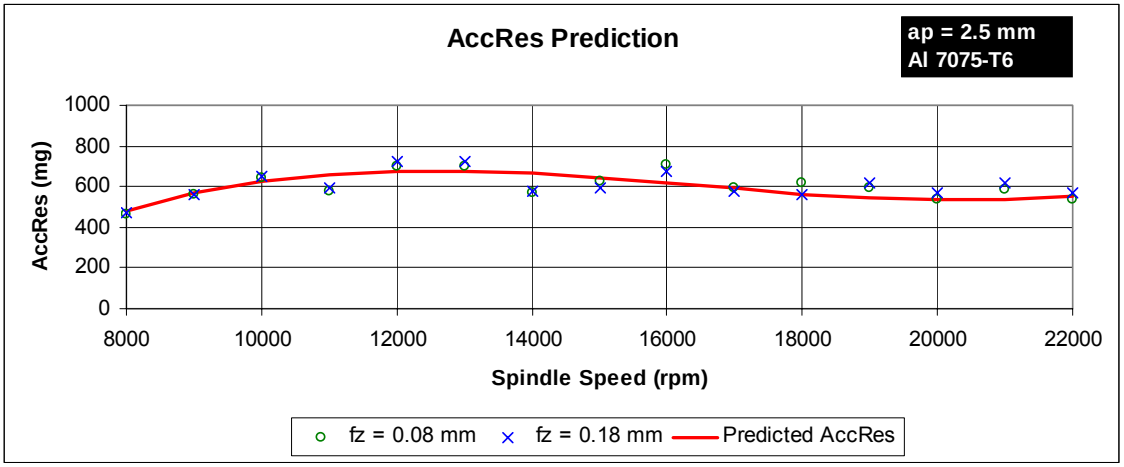

Figure 64. Resultant acceleration model response for 7075-T6 aluminum and ap = 2.5 mm.

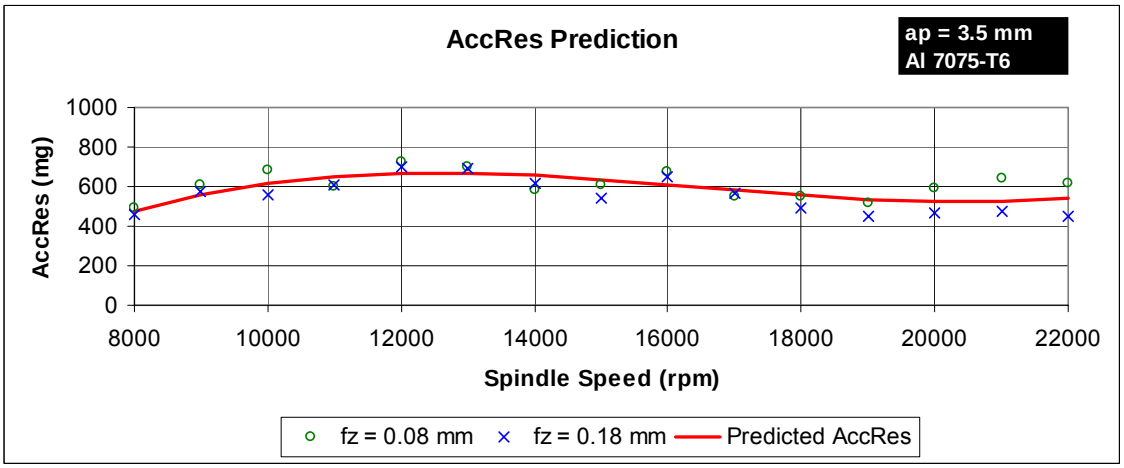

Figure 65. Resultant acceleration model response for 7075-T6 aluminum and ap = 3.5 mm.

SUMMARY OUTPUT

Regression Statistics	
Multiple R	0.259322831
R Square	0.067248331
Adjusted R Square	-0.001001791
Standard Error	0.086609725
Observations	45

ANOVA

	df	*SS*	*MS*	*F*	*Significance F*
Regression	3	0.022173418	0.007391139	0.985321764	0.409133803
Residual	41	0.307551026	0.007501245		
Total	44	0.329724444			

	Coefficients	*Standard Error*	*t Stat*	*P-value*	*Lower 95%*	*Upper 95%*
Intercept	0.002019552	0.332995156	0.006064809	0.995190426	-0.670477801	0.674516905
Vf	0.000155873	0.000140068	1.112832722	0.272262545	-0.000127001	0.000438747
AccRes	0.000812845	0.000588712	1.380718976	0.17484623	-0.000376082	0.002001773
Vf*AccRes	-2.63134E-07	2.52199E-07	-1.043358036	0.302895602	-7.7246E-07	2.46192E-07

Table 20. Regression summary output for the surface roughness prediction and fz = 0.08 mm/t in 7075-T6 aluminum.

After developing the resultant acceleration equation is time to focus on the surface roughness. As well, a regression analysis is done and the resultant equation for fz=0.08 mm/t ends as follows:

$$Ra = 0.002019552 + (0.000155873 * Vf) + (0.000812845 * Acc\,\mathrm{Re}\,s) - (2.63134E-07 * Vf * Acc\,\mathrm{Re}\,s)$$

Figure 66, Figure 67, and Figure 68 correspond to the measured and predicted surface roughness for the model of fz = 0.08 mm/t. These measurements correspond to the scale in micrometers in the left, while the yellow line correspond to the percetange of error in the prediction, and its scale is shown in the right of the graph. Figure 69, Figure 70, and Figure 71 show the same information, but for fz = 0.18 mm/t.

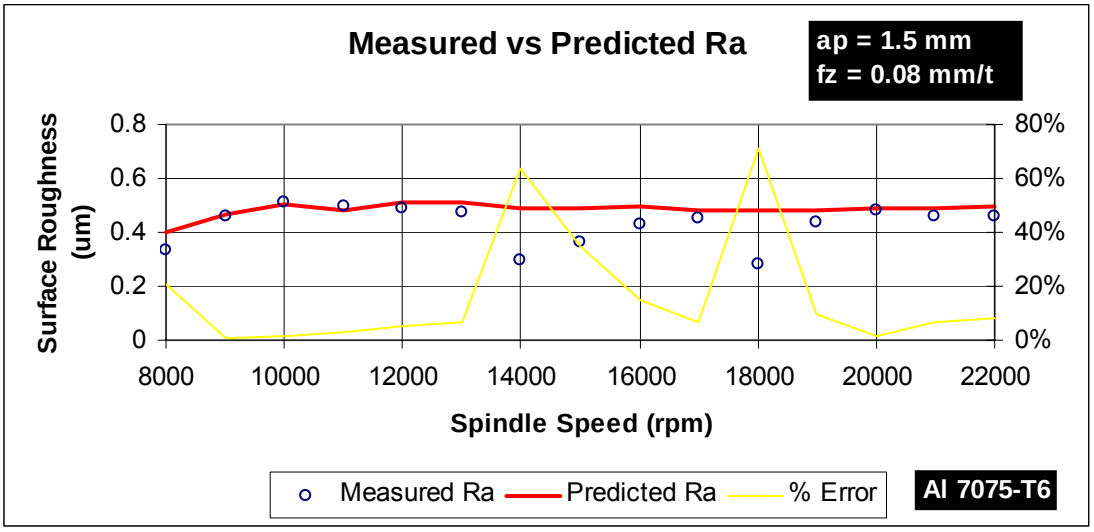

Figure 66. Measured vs Predicted Ra for 7075-T6 aluminum at an ap of 1.5 mm and 0.08 mm/t of feed per tooth.

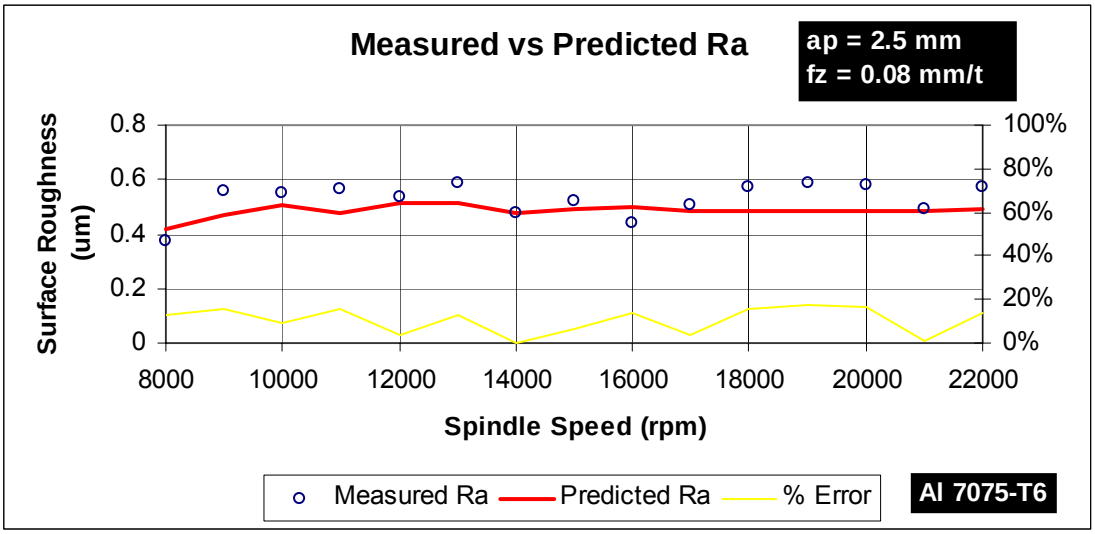

Figure 67. Measured vs Predicted Ra for 7075-T6 aluminum at an ap of 2.5 mm and 0.08 mm/t of feed per tooth.

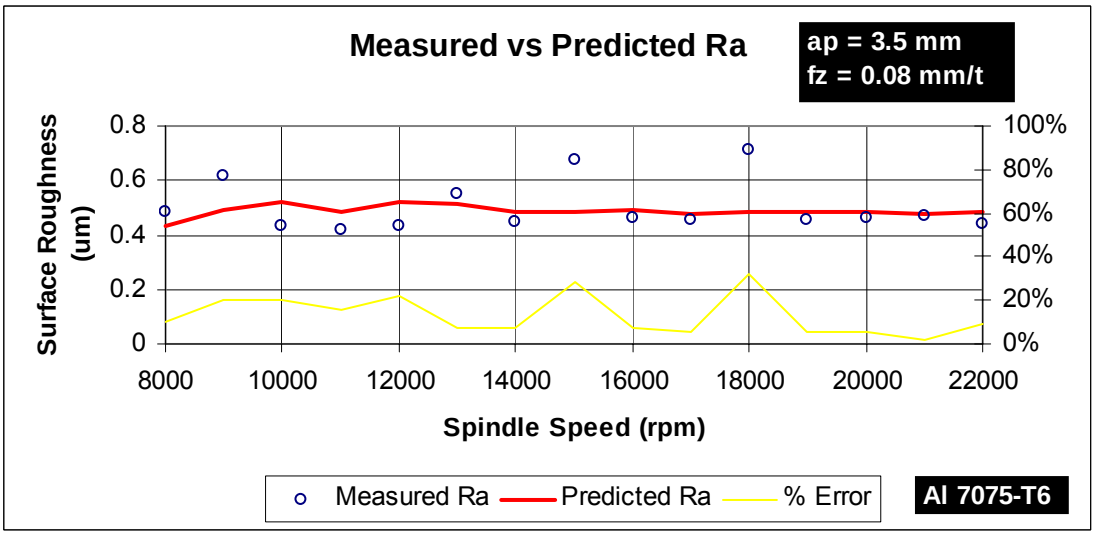

Figure 68. Measured vs Predicted Ra for 7075-T6 aluminum at an ap of 3.5 mm and 0.08 mm/t of feed per tooth.

SUMMARY OUTPUT

Regression Statistics	
Multiple R	0.650066416
R Square	0.422586345
Adjusted R Square	0.380336565
Standard Error	0.305188952
Observations	45

ANOVA

	df	*SS*	*MS*	*F*	*Significance F*
Regression	3	2.794794514	0.931598171	10.00209584	4.49575E-05
Residual	41	3.818752153	0.093140296		
Total	44	6.613546667			

	Coefficients	*Standard Error*	*t Stat*	*P-value*	*Lower 95%*	*Upper 95%*
Intercept	-2.036381137	1.22038966	-1.668631916	0.102810613	-4.501008027	0.428245754
Vf	0.000596896	0.000226961	2.629944923	0.011971778	0.000138538	0.001055253
AccRes	0.005252519	0.002126876	2.469593029	0.017780354	0.000957205	0.009547833
Vf*AccRes	-8.00655E-07	4.03612E-07	-1.983725706	0.054009561	-1.61577E-06	1.44555E-08

Table 21. Regression summary output for the surface roughness prediction and fz = 0.18 mm/t in 7075-T6 aluminum.

A second equation is obtained for the surface roughness but with fz = 0.18 mm/t.

$$Ra = -2.03638 + (0.0005969 * Vf) + (0.00525252 * Acc\,\mathrm{Res}) - (8.00655E-07 * Vf * Acc\,\mathrm{Res})$$

Figure 69, Figure 70, and Figure 71 show the results comparing the measured versus the predicted surface roughness for each depth of cut.

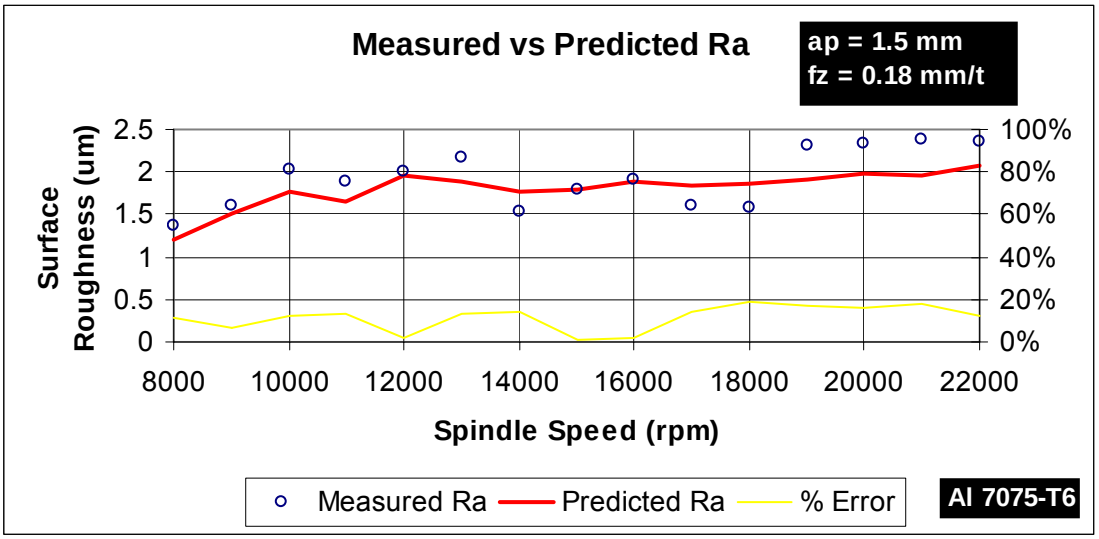

Figure 69. Measured vs Predicted Ra for 7075-T6 aluminum at an ap of 1.5 mm and 0.18 mm/t of feed per tooth.

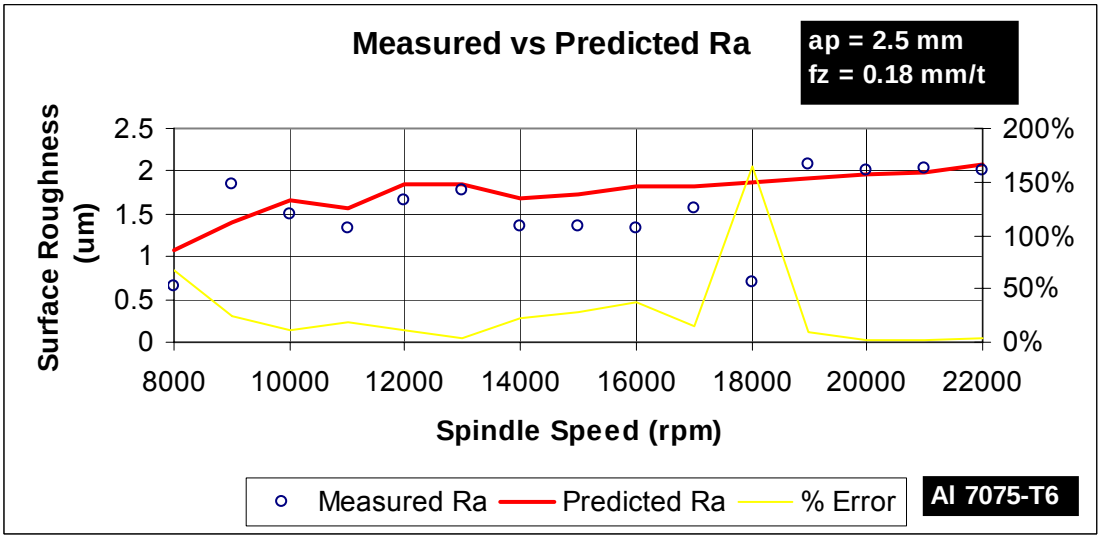

Figure 70. Measured vs Predicted Ra for 7075-T6 aluminum at an ap of 2.5 mm and 0.18 mm/t of feed per tooth.

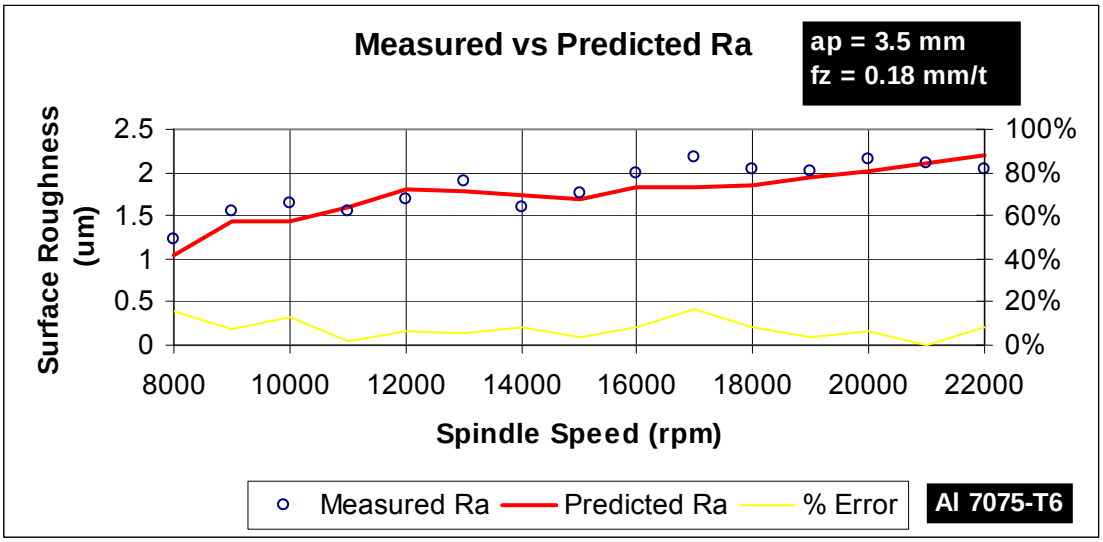

Figure 71. Measured vs Predicted Ra for 7075-T6 aluminum at an ap of 3.5 mm and 0.18 mm/t of feed per tooth.

6061-T6 aluminum

The same procedure is followed with this aluminum. No explanation will be done. For detailed information of the statistical procedures consult the 7075-T6 aluminum information in this appendix.

S	ap	AccX	AccY	AccZ	Accres
8000	2.5	258.8157	260.935	62.91734	372.8689
8000	2.5	319.2301	272.2529	69.49458	425.2752
8000	2.5	323.2779	326.2623	71.14834	464.7771
8000	2.5	311.9814	285.8563	70.23247	428.9275
8000	2.5	331.1539	270.5244	73.4547	433.8685
8000	2.5	362.0915	305.3325	71.19581	478.9646
8000	2.5	349.2083	293.0526	70.00554	461.2234
8000	2.5	329.3436	313.1185	74.71173	460.5347

S	ap	AccX	AccY	AccZ	Accres
9000	2.5	402.2966	366.2117	85.98108	550.7689
9000	2.5	448.9536	350.3477	82.11065	575.3651
9000	2.5	433.4625	342.5742	80.69125	558.3528
9000	2.5	408.8719	378.7464	118.4372	569.7828
9000	2.5	390.1299	351.5715	112.1254	537.0064
9000	2.5	433.2593	369.1789	103.1617	578.4886
9000	2.5	417.3862	310.5213	104.3394	530.5859

S	ap	AccX	AccY	AccZ	Accres
10000	2.5	501.7544	422.5012	73.84702	660.0895
10000	2.5	458.3288	433.4093	77.7612	635.5751
10000	2.5	510.5406	385.8102	80.70903	644.9924
10000	2.5	459.6382	433.0276	96.44726	638.8132
10000	2.5	505.435	437.1025	82.58678	673.308
10000	2.5	492.4455	415.1787	98.61569	651.6142
10000	2.5	505.8303	409.2686	77.45862	655.2594

k	x	Prob	Percentil
1	372.8689	0.0625	389.324
2	425.2752	0.1875	411.0347
3	464.7771	0.3125	424.403
4	428.9275	0.4375	435.5261
5	433.8685	0.5625	446.0839
6	478.9646	0.6875	457.207
7	461.2234	0.8125	470.5753
8	460.5347	0.9375	492.286
Media	440.805	EstDev	33.55733

k	x	Prob	Percentil
1	550.7689	0.071429	529.7791
2	575.3651	0.214286	542.3817
3	558.3528	0.357143	550.3432
4	569.7828	0.5	557.1929
5	537.0064	0.642857	564.0426
6	578.4886	0.785714	572.0041
7	530.5859	0.928571	584.6067
Media	557.1929	EstDev	18.70952

k	x	Prob	Percentil
1	660.0895	0.071429	632.2715
2	635.5751	0.214286	641.0555
3	644.9924	0.357143	646.6046
4	638.8132	0.5	651.3788
5	673.308	0.642857	656.153
6	651.6142	0.785714	661.7021
7	655.2594	0.928571	670.4861
Media	651.3788	EstDev	13.04042

Table 22. Data of populations observed to obtain the Q-Q Plot for 6061-T6 aluminum.

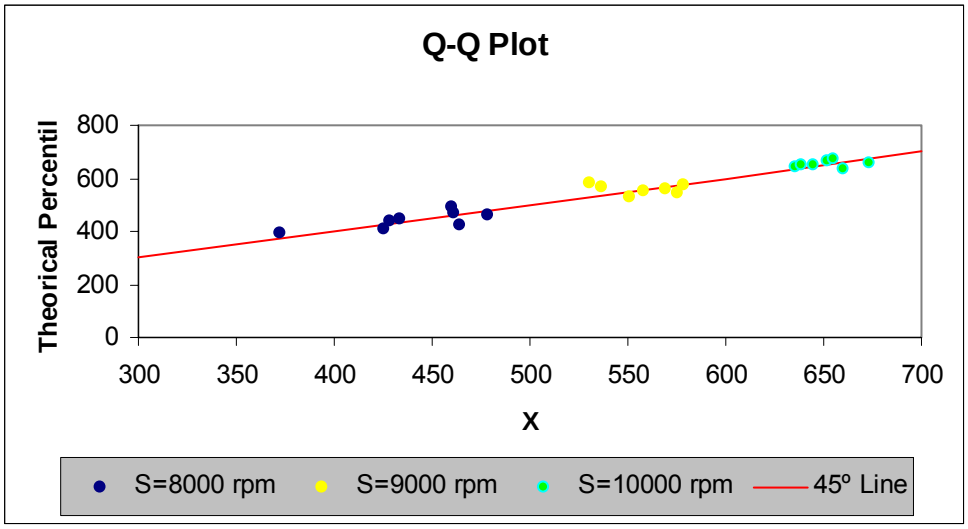

Figure 72. Q-Q Plot graph for 6061-T6 aluminum that shows statistical evidence of a normal distribution of the data.

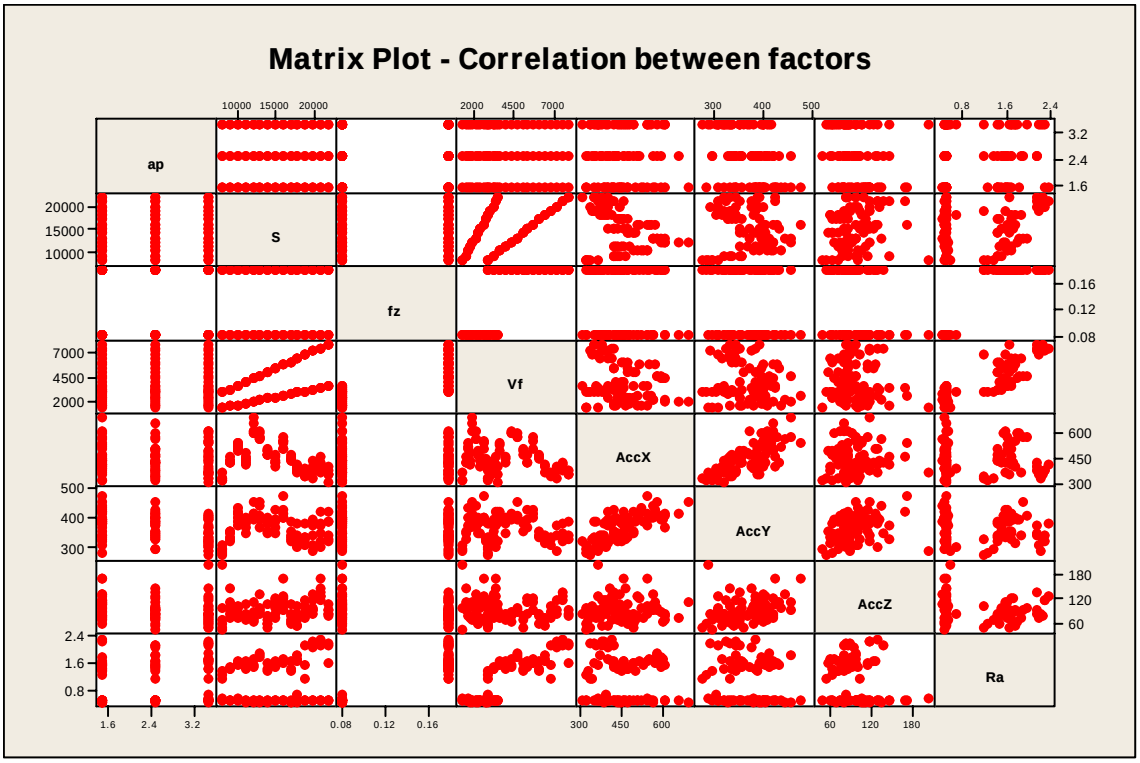

Figure 73. Matrix Plot with the correlation of all factors for 6061-T6 aluminum. The distribution of points suggests if there is linear correlation between factors.

	ap	S	fz	Vf	AccX	AccY	AccZ
S	0.000 1.000						
fz	-0.000 1.000	-0.000 1.000					
Vf	-0.000 1.000	0.584 0.000	0.780 0.000				
AccX	-0.034 0.754	-0.346 0.001	-0.020 0.853	-0.216 0.041			
AccY	-0.372 0.000	-0.058 0.585	-0.090 0.400	-0.118 0.270	0.712 0.000		
AccZ	-0.216 0.041	0.182 0.086	-0.274 0.009	-0.081 0.446	0.032 0.765	0.307 0.003	
Ra	0.058 0.586	0.157 0.141	0.942 0.000	0.861 0.000	-0.048 0.657	-0.091 0.394	-0.180 0.089

Table 23. Correlation matrix between factor for 6061-T6 aluminum.

ap	S	fz	Vf	AccX	AccY	AccZ	Ra	ap	S	fz	Vf	AccX	AccY	AccZ	Ra
1.5	8000	0.08	1280	318.64852	304.41235	9.8028	0.476667	1.5	8000	0.18	2880	316.4615	282.5497	6.105838	1.25
1.5	9000	0.08	1440	416.49202	351.99282	11.424	0.49	1.5	9000	0.18	3240	437.0358	318.4737	7.468691	1.416667
1.5	10000	0.08	1600	518.10841	433.64611	9.88536	0.476667	1.5	10000	0.18	3600	527.6415	388.9527	7.558589	1.58
1.5	11000	0.08	1760	415.74685	397.6997	11.0994	0.466667	1.5	11000	0.18	3960	451.5325	381.6261	7.878338	1.44
1.5	12000	0.08	1920	693.12631	454.15729	11.6013	0.43	1.5	12000	0.18	4320	610.2597	418.1974	7.890043	1.556667
1.5	13000	0.08	2080	564.64161	441.56809	13.3452	0.416667	1.5	13000	0.18	4680	595.7637	395.4136	9.080382	1.82
1.5	14000	0.08	2240	469.27145	404.45124	10.7621	0.443333	1.5	14000	0.18	5040	501.3811	387.7674	7.007385	1.396667
1.5	15000	0.08	2400	399.68716	397.17004	11.6804	0.466667	1.5	15000	0.18	5400	466.8674	369.5079	8.582052	1.476667
1.5	16000	0.08	2560	539.49605	475.18544	17.1291	0.463333	1.5	16000	0.18	5760	573.0644	427.5891	11.35413	1.606667
1.5	17000	0.08	2720	438.42038	392.17364	11.1203	0.41	1.5	17000	0.18	6120	447.3856	342.7469	7.818845	1.406667
1.5	18000	0.08	2880	383.10437	379.87948	10.5069	0.44	1.5	18000	0.18	6480	414.5659	329.2441	6.853251	1.648667
1.5	19000	0.08	3040	388.5098	382.40031	11.7597	0.45	1.5	19000	0.18	6840	362.7935	336.06	8.760105	1.57
1.5	20000	0.08	3200	437.79003	398.29231	13.0806	0.476667	1.5	20000	0.18	7200	379.1574	340.6235	11.82144	2.296667
1.5	21000	0.08	3360	451.80867	420.75797	17.0031	0.453333	1.5	21000	0.18	7560	409.4607	381.3625	12.84493	2.343333
1.5	22000	0.08	3520	399.7454	423.80727	10.7461	0.48	1.5	22000	0.18	7920	347.7379	391.0037	9.538172	1.643333
2.5	8000	0.08	1280	317.02775	292.39228	4.70223	0.446667	2.5	8000	0.18	2880	327.4259	292.9156	7.089358	1.356667
2.5	9000	0.08	1440	426.93948	348.01298	9.5694	0.456667	2.5	9000	0.18	3240	420.4941	351.6994	9.90548	1.473333
2.5	10000	0.08	1600	502.95631	404.60509	8.21307	0.47	2.5	10000	0.18	3600	488.3634	420.0689	8.529546	1.596667
2.5	11000	0.08	1760	430.77512	395.28693	7.72278	0.436667	2.5	11000	0.18	3960	425.0888	401.806	8.496725	1.576667
2.5	12000	0.08	1920	657.53086	417.42709	7.74265	0.456667	2.5	12000	0.18	4320	596.199	411.4076	8.980542	1.516667
2.5	13000	0.08	2080	567.52286	403.31129	9.66947	0.453333	2.5	13000	0.18	4680	575.3232	454.4022	9.505999	1.87
2.5	14000	0.08	2240	474.00363	380.01697	6.13082	0.463333	2.5	14000	0.18	5040	468.0963	381.8309	8.045687	1.41
2.5	15000	0.08	2400	455.92235	390.41047	10.1182	0.48	2.5	15000	0.18	5400	420.4917	430.9448	11.46793	1.563333
2.5	16000	0.08	2560	509.2091	403.39719	12.9225	0.446667	2.5	16000	0.18	5760	510.3544	418.6529	12.54737	1.67
2.5	17000	0.08	2720	432.29437	325.98794	7.26729	0.486667	2.5	17000	0.18	6120	453.8805	353.7735	8.38687	1.676667
2.5	18000	0.08	2880	378.58608	335.64906	5.79747	0.466667	2.5	18000	0.18	6480	366.501	343.4867	7.71909	1.856667
2.5	19000	0.08	3040	344.54153	331.6443	8.45462	0.486667	2.5	19000	0.18	6840	337.4613	329.8406	10.29252	1.163333
2.5	20000	0.08	3200	387.82054	389.09974	9.83529	0.47	2.5	20000	0.18	7200	395.8996	372.9575	9.40697	2.123333
2.5	21000	0.08	3360	405.61587	373.81464	14.5566	0.47	2.5	21000	0.18	7560	417.2979	351.1626	13.63866	2.136667
2.5	22000	0.08	3520	352.61988	385.62391	9.50327	0.476667	2.5	22000	0.18	7920	374.3463	341.4311	8.410161	2.136667
3.5	8000	0.08	1280	361.66423	286.46301	20.4079	0.533333	3.5	8000	0.18	2880	331.1058	272.3962	5.334237	1.156667
3.5	9000	0.08	1440	462.86708	328.17575	14.5794	0.473333	3.5	9000	0.18	3240	438.5575	332.5823	8.530943	1.43
3.5	10000	0.08	1600	541.70522	376.14869	10.5438	0.513333	3.5	10000	0.18	3600	545.6238	415.4498	8.512598	1.68
3.5	11000	0.08	1760	479.98107	366.11767	7.91521	0.47	3.5	11000	0.18	3960	452.8037	351.3809	6.938859	1.68
3.5	12000	0.08	1920	609.34772	407.18931	7.22489	0.493333	3.5	12000	0.18	4320	601.6395	398.1401	6.445733	1.756667
3.5	13000	0.08	2080	608.3126	370.45702	8.53324	0.463333	3.5	13000	0.18	4680	580.9488	412.5036	9.728087	1.94
3.5	14000	0.08	2240	490.75556	349.62204	5.964	0.453333	3.5	14000	0.18	5040	488.6959	356.9837	5.393279	1.64
3.5	15000	0.08	2400	435.1562	348.69312	7.78457	0.456667	3.5	15000	0.18	5400	417.2932	395.4554	12.12621	1.693333
3.5	16000	0.08	2560	553.55468	399.10632	10.5342	0.446667	3.5	16000	0.18	5760	551.7009	399.3166	9.594002	1.746667
3.5	17000	0.08	2720	446.62106	324.32933	6.65859	0.436667	3.5	17000	0.18	6120	470.403	333.5887	5.985224	1.463333
3.5	18000	0.08	2880	391.28546	300.29145	8.29641	0.666667	3.5	18000	0.18	6480	397.0091	311.4258	5.836751	1.733333
3.5	19000	0.08	3040	363.94286	316.57283	8.62122	0.48	3.5	19000	0.18	6840	353.667	304.4322	7.759761	2.163333
3.5	20000	0.08	3200	364.8925	305.51376	9.5927	0.463333	3.5	20000	0.18	7200	330.9703	289.5419	8.679347	2.213333
3.5	21000	0.08	3360	363.8932	303.02259	12.7668	0.46	3.5	21000	0.18	7560	376.0845	320.0954	11.66313	2.29
3.5	22000	0.08	3520	304.49016	318.21847	8.28458	0.46	3.5	22000	0.18	7920	346.0151	331.2296	8.082795	2.226667

Table 24. Data used for regression analysis for 6061-T6 aluminum.

SUMMARY OUTPUT

Regression Statistics	
Multiple R	0.84281188
R Square	0.710331866
Adjusted R Square	0.696700424
Standard Error	50.02863258
Observations	90

ANOVA

	df	*SS*	*MS*	*F*	*Significance F*
Regression	4	521695.1108	130423.7777	52.10981246	4.21486E-22
Residual	85	212743.4466	2502.864078		
Total	89	734438.5574			

	Coefficients	*Standard Error*	*t Stat*	*P-value*	*Lower 95%*	*Upper 95%*
Intercept	-2186.791609	254.5927648	-8.5893706	3.66107E-13	-2692.990223	-1680.592995
(ap*S)^3	-2.1152E-13	6.06994E-14	-3.484705219	0.00078152	-3.32206E-13	-9.08329E-14
S	0.582462322	0.055589484	10.47792276	5.63238E-17	0.471935537	0.692989108
S^2	-3.78886E-05	3.85324E-06	-9.83292057	1.11623E-15	-4.55499E-05	-3.02273E-05
S^3	7.78587E-10	8.53446E-11	9.122856177	3.0451E-14	6.08899E-10	9.48275E-10

Table 25. Regression summary output for the resultant acceleration prediction in 6061-T6 aluminum.

The equation for the resultant acceleration is shown next:

$$Acc\,\mathrm{Re}s = -2186.79161 - 2.1152E-13*(ap*S)^3 + (0.582462*S) - (3.7889E-05*S^2) + (7.7859E-10*S^3)$$

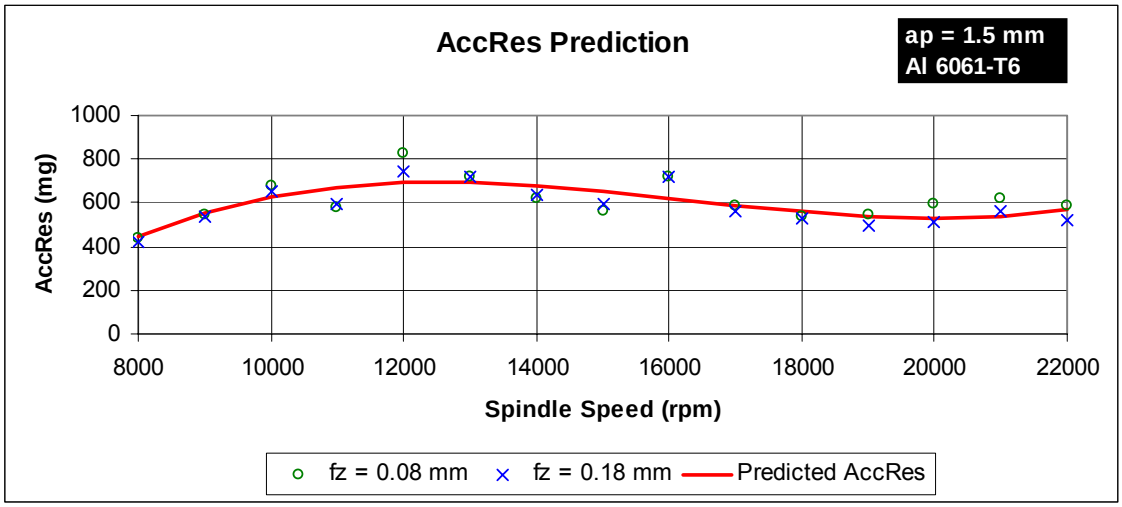

Figure 74. Resultant acceleration model response for 6061-T6 aluminum and ap = 1.5 mm.

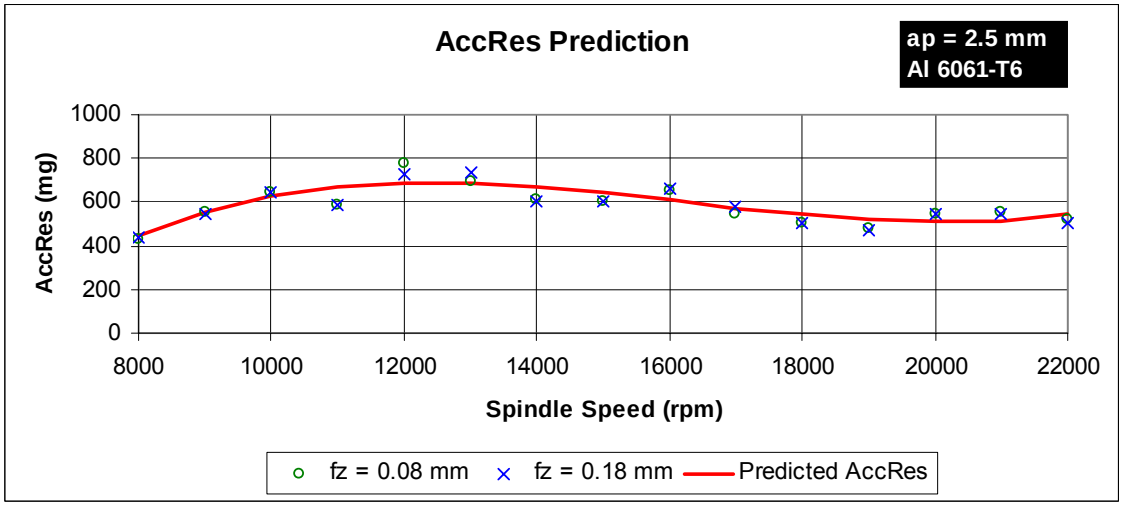

Figure 75. Resultant acceleration model response for 6061-T6 aluminum and ap = 2.5 mm.

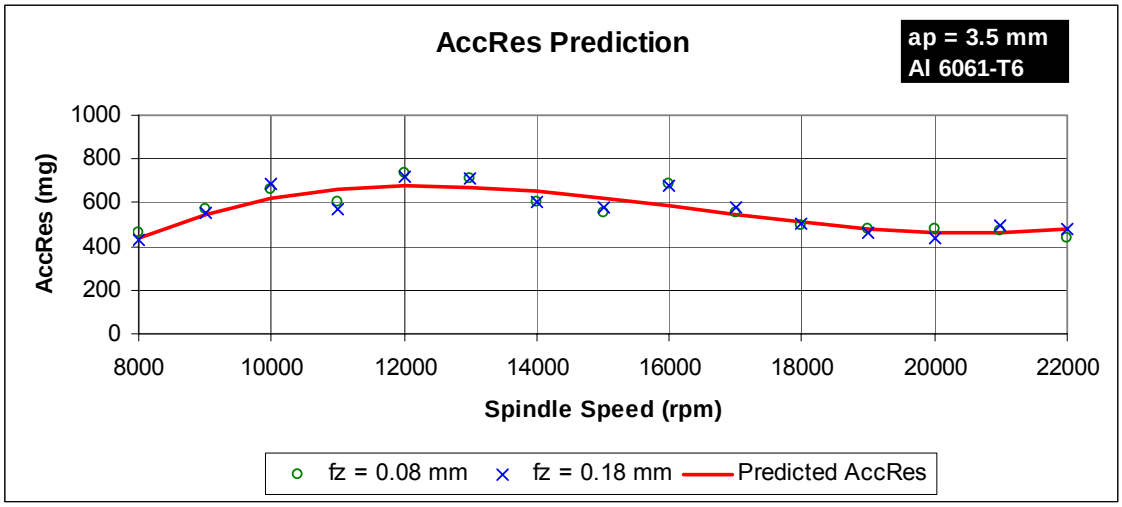

Figure 76. Resultant acceleration model response for 6061-T6 aluminum and ap = 3.5 mm.

SUMMARY OUTPUT

Regression Statistics	
Multiple R	0.309340063
R Square	0.095691275
Adjusted R Square	0.029522344
Standard Error	0.037016846
Observations	45

ANOVA

	df	*SS*	*MS*	*F*	*Significance F*
Regression	3	0.005944815	0.001981605	1.446166247	0.24334575
Residual	41	0.056180124	0.001370247		
Total	44	0.062124938			

	Coefficients	*Standard Error*	*t Stat*	*P-value*	*Lower 95%*	*Upper 95%*
Intercept	0.438936349	0.134329506	3.267609345	0.002197841	0.167652411	0.710220287
Vf	4.75301E-05	6.05378E-05	0.785130003	0.436890884	-7.47285E-05	0.000169789
Acc Res	8.47372E-05	0.000244503	0.346568686	0.730687805	-0.000409047	0.000578521
Vf*AccRes	-9.66617E-08	1.12454E-07	-0.859565298	0.395026894	-3.23768E-07	1.30444E-07

Table 26. Regression summary output for the surface roughness prediction and fz = 0.08 mm/t in 6061-T6 aluminum.

The next equation predicts the surface roughness for an fz = 0.08 mm/t.

$$Ra = 0.34893635 + (4.75301E-05*Vf) + (8.4737E-05*Acc\,\mathrm{Res}) - (9.66617E-08*Vf*Acc\,\mathrm{Res})$$

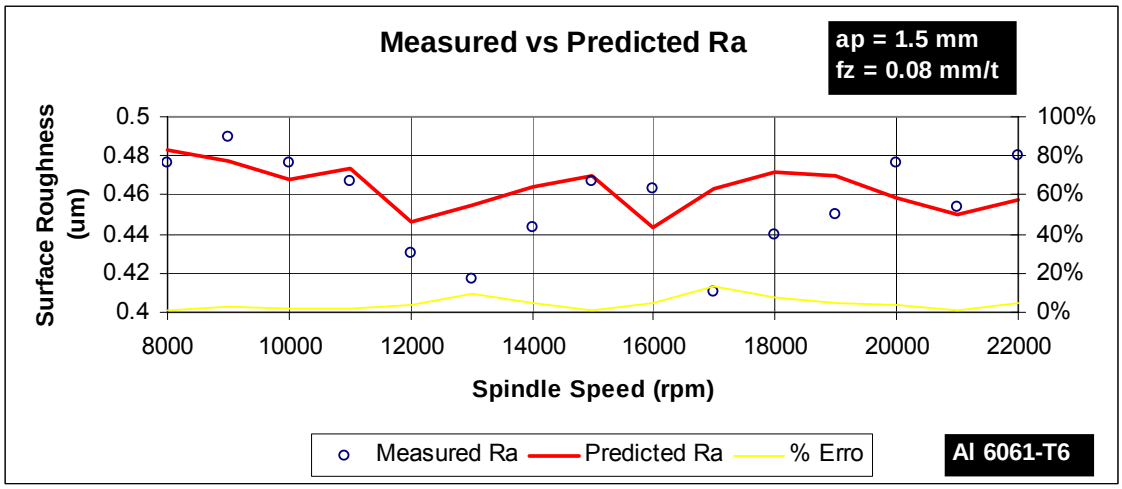

Figure 77. Measured vs Predicted Ra for 6061-T6 aluminum at an ap of 1.5 mm and 0.08 mm/t of feed per tooth.

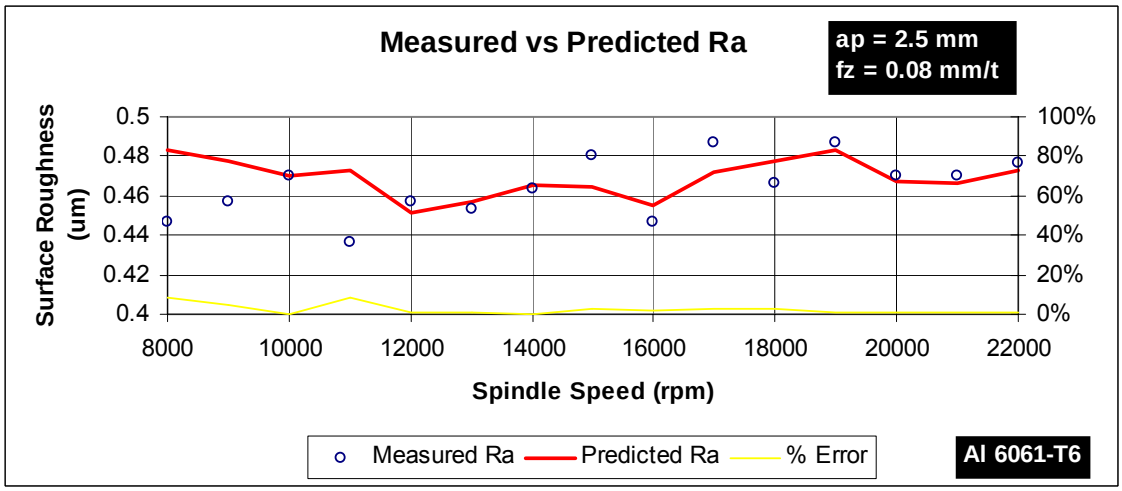

Figure 78. Measured vs Predicted Ra for 6061-T6 aluminum at an ap of 2.5 mm and 0.08 mm/t of feed per tooth.

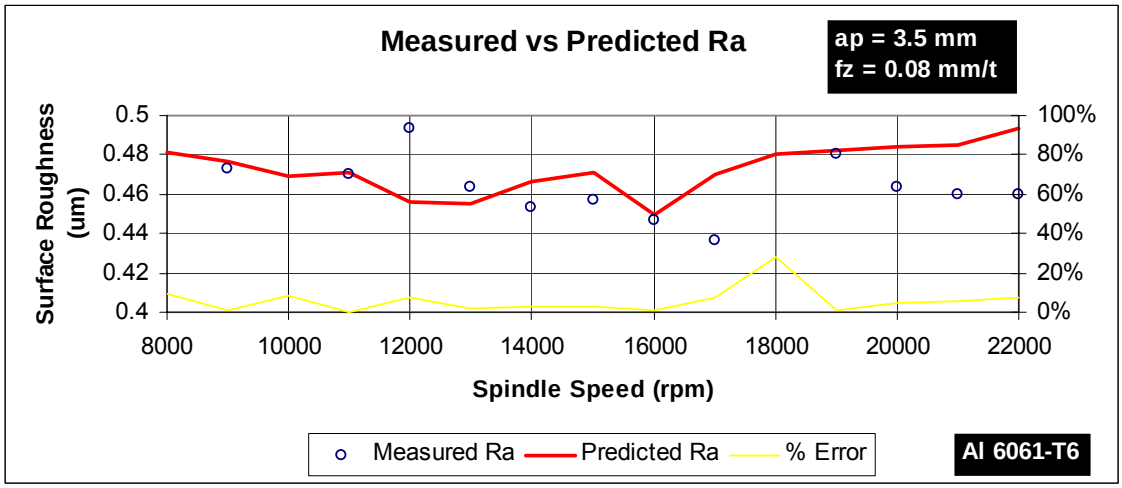

Figure 79. Measured vs Predicted Ra for 6061-T6 aluminum at an ap of 3.5 mm and 0.08 mm/t of feed per tooth.

SUMMARY OUTPUT

Regression Statistics	
Multiple R	0.71056957
R Square	0.504909113
Adjusted R Square	0.468682951
Standard Error	0.226808437
Observations	45

ANOVA

	df	*SS*	*MS*	*F*	*Significance F*
Regression	3	2.150951151	0.716983717	13.93769253	2.08157E-06
Residual	41	2.10912476	0.051442067		
Total	44	4.260075911			

	Coefficients	*Standard Error*	*t Stat*	*P-value*	*Lower 95%*	*Upper 95%*
Intercept	-0.982117576	0.891544264	-1.101591491	0.277064371	-2.782627725	0.818392574
Vf	0.00049374	0.000182356	2.707566163	0.009838771	0.000125465	0.000862015
Acc Res	0.003675913	0.001679439	2.188774683	0.034364174	0.000284218	0.007067609
Vf*AccRes	-6.85312E-07	3.49951E-07	-1.958307428	0.05702134	-1.39205E-06	2.14287E-08

Table 27. Regression summary output for the surface roughness prediction and fz = 0.18 mm/t in 7075-T6 aluminum.

Next equation helps predicts the surface roughness for an fz = 0.18 mm/t.

$$Ra = -0.982117576 + (0.00049374 * Vf) + (0.003675913 * Acc\,\mathrm{Re}\,s) - (6.85312E-07 * Vf * Acc\,\mathrm{Re}\,s)$$

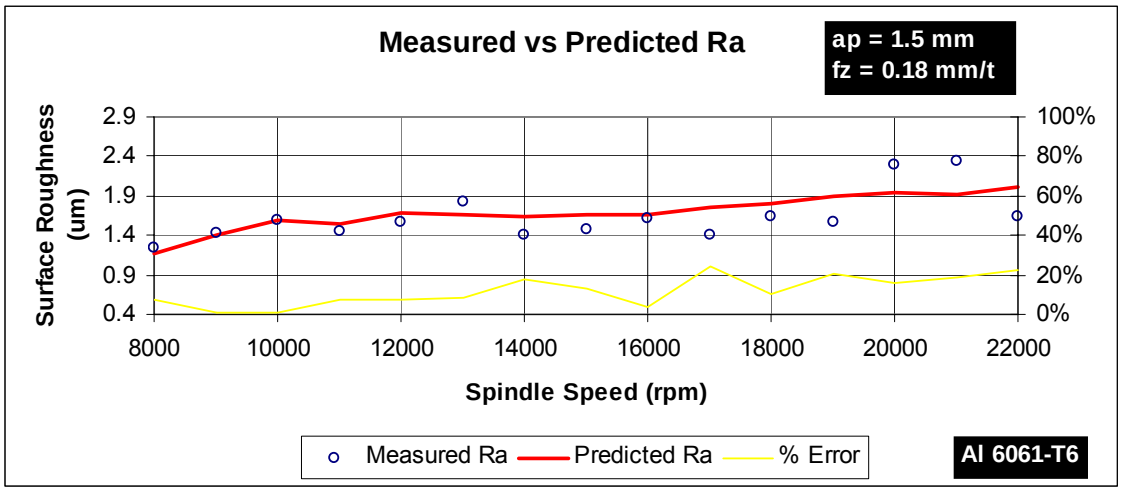

Figure 80. Measured vs Predicted Ra for 6061-T6 aluminum at an ap of 1.5 mm and 0.18 mm/t of feed per tooth.

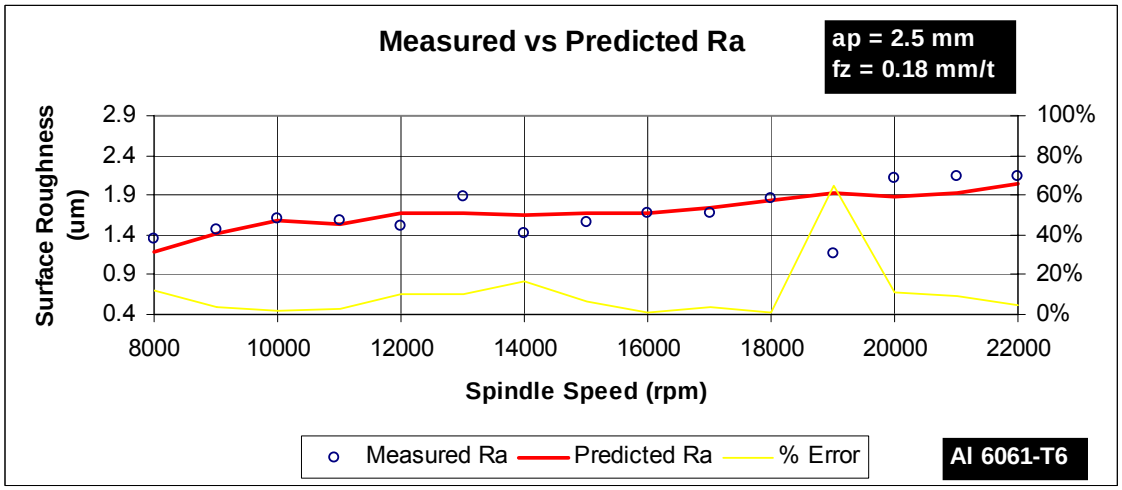

Figure 81. Measured vs Predicted Ra for 6061-T6 aluminum at an ap of 2.5 mm and 0.18 mm/t of feed per tooth.

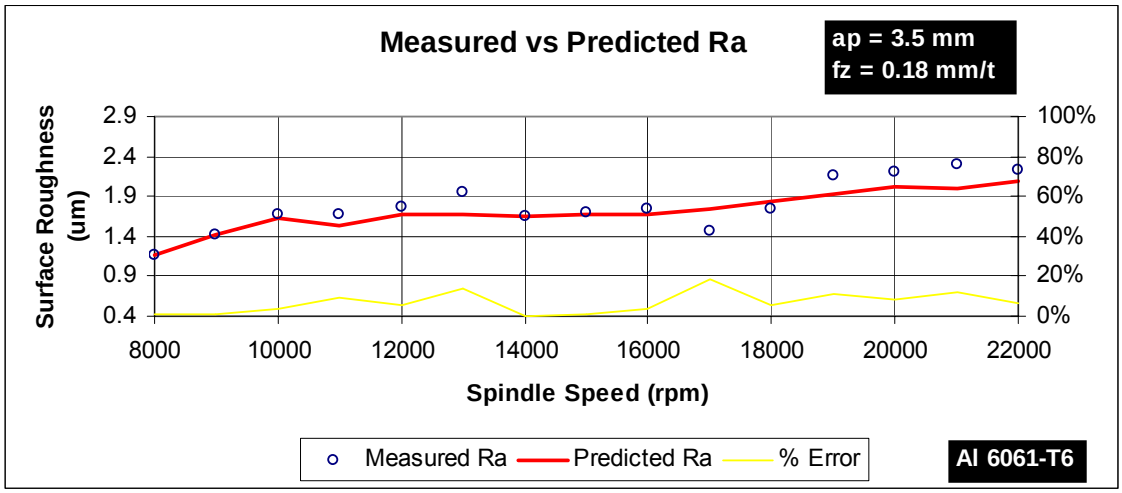

Figure 82. Measured vs Predicted Ra for 6061-T6 aluminum at an ap of 3.5 mm and 0.18 mm/t of feed per tooth.

1045 Steel

The complete analysis was made to 1045 Steel. The experiments are made under different conditions than the aluminum materials. The difference is due to the hardness of the material and the properties of the cutter. This differences are explained in section 4.3 and 4.4.

S	ap	AccX	AccY	AccZ	Accres
11000	0.4	499.1473	400.438	109.4801	649.2184
11000	0.4	529.1786	354.231	118.3601	647.7026
11000	0.4	429.2506	370.7244	117.9937	579.323
11000	0.4	441.9377	372.0557	119.5355	589.9348
11000	0.4	472.1769	376.4562	116.0952	614.9377
11000	0.4	468.4643	377.7859	121.3443	613.9262
11000	0.4	470.9362	371.4411	111.61	610.0871
11000	0.4	402.1037	359.8529	103.5555	549.459

k	x	Prob	Percentil
1	649.2184	0.0625	555.1962
2	647.7026	0.1875	576.9687
3	579.323	0.3125	590.3749
4	589.9348	0.4375	601.5297
5	614.9377	0.5625	612.1175
6	613.9262	0.6875	623.2723
7	610.0871	0.8125	636.6785
8	549.459	0.9375	658.451
Media	606.8236	EstDev	33.65276

S	ap	AccX	AccY	AccZ	Accres
12000	0.4	533.5999	377.613	111.9497	663.2142
12000	0.4	496.4066	414.7098	108.8305	655.9327
12000	0.4	517.6338	410.4168	107.9665	669.3605
12000	0.4	482.3459	437.2131	107.5201	659.8284
12000	0.4	522.0534	409.3122	113.0658	672.9488
12000	0.4	529.7958	372.2021	113.4032	657.3267
12000	0.4	555.3544	389.3507	104.4232	686.2337

k	x	Prob	Percentil
1	663.2142	0.071429	650.6907
2	655.9327	0.214286	657.9155
3	669.3605	0.357143	662.4797
4	659.8284	0.5	666.4064
5	672.9488	0.642857	670.3332
6	657.3267	0.785714	674.8974
7	686.2337	0.928571	682.1222
Media	666.4064	EstDev	10.72576

S	ap	AccX	AccY	AccZ	Accres
13000	0.4	534.5515	401.2536	117.7616	678.6881
13000	0.4	577.6395	433.3298	118.1472	731.7109
13000	0.4	579.1809	433.2449	112.4169	731.9763
13000	0.4	583.8585	407.1357	116.7093	721.2983
13000	0.4	589.9578	412.8908	123.4823	730.6004
13000	0.4	626.0645	406.7041	130.6328	757.9115
13000	0.4	579.8271	418.6748	129.5174	726.8169

k	x	Prob	Percentil
1	678.6881	0.071429	690.858
2	731.7109	0.214286	706.8166
3	731.9763	0.357143	716.8981
4	721.2983	0.5	725.5718
5	730.6004	0.642857	734.2454
6	757.9115	0.785714	744.3269
7	726.8169	0.928571	760.2855
Media	725.5718	EstDev	23.69159

Table 28. Data of populations observed to obtain the Q-Q Plot in 1045 Steel.

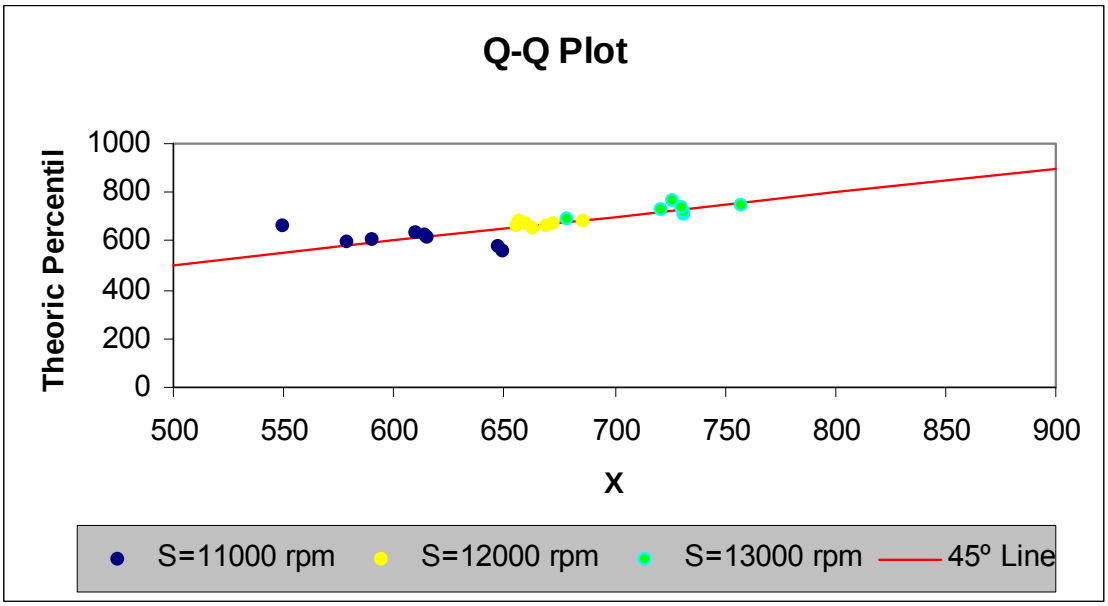

Figure 83. Q-Q Plot graph for 1045 Steel which shows statistical evidence of a normal distribution.

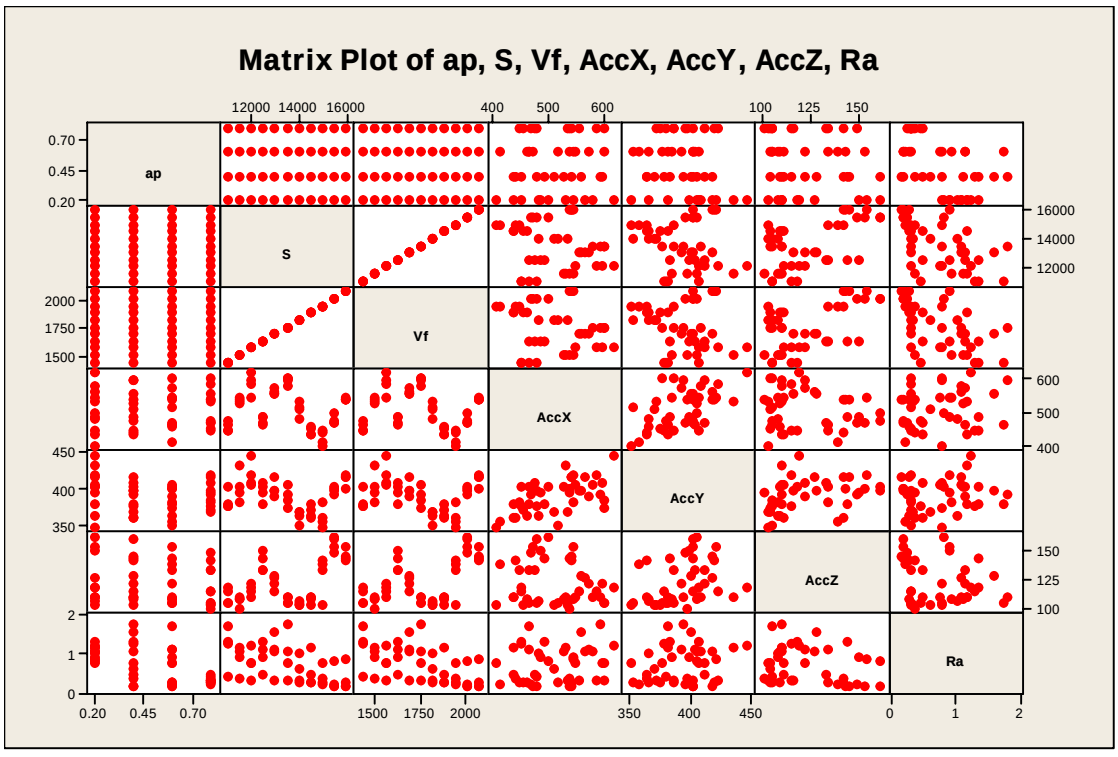

Figure 84. Matrix Plot with the correlation of all factors for 1045 Steel. The distribution of points suggests if there is linear correlation between factors.

	ap	S	Vf	AccX	AccY	AccZ
S	0.000 1.000					
Vf	-0.000 1.000	1.000 *				
AccX	0.040 0.794	-0.220 0.152	-0.220 0.152			
AccY	-0.157 0.309	-0.183 0.234	-0.183 0.234	0.561 0.000		
AccZ	-0.137 0.374	0.521 0.000	0.521 0.000	-0.161 0.296	0.337 0.025	
Ra	-0.563 0.000	-0.536 0.000	-0.536 0.000	0.157 0.307	0.180 0.243	-0.213 0.165

Cell Contents: Pearson correlation
P-Value

Table 29. Correlation matrix between factor for 1045 Steel.

ap	S	fz	Vf	Acc X	Acc Y	Acc Z	Ra
0.2	11000	0.065	1430	451.3914	405.3879	117.6868	1.346667
0.2	11500	0.065	1495	532.3773	434.4817	109.9922	1.156667
0.2	12000	0.065	1560	618.5632	447.0681	118.4932	1.233333
0.2	12500	0.065	1625	487.1068	397.7623	150.7929	0.9
0.2	13000	0.065	1690	564.5597	416.9468	126.7638	1.066667
0.2	13500	0.065	1755	578.5886	406.9511	109.6219	1.066667
0.2	14000	0.065	1820	480.6042	363.7981	107.1038	1.01
0.2	14500	0.065	1885	436.5966	380.2249	109.2574	1.163333
0.2	15000	0.065	1950	404.6057	348.932	102.7156	0.776667
0.2	15500	0.065	2015	500.2926	405.1455	162.2831	0.816667
0.2	16000	0.065	2080	543.113	421.4002	154.3643	0.89
0.4	11000	0.065	1430	451.1615	376.6488	114.5181	1.29
0.4	11500	0.065	1495	526.9422	403.985	108.904	1.096667
0.4	12000	0.065	1560	595.194	411.0838	121.5761	0.786667
0.4	12500	0.065	1625	491.0591	381.3817	144.1291	1.34
0.4	13000	0.065	1690	558.834	400.0651	127.8816	1.57
0.4	13500	0.065	1755	594.6975	393.4493	109.3664	1.8
0.4	14000	0.065	1820	508.835	368.9492	103.6506	0.61
0.4	14500	0.065	1885	436.322	362.0618	110.3299	0.473333
0.4	15000	0.065	1950	440.9878	361.7699	142.6886	0.37
0.4	15500	0.065	2015	479.9676	400.6728	161.7479	0.173333
0.4	16000	0.065	2080	539.8395	417.3564	145.403	0.15
0.6	11000	0.065	1430	464.3843	379.5693	104.1835	1.736667
0.6	11500	0.065	1495	545.4961	384.2536	107.8709	0.913333
0.6	12000	0.065	1560	548.2805	406.1144	110.5248	0.76
0.6	12500	0.065	1625	464.1348	403.4312	134.2162	1.12
0.6	13000	0.065	1690	573.0147	391.9451	121.5137	1.14
0.6	13500	0.065	1755	600.4946	375.3503	104.0016	0.766667
0.6	14000	0.065	1820	517.1188	351.3415	104.0632	0.283333
0.6	14500	0.065	1885	459.5997	363.2746	109.0543	0.27
0.6	15000	0.065	1950	413.7812	355.6686	138.9071	0.21
0.6	15500	0.065	2015	473.1705	401.2314	153.3425	0.186667
0.6	16000	0.065	2080	537.8593	400.9136	143.2024	0.18
0.8	11000	0.065	1430	480.1017	378.5188	105.0299	0.433333
0.8	11500	0.065	1495	538.7579	396.0705	100.0764	0.37
0.8	12000	0.065	1560	587.0377	421.7889	114.8956	0.296667
0.8	12500	0.065	1625	473.4865	411.2369	132.9026	0.47
0.8	13000	0.065	1690	555.698	400.6304	115.4843	0.31
0.8	13500	0.065	1755	600.3274	384.7027	104.1073	0.3
0.8	14000	0.065	1820	533.2502	370.685	102.6138	0.323333
0.8	14500	0.065	1885	454.4686	373.406	103.7836	0.293333
0.8	15000	0.065	1950	448.853	384.5925	134.3626	0.29
0.8	15500	0.065	2015	469.1492	394.6067	149.522	0.24
0.8	16000	0.065	2080	539.7237	419.0007	142.3159	0.273333

Table 30. Data used for regression analysis for 1045 Steel.

SUMMARY OUTPUT

Regression Statistics	
Multiple R	0.747639
R Square	0.558964
Adjusted R Square	0.525887
Standard Error	37.04046
Observations	44

ANOVA

	df	*SS*	*MS*	*F*	*Significance F*
Regression	3	69554.169	23184.723	16.89854	3.03454E-07
Residual	40	54879.83	1371.9957		
Total	43	124434			

	Coefficients	*tandard Erro*	*t Stat*	*P-value*	*Lower 95%*	*Upper 95%*
Intercept	-30048.13	4547.7562	-6.6072428	6.63E-08	-39239.48761	-20856.77144
S	6.921679	1.0245553	6.7557889	4.11E-08	4.850975764	8.992382706
S^2	-0.000515	7.639E-05	-6.746661	4.23E-08	-0.000669741	-0.000360973
S^3	1.27E-08	1.885E-09	6.7227207	4.57E-08	8.86291E-09	1.64826E-08

Table 31. Regression summary output for resultant acceleration prediction in 1045 Steel.

Since the regression analysis showed that the factor depth of cut is insignificant to the prediction there is only one resultant acceleration prediction graph, shown below. The resultant acceleration prediction equation has the next form:

$$Acc\,\mathrm{Re}\,s = -30048.13 + (6.921679 * S) - (0.000515 * S^2) + (1.27E - 08 * S^3)$$

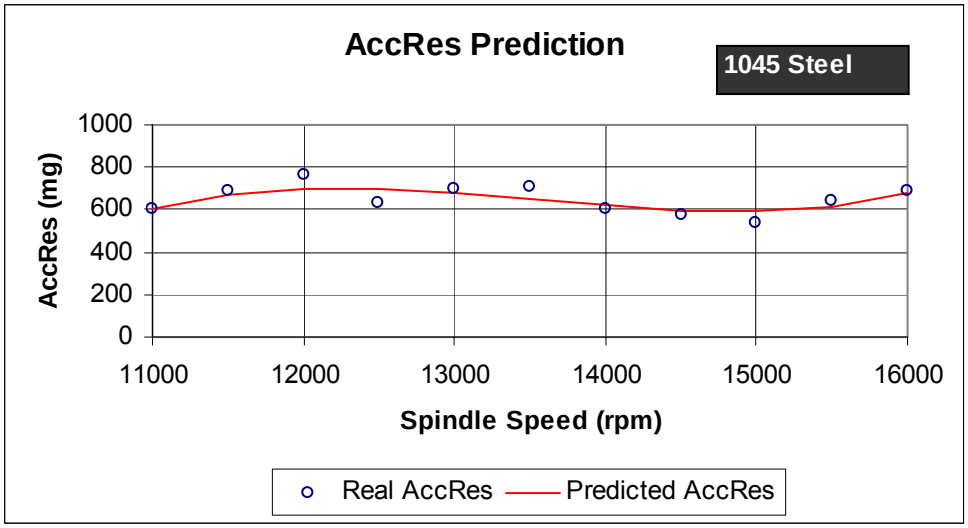

Figure 85. Resultant acceleration model response for 1045 Steel.

SUMMARY OUTPUT

Regression Statistics	
Multiple R	0.536244422
R Square	0.28755808
Adjusted R Squ	0.270595177
Standard Error	0.398964472
Observations	44

ANOVA

	df	*SS*	*MS*	*F*	*Significance F*
Regression	1	2.698322449	2.698322	16.95217	0.000175508
Residual	42	6.685251288	0.159173		
Total	43	9.383573737			

	Coefficients	*Standard Error*	*t Stat*	*P-value*	*Lower 95%*	*Upper 95%*
Intercept	2.847416667	0.517047097	5.507074	2.03E-06	1.803973394	3.89085994
Vf	-0.001204779	0.000292614	-4.117302	0.000176	-0.001795297	-0.00061426

Table 32. Regression summary output for surface roughness prediction in 1045 Steel

For this material only one feed per tooth was used, for such reason we only have one equation to predict surface roughness.

$$Ra = 2.847416667 - (0.001204779 * Vf)$$

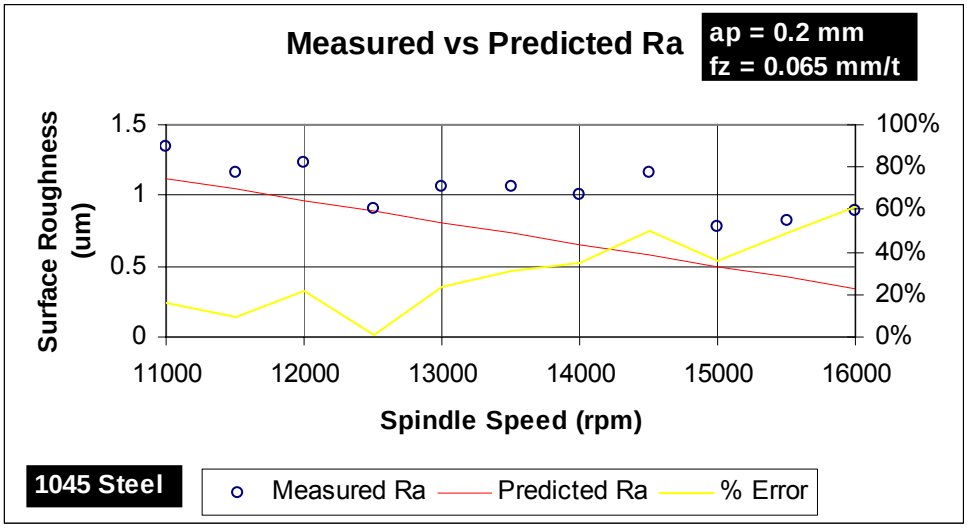

Figure 86. Measured vs Predicted Ra for 1045 Steel at an ap of 0.2 mm and 0.065 mm/t of feed per tooth.

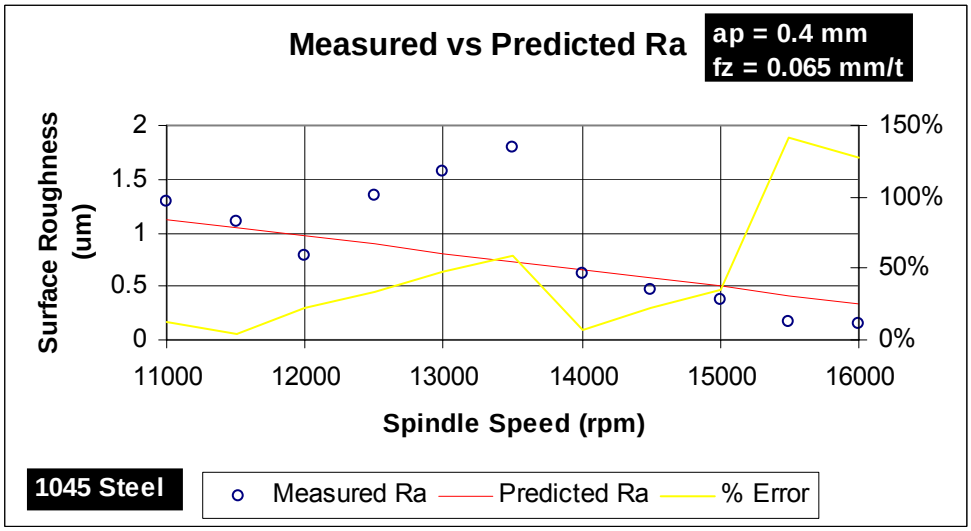

Figure 87. Measured vs Predicted Ra for 1045 Steel at an ap of 0.4 mm and 0.065 mm/t of feed per tooth.

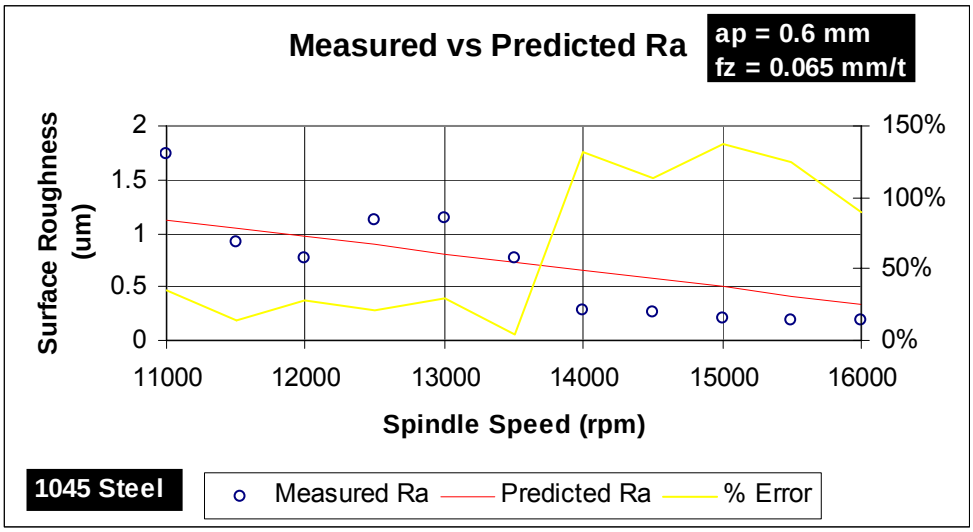

Figure 88. Measured vs Predicted Ra for 1045 Steel at an ap of 0.6 mm and 0.065 mm/t of feed per tooth.

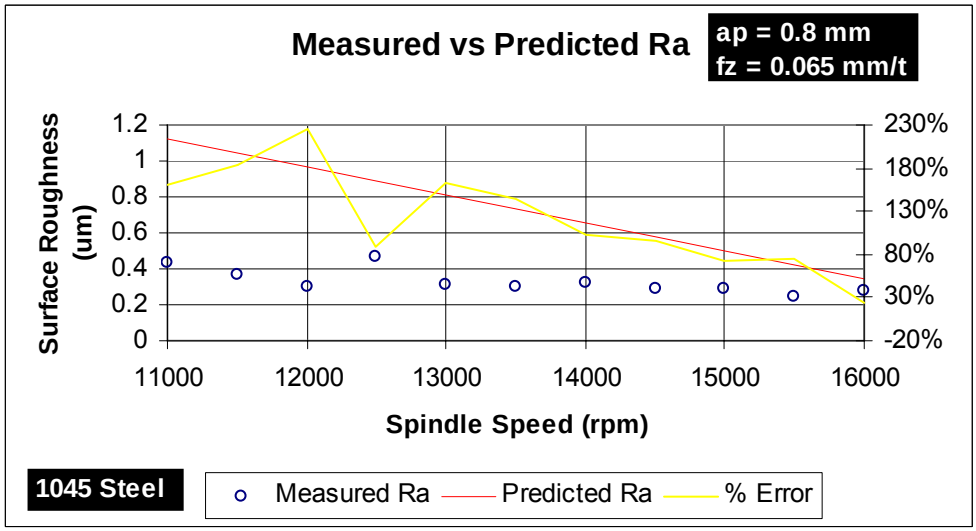

Figure 89. Measured vs Predicted Ra for 1045 Steel at an ap of 0.8 mm and 0.065 mm/t of feed per tooth.